IMPLICATIONS OF WIDESPREAD DARK PRODUCTION AND DECAY OF REACTIVE OXYGEN SPECIES IN NATURAL WATERS

by

Ryan M. Marsico

A thesis submitted to the Faculty and the Board of Trustees of the Colorado School of Mines in partial fulfillment of the requirements for the degree of Doctor of Philosophy (Geochemistry).

Golden, Colorado

Date _____

Signed: _____

Ryan M. Marsico

Signed: _____

Dr. Bettina M. Voelker
Thesis Advisor

Golden, Colorado

Date _____

Signed: _____

Dr. David T.W. Wu
Professor and Head
Department of Chemistry and Geochemistry

ABSTRACT

Light dependent and independent reactions produce and consume reactive oxygen species (ROS), including hydrogen peroxide (H_2O_2) and superoxide (O_2^-), in natural waters. ROS can act as oxidants or reductants to biologically important metals such as Fe, Cu, and Mn influencing their bioavailability. ROS produced in natural waters have also been linked to global phenomena such as harmful algal bloom fish kills and coral bleaching. In this thesis, we focus on the light independent (dark) reactions of ROS that are produced and decomposed by particle-associated processes, most likely microorganisms. However, before microorganisms can be implicated in ROS reactions we need to understand where, why, and how microorganisms as well as abiotic processes produce and decompose ROS.

Ecological and geochemical stress factors that trigger ROS production and decomposition in natural waters are largely unknown. Therefore, we set out to measure the temporal and spatial variability of dark H_2O_2 production rates (P_{H2O2}) and dark decay rate coefficients ($k_{loss,H2O2}$) in freshwaters with a range of trophic states. Production rates were found to be comparable to production by photochemical processes. Furthermore, $k_{loss,H2O2}$ correlated well with biological indicators (chlorophyll and cell counts) while P_{H2O2} did not. This suggests that while microorganisms are a common sink of H_2O_2, dark production may vary with microbial composition. We suspect that both a lake's trophic state and the specific microbial consortia present in the system, at a given time, lead to the observed variability of ROS production in freshwater.

The method for measuring dark P_{H2O2} in project one, which utilized an isotope tracer ($H_2{}^{18}O_2$), proved tedious, costly, and time consuming. Therefore, we used Amplex Red (AR) oxidation by H_2O_2 in the presence of horseradish peroxidase (HRP) catalyst as an effective

alternative. We show that AR/HRP is suitable for measuring dark P_{H2O2} in freshwater by examining possible false positive and negative interferences, and methods to eliminate them. Catalase and HRP-free controls helped validate the AR method and revealed dark P_{H2O2} values of comparable magnitude and natural variability as previous studies.

The dark redox cycling of mercury (Hg), especially the production of Hg(II), can lead to the formation of toxic methylated Hg compounds. Because dark reactions of Hg are largely an enigma and ROS are known to affect the redox cycling of metals in the ocean (e.g. Cu and Mn), we set out to understand if O_2^- plays a role in the dark biogeochemical cycle of Hg. Here, we measured O_2^- oxidation and reduction of Hg in filtered coastal (Vineyard Sound) seawater. O_2^- appeared to indirectly oxidize Hg^0 in two seawater samples and O_2^- reduced Hg(II) in one seawater sample. We did not observe evidence of oxidation or reduction of Hg via secondary O_2^- reactions involving Mn, Cu, and nicotinamide adenine dinucleotide (NADH). However, our samples were filtered, and the proximity of NADH to cell surfaces may reveal a potential biological mechanism of Hg(II) reduction. The calculated reduction rate constant of Hg(II), 6.9 (3.1) $x10^2$ M^{-1} s^{-1}, would cause a Hg(II) reduction rate of ~1% day^{-1} similar to the rate observed in previous studies of dark microbial Hg(II) reduction. Our study suggests that O_2^- may play an important role in the dark biogeochemical cycling of Hg in coastal ocean waters by indirectly oxidizing Hg^0 and slowly reducing Hg(II).

TABLE OF CONTENTS

LIST OF FIGURES

LIST OF TABLES

ACKNOWLEDGEMENTS

There are countless people and organizations that I would like to thank for their help during my career at the Colorado School of Mines from funding sources and mentors to friends and family members.

First I would like to thank the Department of Chemistry and Geochemistry at the Colorado School of Mines for providing partial funding as a Teaching Assistant. Interacting with undergraduate students in Chemistry Lab was a rewarding experience, and helped me keep a fresh perspective for my own learning. The National Science Foundation funded a large part of my graduate research and I'm very grateful that they help foster scientific research at many levels.

Our work requires laboratory experiments as well as heading out to the field, and without the help of others it sometimes would be a difficult experience. I would like to thank Paul Flannigan and the folks at Big Elk Meadows that were gracious enough to let us sample their private lake. I've also traveled to Woods Hole Oceanographic Institution a few times to complete my final mercury seawater project, and if it were not for the help of Carl Lamborg, Gretchen Swarr, Priya Ganguli, Tong Zhang, Julia Diaz, and Colleen Hansel my visit would have been less pleasant and speedy. I also cannot forget the help of Ed Dempsey on numerous occasions. No matter how busy or overwhelmed Ed was he would find time to help, and always with a smile on his face. Others in the department were also very helpful including Joe Stranahan, Ramona Figueroa, and the many people working tirelessly in the head office.

The Voelker group, while always changing, helped me be a better scientist on a daily basis. I would like to thank Robin Schneider who was very helpful my first year of graduate school when Tina was on sabbatical, and with her help on the hydrogen peroxide freshwater field survey

project. I would like to thank Shuichi Ushijima who, at the time, was an undergraduate student that helped me with field sampling for my first two projects, and a very impressive scientist for his young age. Many thanks to Shubham Vyas and Kelly Roe who provided invaluable guidance as post docs in Tina's lab. Observing their work, presentations, and professionalism were a lesson in and of themselves.

Thanks to my committee members, Dr. Jim Ranville, Dr. John Spear, Dr. Ron Cohen, and Dr. Colleen Hansel for their time and input. My committee is an extremely intelligent group of scholars that would never turn you away if you needed help. I could not thank my advisor and mentor Dr. Tina Voelker enough for her guidance throughout graduate school. She is one of the most patient and unselfish human beings I have ever encountered. I could not have had a better graduate school experience that is largely due to the help of Tina. It's still hard to comprehend the amount of information I've learned from her and her group, especially since I had no idea what a reactive oxygen species was until I met her.

I'd also like to thank my friends and family. I'm incredibly lucky to have such a loving and supportive family. My parents, brother, sister-in-law, and nephews are the most important people in my life. Skyping with them just about every week while living in Colorado really kept me happy and sane during my graduate school career. Thanks to the many friends that I've made in Colorado including Val, Charlie, Doreen, Kevin, Sean, Ben, Erich, Assaf, and Heidi, just to name a few. Our adventures around Golden and in the mountains were always a great escape from the rigors of graduate school. Lastly, I would like to thank my second family here in Colorado. One of my biggest support systems were Myndi, Mason, and Marin. You always encouraged during my endeavors, were always patient, and were there through the best and toughest times. I will forever be grateful.

CHAPTER 1
INTRODUCTION

1.1 Introduction and thesis organization

This thesis focuses on two reactive oxygen species (ROS), hydrogen peroxide (H_2O_2) and superoxide (O_2^-), in natural waters, and their possible sources and reactions. ROS are important to aquatic life because of their involvement in the redox cycling of metals important to biological processes. For example, H_2O_2 is an oxidant of ferrous iron in the Fenton reaction and a reductant of manganese oxides (Moffett & Zika 1987, Sunda & Huntsman 1994, Vermilyea et al. 2010). Superoxide can oxidize and reduce metals such as Cu, Mn, and Fe, ultimately affecting their bioavailability (Bielski et al. 1985, Voelker & Sedlak 1995, Zafiriou et al. 1998, Hansard et al. 2010).

Photo-excitation of chromophoric dissolved organic matter (CDOM) produces ROS in natural waters by transferring electrons to O_2 (Cooper et al. 1988, Scully et al. 1995, Andrews et al. 2000). However, aquatic microorganisms (e.g. algae and bacteria) can also produce and decompose ROS in the dark (Diaz et al. 2013, Oda et al. 1997, Kim et al. 2000, Kim et al. 2005, Garg et al. 2007a, Kim et al. 2007, Liu et al. 2007, Aguirre et al. 2005, Silar 2005, Rose 2012). Previous studies have measured dark production (P_{H2O2}) and decay ($k_{loss,H2O2}$) of H_2O_2 in natural waters (Dixon et al. 2013, Vermilyea et al 2010a, Vermilyea et al. 2010b), but it was left unclear if dark P_{H2O2} and $k_{loss,H2O2}$ were widespread and occurred in various types of waters (e.g. oligotrophic to eutrophic). It also remained largely unknown if dark P_{H2O2} and $k_{loss,H2O2}$ in natural waters resulted from microbial processes. Therefore, Chapter 2 presents a freshwater field survey of dark P_{H2O2} and $k_{loss,H2O2}$ from 16 different sites in Colorado and Massachusetts. Additional goals of this project were to relate the magnitudes of dark P_{H2O2} and $k_{loss,H2O2}$ to

biological indicators (chlorophyll and microbial cell numbers) and to geochemical parameters (e.g. metals and nutrients). A manuscript based on Chapter 2 was accepted for publication in the Journal of Aquatic Sciences in June 2015 (DOI 10.1007/s00027-015-0399-2).

The main method used in Chapter 2, involving an isotope tracer of hydrogen peroxide ($H_2{}^{18}O_2$), is tedious and time consuming, and often needs two people to complete. Therefore, Chapter 3 set out to validate and apply an alternative analytical method to determine dark P_{H2O2} in freshwater using Amplex Red or AR (N-acetyl-3,7-dihydroxyphenoxazine). Unlike the technique used in Chapter 2, this method measures P_{H2O2} directly. Various studies have used AR in biological, natural, and aqueous fluids (Rhee et al. 2010, Burns et al. 2012, Snyrychova et al. 2009, Zhou et al. 1997, Mishin et al. 2010, Gajovic-Eichelmann & Bier 2005) to detect H_2O_2, but many pitfalls exist including false positive interferences from direct oxidation of AR or inhibition of the catalyst enzyme, horse radish peroxidase or HRP (Rodrigues & Gomes 2010, Votyakova & Reynolds 2004, Wetzel 1992, Reszka et al. 2005). Our goals were to validate AR/HRP for dark P_{H2O2} measurements in freshwater by determining false positive and negative interferences via AR and resorufin (measurable reaction product) stability experiments. Catalase (scavenges H_2O_2) controls and controls removing the HRP catalyst were also used to validate true dark P_{H2O2} measurements in freshwaters. A manuscript based on Chapter 3 will be submitted to the journal Analytica Chimica Acta.

Dark O_2^- oxidation and reduction of mercury (Hg) in the Vineyard Sound are the focus of Chapter 4. Little is known about the dark mechanisms of Hg oxidation/reduction in sweater. However, because O_2^- rapidly reacts with metals like Cu and Mn in seawater (Zafiriou et al. 1998, Voelker et al. 2000, Hansard et al. 2011) we set out to determine if an abiotic source of O_2^- is also involved in the dark redox reactions of Hg. It is important to determine if O_2^- is involved

in the dark Hg redox cycle because, for example, the production of Hg(II) through oxidation reactions leads to the formation of toxic methylated Hg compounds (Fitzgerald et al. 2007). The aim of Chapter 4 is to determine whether O_2^- production can lead to dark Hg oxidation/reduction, which would shift our understanding of the dark biogeochemical cycle of Hg in the ocean. Other goals included determining if secondary reactions with O_2^- can oxidize/reduce Hg in seawater. For example, O_2^- can oxidize Mn(II) to Mn(III/IV), and Mn(III/IV) may then oxidize Hg. The implications would be that even if O_2^- does not directly oxidize/reduce Hg, it would link other global metal cycles to the Hg cycle. A manuscript based on Chapter 4 is being prepared for a submission for publication.

CHAPTER 2

SPATIAL AND TEMPORAL VARIABILITY OF WIDESPREAD DARK PRODUCTION AND DECAY OF HYDROGEN PEROXIDE IN FRESHWATER

This Chapter was published in *Aquatic Sciences* (DOI 10.1007/s00027-015-0399-2)

Ryan M. Marsico[1*], Robin J. Schneider[2*], Bettina M. Voelker[3*], Tong Zhang[4†], Julia M. Diaz[5†], Colleen M. Hansel[6†], Shuichi Ushijima[7*]

[1] Graduate student, primary researcher and author
[2] Graduate student, primary researcher, and co-author
[3] Professor, Principal Investigator, and corresponding author
[4] Post-doctoral Investigator and contributing researcher
[5] Post-doctoral Investigator and contributing researcher
[6] Associate Scientist, co-Principal Investigator, and corresponding author
[7] Undergraduate student, field work contributor
*Colorado School of Mines, Department of Chemistry & Geochemistry, 1500 Illinois St., Golden, CO 80401
†Woods Hole Oceanographic Institution, Marine Chemistry & Geochemistry, 266 Woods Hole Rd. MS# 52, Woods Hole, MA 02543-1050

2.1 Abstract

Hydrogen peroxide (H_2O_2) is an oxidant and reductant of redox active metals and a potential source of strong oxidants such as the hydroxyl radical (·OH). H_2O_2 production in freshwater has been largely attributed to photo-oxidation of chromophoric dissolved organic matter (CDOM), while its decay has been linked to enzymatic processes as well as to chemical reactions with metals. More recently, however, microorganisms were postulated as a significant source and sink of H_2O_2 in freshwater. In this study, we examined the spatial and temporal variability of dark H_2O_2 production rates (P_{H2O2}) and pseudo-first order dark decay rate coefficients ($k_{loss,H2O2}$) in incubations of water samples from sites with a range of trophic states in Colorado (CO) and Massachusetts (MA). Observed values of P_{H2O2} and $k_{loss,H2O2}$ ranged from 3 to 259 nM h^{-1} and 0.02 to 8.87 h^{-1}, respectively. Filtering the freshwater samples removed the majority of $k_{loss,H2O2}$

while microbial cell numbers and chlorophyll content correlated strongly with $k_{loss,H2O2}$, indicating breakdown by biota as the major sink of H_2O_2. Dark production of H_2O_2 was also ubiquitous, but P_{H2O2} was not well correlated with indicators of microbial abundance. For instance, several oligotrophic sites with low $k_{loss,H2O2}$ exhibited moderately high $P_{H2O2,}$ while a sample with unusually high chlorophyll content and a correspondingly high $k_{loss,H2O2}$ had a relatively low P_{H2O2}. One possible explanation for this phenomenon is that the ability to break down H_2O_2 is similar among different microorganisms, but the ability to produce H_2O_2 may vary with microbial composition.

Keywords: reactive oxygen species; hydrogen peroxide; freshwater; dark production and decay; spatial and temporal variability

2.2 Introduction

Hydrogen peroxide (H_2O_2), a reactive oxygen species (ROS), plays an important role for aquatic life in freshwater due to its involvement in the redox cycling of metals. For example, H_2O_2 is known to be an oxidant of ferrous iron in the Fenton reaction and a reductant of manganese oxides (Moffett & Zika 1987, Sunda & Huntsman 1994, Vermilyea et al. 2010a). The Fenton reaction produces hydroxyl radical ($^{\cdot}OH$) and other strong oxidants, which can break down environmentally relevant recalcitrant organic molecules (Pignatello et al. 2006, Vermilyea & Voelker 2009).

In natural aquatic environments, H_2O_2 is generated from both light dependent and independent processes. Photochemically excited chromophoric dissolved organic matter (CDOM) can reduce dissolved oxygen to form superoxide ($O_2^{\cdot -}$) as an intermediate to production of H_2O_2 (Cooper et al. 1988, Scully et al. 1995, Andrews et al. 2000). However, several field studies have observed non-zero steady state concentrations of H_2O_2 in freshwater systems during

the night. Since H_2O_2 decomposition continues in the dark (abiotically via redox reactions or biotically via catalase or peroxidase enzymes), H_2O_2 would decay to low levels if it were not simultaneously produced. Thus, H_2O_2 must be actively produced in the absence of light (Zepp et al. 1987). Indeed, overnight studies at Jack's Lake, Ontario, Canada and in a New Zealand stream demonstrated non-zero steady state H_2O_2 concentrations of 20-60 nM and 15-80 nM, respectively (Cooper & Lean 1989, Richard et al. 2007).

Simultaneous dark production and decay rates of H_2O_2 were previously confirmed by using lake water incubations with an added isotope labeled tracer ($H_2{}^{18}O_2$), the first experiments of this kind performed in freshwater (Vermilyea et al. 2010a). Dark H_2O_2 production rates (P_{H2O2}) varied among several Denver Metropolitan area lakes (e.g. 29-122 nM h^{-1}), and were up to an order of magnitude higher than the calculated photochemical production (Vermilyea et al. 2010a). Pseudo first order decay rates coefficients ($k_{loss,H2O2}$) in this study ranged from 0.33 to 1.7 h^{-1}. A second study applied the $H_2{}^{18}O_2$ tracer technique to *in-situ* mesocosms in a Nebraska agricultural headwater (Maple Creek), and showed that total production of H_2O_2 in the stream was far greater than that expected from abiotic photoproduction alone (Dixon et al. 2013).

Both Vermilyea et al. (2010a) and Dixon et al. (2013) attributed dark production of H_2O_2 to biological sources, since the ability of both bacteria and algae to produce extracellular ROS in the dark has been demonstrated in culture studies. For example, dark superoxide production has been observed in a broad diversity of heterotrophic bacteria isolated from marine, freshwater, and terrestrial environments (Diaz et al. 2013). Cultured algae have also been shown to produce extracellular ROS in the dark (Oda et al. 1997, Kim et al. 2000, Kim et al. 2005, Garg et al. 2007a, Kim et al. 2007, Liu et al. 2007). In addition, fungal species are capable of producing H_2O_2 for cell signaling within laboratory incubations (Aguirre et al. 2005, Silar 2005, Rose

2012). While culture experiments provide us insight into the diversity of organisms that produce ROS in the laboratory, little knowledge is available regarding the range of biological production and decay rates that occur in freshwater environments, and the ecological and/or geochemical factors affecting their magnitude.

The goals for this study were (i) to quantify the extent of spatial and temporal variability in the rates of dark H_2O_2 production and decay in natural freshwater systems, (ii) to determine whether there is a relationship between standard geochemical parameters (such as nutrients, DOM, and dissolved metals) and rates of dark production and decay , and (iii) to examine the contributions of different types of microbial organisms (i.e. bacteria versus phototrophs) to dark H_2O_2 production and decay. We conducted a field survey to quantify dark P_{H2O2} and $k_{loss,H2O2}$ in widely varying freshwater settings and conditions. We also measured nutrients, dissolved metals, DOM, and indicators of biological abundance (chlorophyll content and cell density) for specific sites.

2.3 Materials and Methods

The methodological details for measuring dark hydrogen peroxide production (P_{H2O2}) and decay ($k_{loss,H2O2}$) are described in the section. Field sites and auxiliary measurements are also described.

2.3.1 Field sites

The field sites sampled in Colorado (CO) and Massachusetts (MA) include bodies of water with different trophic states influenced by assorted land uses. Badger, Bijou, and Box Elder Creeks are streams that flow through agricultural plains near the towns of Wiggins, Fort Morgan, and Brush, CO, respectively. South Pawnee Creek flows through the Pawnee National Grasslands in northern CO. Cold Spring (North Boulder Creek) is a stream north of the foothill

town of Nederland, CO while Barker Reservoir is a treated stream-fed lake residing within Nederland's border. Mirror Lake at Big Elk Meadows (referred to as Mirror Lake herein) is one of five lakes nestled in a catchment area adjacent to a development in the Rocky Mountain foothills near the town of Lyons, CO. Big Elk Meadow's private homeowner's association lake management determined that Mirror Lake is hypereutrophic, and receives high inputs of nutrients from septic tank leakage. Clear Creek was sampled upstream and downstream from Black Hawk, CO with the downstream water potentially influenced by acid mine drainage. Boulder Creek flows from mountain sources through Boulder Canyon, and water samples were collected near CO Route 119. Crown Hill Lake resides in the Denver suburb of Wheat Ridge, CO and is fed by storm drainage. Spring-fed Sloan's Lake exists within Denver's city limits, the most densely populated area that we sampled. Denver area lakes, including Sloan's Lake, are known to be eutrophic to hypereutrophic (Dudley 2004).

The MA sites provide a geographically different sample set in which all are in low population density suburban areas. All MA sites have a pH < 6, opposed to all Colorado sites having a pH > 8. Additionally, Ashumet Pond is known to have relatively high Mn concentrations. Therefore, the MA sites were targeted as bodies of freshwater with different pH values, and possibly different microbial communities, than the CO sites that could possibly influence P_{H2O2} and $k_{loss,H2O2}$ differently. Three freshwater ponds on Cape Cod were sampled, including Santuit, Ashumet, and John's Ponds. The Assabet River, the largest stream sampled in terms of volume, and Lake Boon, a dammed lake adjacent to the Assabet River, are approximately 30 miles west of Boston, MA. Table A.1 in the supplementary Appendix A contains information on pH, conductivity (μS), and water temperature of each field site. Figures

A.2 and A.3 contain the relative locations and GPS coordinates of the CO and MA field sites, respectively.

2.3.2 Natural water sample collection and transfer

Unfiltered freshwater samples were taken from the field sites near the shore-line (littoral zone) during mid-day. They were collected using 1 L amber Nalgene bottles filled to ¾ full for the dates 7/25/11 through 6/20/2012. Once collected, the samples were kept on ice in a standard cooler and transferred to the lab for storage and/or analysis. For all dates after 6/20/12, 5-10 L of unfiltered freshwater samples were collected in 19 L carboys. The carboys were brought back to the laboratory immediately for redistribution into 1 L amber Nalgene bottles for storage and analysis.

2012 Sloan's Lake samples were incubated and analyzed within 1–2 h of sample collection, which took place before 10 a.m. local time. All 2011 samples were obtained between 10 a.m. and 3 p.m while 2012 Mirror Lake samples were obtained between noon and 12:30 p.m., and stored in the dark overnight (14–15 h) either on ice or in a standard refrigerator (4 _C) before being incubated and analyzed the following day.

Nalgene bottles were cleaned before use by soaking in 30% isopropyl alcohol (IPA) overnight, rinsing with nanopure water, soaking in 3% nitric acid at least overnight, and then rinsing with nanopure water. The carboys were rinsed with nanopure water, soaked in 30% IPA overnight and rinsed with nanopure water, 3% nitric acid, and, again, nanopure water on the same day as it was used.

2.3.3 Incubation experiments

To measure both P_{H2O2} and $k_{loss,H2O2}$ during incubations of freshwater samples, we utilized the isotope-tracer procedure as described in Vermilyea et al. (2010a). $H_2{}^{18}O_2$ is not

produced naturally in significant quantity, but decays by the same processes as total H_2O_2. Measurement of both the absolute decay rate of $H_2{}^{18}O_2$ as well as the change in total H_2O_2 (which is affected by both production and decay) allows for the calculation of the H_2O_2 production rates (P_{H2O2}).

Before analysis, the freshwater samples were brought to and incubated at room temperature (~22-25 ^{o}C) in a water bath and then spiked with 300-800 nM $H_2{}^{18}O_2$. The 2011 freshwater samples were incubated in 60 mL syringes which were covered with aluminum foil to prevent exposure to ambient light. The 2012 freshwater samples were incubated in 1 L opaque amber Nalgene bottles with minimum headspace (<20 mL) which were placed in a water bath at room temperature. Filtered controls were incubated under the same conditions after passing the water sample through a membrane filter (Pall Corp. 0.2 µm Acropak). To eliminate any interference from the filter material, the filter was pre-rinsed with at least 0.5 L of the water sample.

Aliquots from the incubations were removed at a minimum of every hour until a steady state signal was reached after spiking with $H_2{}^{18}O_2$ (typically from 3-7 hours). Each sample was syringe filtered (Millipore 0.2 µm PES), and the filtrate was analyzed for total [H_2O_2] and [$H_2{}^{18}O_2$]. The syringe filters were pre-cleaned with 3 mL of 0.1 M HCl followed by 5 mL of nanopure water (Vermilyea et al. 2010a). Total [H_2O_2] was measured the same day as the dark incubation, using flow injection analysis (FIA) (see following section for details). Samples for $H_2{}^{18}O_2$ were prepared simultaneously (alongside the total measurements). They were preserved, and analyzed within a week using gas chromatography mass spectrometry (GCMS). See Vermilyea et al (2010a) for preservation and analysis details.

On 8/17/12 and 9/4/12-9/20/12, incubations were not conducted with $H_2{}^{18}O_2$. Instead, P_{H2O2} and $k_{loss,H2O2}$ were obtained from a set of parallel incubations as described by a previously published procedure (Vermilyea et al. 2010b) which we will refer to here as "Spiked batch incubations". Briefly, an unaltered sample was incubated alongside 2 to 3 samples of the same water spiked with additional H_2O_2 (e.g. +100 nM, +200 nM, and + 300 nM H_2O_2). Aliquots drawn from each bottle were syringe-filtered, and total [H_2O_2] was measured hourly using FIA. The decay rate coefficient ($k_{loss;H2O2}$) was then determined by the rate of loss of H_2O_2 spiked in the samples compared to the unaltered sample.

2.3.4 Total and labeled H_2O_2 analysis

The analysis of H_2O_2 is described in this section. Two simultaneous techniques were used to measure total H_2O_2 (naturally existing H_2O_2 and the added amount of $H_2{}^{18}O_2$) using flow injection analysis (FIA) and the absolute decay rate of $H_2{}^{18}O_2$ using cryogenic gas chromatography mass spectrometry (GCMS).

2.3.4.1 Total H_2O_2 analysis

Total H_2O_2 was measured using FIA on a FeLume (Waterville Analytical, Maine) and the acridinium ester (AE) method (Cooper et al. 2000, Vermilyea et al. 2010a). Briefly, a sample aliquot of sample was injected into a stream of carrier (DI water treated with 10 units catalase L^{-1}) and then combined with AE solution (1 µM, pH 3). As the sample/AE mixture entered a spiral flow cell adjacent to the photomultiplier tube, it was combined with a carbonate buffer (pH 10.2-10.5) solution, which initiated the base-catalyzed reaction of AE with H_2O_2.

2.3.4.2 $H_2{}^{18}O_2$ analysis

$H_2{}^{18}O_2$ sample preparation and measurement was conducted as previously described by Vermilyea et al. (2010a). All measurements were analyzed on a cryogenic Hewlett Packard (HP)

Agilent 5973 gas chromatograph with a 6890 HP mass spectrometer detector equipped with a mole sieve column (HP-PLOT MoleSieve, 30m×320 mm ID, 12 μm film thickness). Our temperature program used a -60 °C oven temperature held for 4.5 min, followed by a ramp up to 120 °C at 120 °C/minute. The detector was set to approximately 1700 V. All concentrations are reported in terms of $H_2{}^{18}O_2$, rather than the true $^{18}O_2$ headspace concentration. Calibration standards of 0, 200, 400, and 600 nM $H_2{}^{18}O_2$ were prepared in nanopure water.

Quality control standards of 400 nM $H_2{}^{18}O_2$ in nanopure water were also prepared and stored for the same amount of time as the freshwater samples before analysis on the GCMS. A quality control standard was measured on the GCMS after every 10 samples.

2.3.5 Determination of production and decay rates

We assume that the concentration of isotope-labeled H_2O_2 , $[H_2{}^{18}O_2]$, undergoes simple exponential decay, and can be modeled by the equation:

$$\left[H_2{}^{18}O_2\right] = \left[H_2{}^{18}O_2\right]_0 e^{-k_{loss,H2O2}t} \qquad \text{(Equation 2.1)}$$

We further assume that the change in the concentration of total H_2O_2, $[H_2O_2]$, is the net result of a constant rate of production as well as first-order decay:

$$\frac{d[H_2O_2]}{dt} = P_{H2O2} - k_{loss,H2O2}[H_2O_2] \qquad \text{(Equation 2.2)}$$

This differential equation has the solution:

$$[H_2O_2] = \frac{P_{H2O2}}{k_{loss,H2O2}} - \left\{\left(\frac{P_{H2O2}}{k_{loss,H2O2}} - [H_2O_2]_0\right) e^{-k_{loss,H2O2}t}\right\} \qquad \text{(Equation 2.3)}$$

Data from the isotope-tracer method were modeled using Eqs. 2.1–2.3. $H_2{}^{18}O_2$ data were fitted to Eq. (2.1) and the data for total $[H_2O_2]$ were fitted to Eq. (2.3) simultaneously, using the Solver function in Microsoft Excel. Decay and production rate data from the spiked batch incubations were modeled using Eqs. 2.2–2.3 only, as described in Vermilyea et al. (2010b), since an

isotope-tracer was not used. In this case, the data of the parallel spiked batch incubations were fitted simultaneously to Eq. (2.3) also using the Solver function of Microsoft Excel.

To determine background P_{H2O2} and $k_{loss,H2O2}$ for our experiments, we incubated nanopure water in a syringe on 8/10/2011 (same date as the Clear Creek sample collections) and in a dark Nalgene bottle on 8/1/2012 (same date as a Mirror Lake sample collection). These two nanopure controls both had P_{H2O2} values of 0 nM h^{-1} and the $k_{loss,H2O2}$ values were 0.03 and 0.02 h^{-1} for Clear Creek and Mirror Lake, respectively. These background signals were similar to those determined previously by our lab, where $P_{H2O2} = 11 \pm 9$ nM h^{-1} and $k_{loss,H2O2} = 0.016 \pm 0.015$ h^{-1} (N =4, Vermilyea et al. 2010a).

Replicate incubation experiments were not always conducted due to the limited throughput of sample analysis. However, we did obtain duplicate measurements using the isotope-tracer method with unfiltered water samples from six different field sites, each conducted on a different day (Table 2.1) Using these duplicate measurements, we calculated a pooled percent relative standard deviation ($\%RSD_{pooled}$) of 32 % for production rates. Using the same strategy for decay, we determined a pooled % RSD_{pooled} of ±15 %. These standard deviations imply high uncertainties in production rates, with 95 % confidence limits of ±78 % of the value of individual measurements and ±55 % of the average value of two duplicate measurements. For decay rate coefficients, the 95 % confidence limits are ±37 % of individual measurements and ±26 % of the average of two duplicate measurements. These confidence limits were used to place error bars on the measurements of unfiltered samples obtained by the isotope tracer method.
To determine the uncertainty for the spiked batch incubation method, we duplicated 3 separate unfiltered incubation experiments (all from Sloan's Lake) and calculated a % RSD_{pooled} of ±23 and ±16 % for production rates and decay rate coefficients, respectively (Table 2.1). Therefore,

95 % confidence limits on production rates measured by this technique are ±73 % of the value of individual measurements and ±52 % of the average value of two duplicate measurements. For decay rate coefficients, the 95 % confidence limits are ±52 % of individual measurements and ±36 % of the average of two duplicate measurements. These confidence limits were used to place error bars on the measurements of unfiltered samples obtained by the spiked batch incubation method.

Table 2.1 Example calculation of the pooled percent relative standard deviation (*%RSD$_{pooled}$*) using duplicates of unfiltered P_{H2O2} (P_1 and P_2) and $k_{loss,H2O2}$ (k_1 and k_2) measurements for the isotope-tracer method and the spiked batch incubation method

Sites – Isotope-tracer Method	Replicate P_1 (nM h^{-1})	Replicate P_2 (nM h^{-1})	Mean	P_1/Mean	P_2/Mean	%RSD
Badger Creek	70	137	104	68	132	46
Bijou Creek	91	133	112	81	119	27
Box Elder Creek	42	74	58	72	128	39
Barker Reservoir	3.1	2.6	2.9	108	92	12
Mirror Lake 8/10/12	172	199	185.5	93	107	10
Sloan's Lake 8/24/12	135	74	104.5	129	71	41
					%RSD$_{pooled}$	*32.4*
Sites – Spiked batch incubation Method						
Sloan's Lake 9/4/12	90	150	120	75	125	35
Sloan's Lake 9/11/12	96	105	101	96	104	6
Sloan's Lake 9/20/12	101	79	90	112	88	17
					%RSD$_{pooled}$	*23.0*
Sites – Isotope-tracer Method	**Replicate k_1 (h^{-1})**	**Replicate k_2 (h^{-1})**	**Mean**	**k_1/Mean**	**k_2/Mean**	**%RSD**
Badger Creek	0.66	0.58	0.62	106	94	9
Bijou Creek	0.56	0.49	0.53	106	94	9
Box Elder Creek	0.53	0.56	0.55	97	103	4
Barker Reservoir	0.11	0.16	0.14	81	119	27
Mirror Lake 8/10/12	1.22	1.54	1.38	89	111	16
Sloan's Lake 8/24/12	0.75	0.61	0.68	110	90	14
					%RSD$_{pooled}$	*15.0*
Sites – Spiked batch incubation Method						
Sloan's Lake 9/4/12	1.80	2.40	2.10	86	114	20
Sloan's Lake 9/11/12	1.06	1.20	1.13	94	106	9
Sloan's Lake 9/20/12	0.75	0.59	0.67	112	88	17
					%RSD$_{pooled}$	*16.0*

2.3.6 Auxiliary parameters

Auxiliary measurements (e.g. nutrients and metals) were made at the field sites, and this section describes how these measurements were made.

2.3.6.1 Nutrients and anions by Ion Chromatography (IC)

Nutrients (NO_3^-, PO_4^{3-}) and other salt anions (F^-, Cl^-, Br^-, SO_4^{2-}) were measured using an ion chromatograph (Dionex ICS-90, EPA method 300.1). Pre-packaged sterile 15 mL Falcon™ tubes were used to collect filtered samples in the field. The 2011 samples were filtered using 0.2 µm PES syringe filter (Millipore) and the 2012 samples were filtered through a 0.22 µm Sterivex GP filter. After filtering, the IC samples were transported on ice, and stored frozen for up to 3 weeks before analysis. Nanopure field blanks were below detection limit (BDL) except for nitrate (ranged from BDL to 0.09 mg L^{-1}). The blank values were not subtracted from values reported.

2.3.6.2 Dissolved Organic Carbon (DOC)

DOC was measured using a Total Organic Carbon Analyzer (Sievers model 5310C). Environmental Sampling and Supply's certified pre-cleaned (of trace organics) 125-250 mL amber glass bottles were used to collect filtered samples in the field. The 2011 samples were filtered through a 0.2 µm PES syringe filters (Millipore) and the 2012 samples were filtered using 0.22 µm Sterivex GP filters. After filtering, the DOC samples were transported on ice, and refrigerated for up to 3 weeks before analysis. Before refrigeration, the samples were acidified to pH < 2 using concentrated phosphoric acid. Nanopure field blank DOC ranged from 0.33 to 1.50 mg L^{-1} and were not subtracted from values shown.

2.3.6.3 Dissolved metals (Cu, Fe, Mn) by Inductively Coupled Plasma – Atomic Emission Spectroscopy (ICP-AES)

Dissolved Cu, Fe, and Mn were quantified by ICP-AES (Perkin Elmer 3000). Pre-packaged sterile 15 mL Falcon™ tubes were used to collect the filtered samples in the field. The 2011 samples were filtered using 0.2 µm PES syringe filter (Millipore) and the 2012 samples were filtered using 0.22 µm Sterivex GP filter. After filtration, the dissolved metal samples were transported on ice, and refrigerated for up to 3 weeks before analysis. Before refrigeration, the samples were acidified to pH < 2 using concentrated nitric acid. Nanopure field blank values for Cu were BDL; Fe blanks ranged between 0.5 to 7.5% of individual sample concentrations depending on the date sampled; Mn blanks were BDL to 7% of individual sample concentrations. Reported concentrations were not corrected for these blanks.

2.3.6.4 Chlorophyll by Ultraviolet-Visible Spectroscopy (UV-Vis)

Total chlorophyll concentrations were determined by an UV-Visible spectrometer (Hewlett Packard 8453 Chemstation Software, with a Tungsten Lamp) utilizing EPA method 446.0. The samples were collected in 250 mL Nalgene amber bottles, and transported back to the laboratory on ice. Chlorophyll samples were processed in the laboratory by concentrating them on 47 mm 0.7 µm nominal porosity (GF/F Whatman Millipore AP-40) filter paper immediately upon return. They were then wrapped in aluminum foil and stored in the dark at -20 °C for up 2 weeks before analysis. The chlorophyll data are averages of triplicate measurements on all occasions except for Crown Hill Lake (8/23 and 9/29), Boulder Creek, and Santuit Pond when duplicate measurements were made. Standard deviations of chlorophyll measurements are provided in the Appendix A. Nanopure field blanks that were brought on site were also processed and analyzed in the same manner and values were <5% of the sample values.

2.3.6.5 Water temperature, conductivity, and pH

Water temperature (T_{water}, °C) and conductivity (µS) were measured using a CHEMetrics, Inc. field conductivity meter by directly submerging the meter into the body of water. pH was measured in a similar manner using a CHEMetrics, Inc. field pH meter. See Table A.1 in the supplementary Appendix A.

2.3.6.6 Cell counts

Natural water taken from Mirror Lake on 7/19/12 and Sloan's Lake from 8/17 to 9/20/12 was preserved to count algae, cyanobacteria, and bacteria using fluorescence microscopy. Cells were fixed with 4% formaldehyde and then stored at -20℃. Natural water samples were thawed and stained with 4',6-diamidino-2-phenylindole (DAPI) prior to counting bacterial cells. The abundance of bacterial cells were represented by DAPI counts of spherical cells with a diameter < 1 µm and rod-shaped cells with a diameter < 1 µm and length < 4 µm. Round-shaped algal cells and filamentous cyanobacterial cells were also observed and counted in the water samples. All cell counts were performed for 20 random fields of view on an epifluorescence microscope. See Figure A.1 and Table A.4 in the supplementary Appendix A for cell counts per mL.

2.4 Results and Discussion

This section presents the first results showing the widespread dark production and decay of H_2O_2 in freshwater. It also describes the correlations of dark production and decay with biological abdundance indicators such as chlorophyll and microbial cell numbers.

2.4.1 Spatial and temporal variability of dark P_{H2O2} and $k_{loss,H2O2}$

A two-year survey of freshwater systems in CO and MA shows that the dark production and decay of H_2O_2 are ubiquitous, with rates that vary widely in magnitude. Our 2011 data establishes the spatial variability in P_{H2O2} and $k_{loss,H2O2}$ among 16 different sites with a range of

trophic states (Figures 2.1a and 2.1b, respectively). The 2012 data constitutes a study of temporal variability of P_{H2O2} and $k_{loss,H2O2}$ at 2 sites over the course of late spring to mid-summer for Sloan's Lake and from July to August for Mirror Lake (Figures 2.2a and 2.2b, respectively). Both Sloan's Lake and Mirror Lake are considered to be eutrophic to hypereutrophic (within typical ranges) based on our chlorophyll measurements and consistent with past knowledge of their trophic states (Dudley 2004).

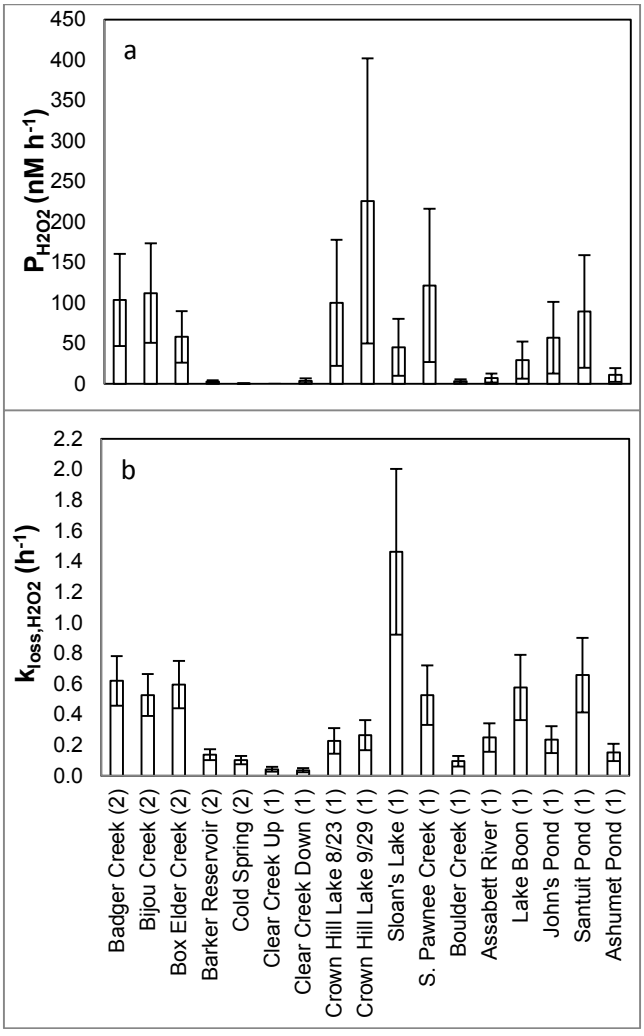

Fig. 2.1 The spatial variability of a.) dark P_{H2O2} in nM h^{-1} and b.) dark $k_{loss,H2O2}$ in h^{-1} from CO and MA during 2011. The error bars of P_{H2O2} and $k_{loss,H2O2}$ are 95% confidence intervals using the pooled %RSD in Table 2.1. The symbol (2) beside a field site indicates an average of duplicate measurements and the symbol (1) indicates a single measurement

While much of the variability in P_{H2O2} observed in the spatial study falls within the uncertainty of our measurements, very low P_{H2O2} values were observed at some of the oligotrophic sites (Figure 2.1). For example, Barker Reservoir and Boulder Creek had H_2O_2 dark production rates similar to background signals (P_{H2O2} ~3.0 nM h^{-1}). Agriculturally influenced streams generally had much higher production rates. For example, P_{H2O2} at Bijou Creek was as high as 112 nM h^{-1} and Crown Hill Lake, a lake in a Denver suburb, had one of the highest dark production rates of H_2O_2 (226 nM h^{-1}).

The same oligotrophic CO foothill lakes and streams also had some of the lowest decay rates, though these were somewhat higher than those we measured in nanopure blanks (e.g. Barker Reservoir, 0.11-0.16 h^{-1}, Figure 2.1b). Higher $k_{loss,H2O2}$ was observed for sites influenced by agriculture (e.g. Bijou Creek, 0.49-0.56 h^{-1}). The highest decay rate for the 2011 spatial variability study was at urban Sloan's Lake with $k_{loss,H2O2}$ = 1.46 h^{-1}.

The variation of dark H_2O_2 production and decay rates in the temporal study (Figure 2.2) was smaller than in the spatial study, except for the unusually high decay rate observed in Sloan's Lake water on 8/29. This decay rate (8.87 h^{-1}) occurred during a visually observed, unusually dense algal bloom, and did not correspond to a particularly high value of P_{H2O2} (137 nM h^{-1}). The peak P_{H2O2} at Sloan's Lake was 259 nM h^{-1} on 8/17 during another noticeable algal bloom, while the lowest P_{H2O2} was roughly an order of magnitude lower on 6/14 at 38 nM h^{-1}. In Mirror Lake water, the highest P_{H2O2} and $k_{loss;H2O2}$ were also measured during a visually observed algal bloom on 7/18 at values of 219 nM h^{-1} and 2.27 h^{-1}, respectively. The lowest P_{H2O2} and $k_{loss;H2O2}$ values at Mirror Lake occurred on separate dates without observed algal blooms, with values of 56 nM h^{-1} and 0.81 h^{-1}, respectively. Even the lowest P_{H2O2} and $k_{loss;H2O2}$ measured at

hypereutrophic Mirror Lake were still similar to or higher than the larger values observed in eutrophic sites (e.g. Box Elder Creek) inthe 2011 spatial variability study (Figure 2.1).

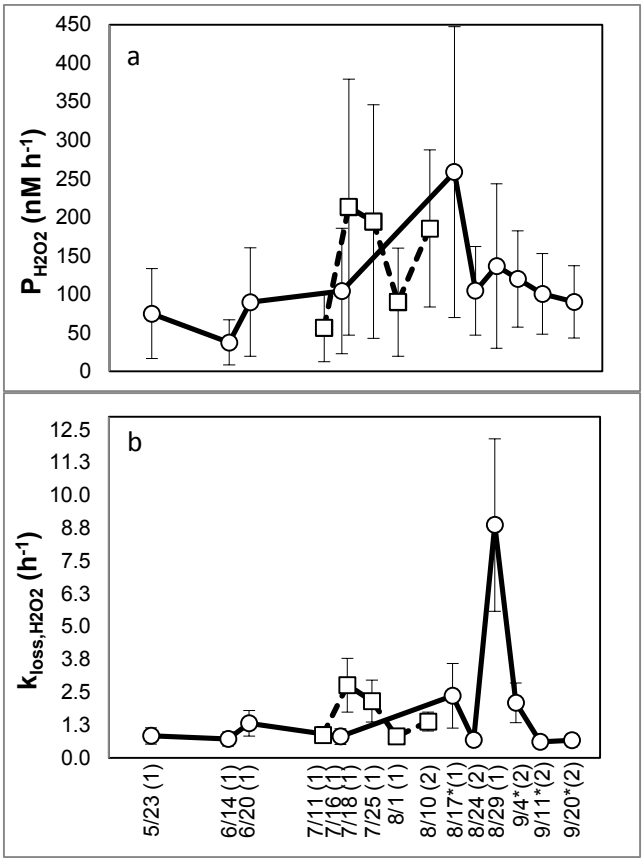

Fig. 2.2 The temporal variability of a.) dark P_{H2O2} in nM h^{-1} and b.) dark $k_{loss,H2O2}$ in h^{-1} over the summer months of two field sites in CO (2012): Sloan's Lake (○, solid line) and Mirror Lake (□ , dashed line). Asterisks (*) indicate dates when the spiked batch incubation method was used rather than the isotope-tracer method. The error bars of P_{H2O2} and $k_{loss,H2O2}$ are 95% confidence intervals using the pooled %RSD in Table 2.1. The symbol (2) beside a date indicates an average of duplicate measurements and the symbol (1) indicates a single measurement

2.4.2 Attributing dark P_{H2O2} and $k_{loss,H2O2}$ to microorganisms

Filtering (0.22 µm) of the freshwater samples consistently decreased $k_{loss;H2O2}$, and decreased P_{H2O2} in Sloan's Lake samples, but not always in Mirror Lake samples (Figure 2.3a). Student's t test was conducted when replicate measurements of both unfiltered and filtered

samples were obtained (Sloan's Lake samples on 8/24, 9/4, 9/11, and 9/20), and showed that the difference between unfiltered and filtered production rates (Figure. 2.3a) was significant ($p<0.05$ on 9/20 and $p<0.1$ in the other three). The difference between filtered and unfiltered decay rates was highly significant in all four of the cases tested (Figure 2.3b). The strong effect of filtering on $k_{loss;H2O2}$ may indicate that microbes are a significant sink of H_2O_2 (i.e. $k_{loss;H2O2}$) since filtering also removed >99 % of microbial cells (with a few exceptions; see Table A.4 in the Appendix A for cell counts in filtered water). Microbes are often equipped with anti-oxidant enzymes (e.g. catalase and superoxide dismutase) that break down ROS in the environment (Cooper & Zepp 1990, Cooper et al. 1994). While we cannot rule out reactions with inorganic particulates larger than 0.22 µm as a loss mechanism, these reactions are probably too slow to account for the rapid decay rates we observed in these systems (Kwan and Voelker 2002;. Petigara et al.2002; Scott et al. 2002).

The difference between unfiltered and filtered production rates in Sloan's Lake water (Fig. 2.3a) indicates that dark PH2O2 is also predominantly attributable to particles (>0.22 µm), probably biota. However, the larger residual dark P_{H2O2} in Mirror Lake filtered samples, observed on 7/18, 7/25, and 8/10 (Fig. 2.3a), suggests that the dissolved fraction (<0.22 µm) can also be a source of H_2O_2 at Mirror Lake. Oxidation of reduced natural organic matter (Page et al. 2012), enzymes exuded from microbial cells, or enzymes released from cell surfaces during filtering may be responsible for dark P_{H2O2} in filtered solutions (Learman et al. 2011, 2013).

The decay parameter, $k_{loss,H2O2,}$ was generally well correlated with total microbial cell counts per mL ($R^2 = 0.91$, $p < 0.001$, $N = 7$, Table 2.2) as well as with algal cell counts ($R^2 = 0.95$, $p < 0.001$, $N = 7$, Table 2.2) in unfiltered freshwater water samples (see Figure A.1 in the Appendix A for cell counts). Additionally, $k_{loss,H2O2}$ was moderately correlated with chlorophyll

content measured in the spatial study ($R^2 = 0.56$, $p < 0.05$, N = 10, Figure 2.4a) and well correlated in the temporal study ($R^2 = 0.96$, $p < 0.001$, N = 15, Figure 2.4b). This trend suggests that microbial decomposition is a key factor of $k_{loss;H2O2}$ in the unfiltered samples.

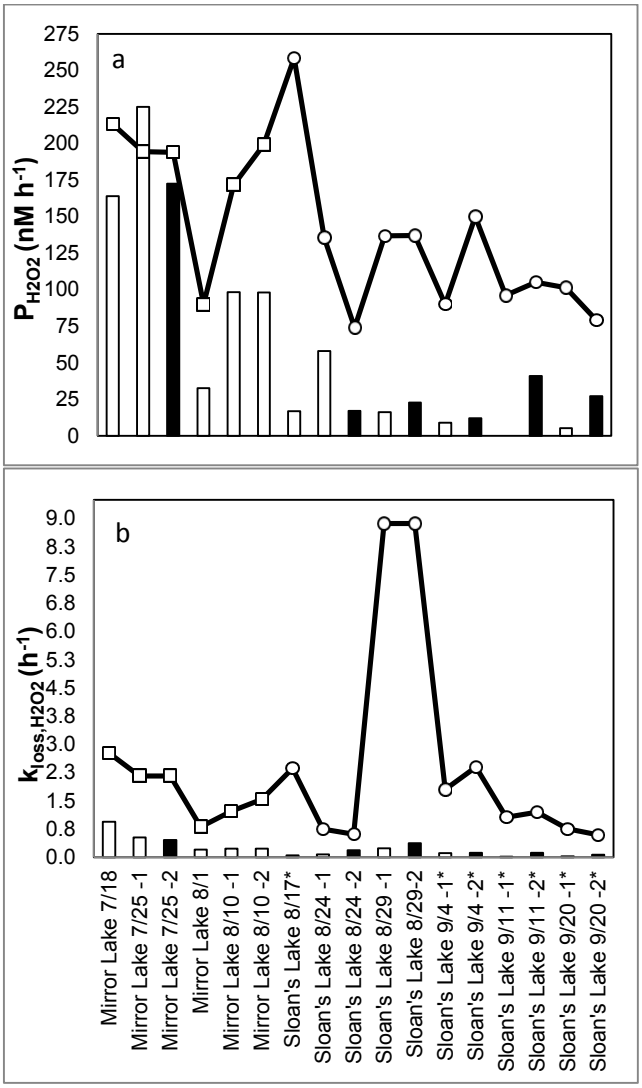

Fig. 2.3 A comparison of a.) dark P_{H2O2} in nM h^{-1} and b.) dark $k_{loss,H2O2}$ in h^{-1} in unfiltered (solid line) and filtered (bars) samples. Replicates of filtered samples (black bars) are sometimes compared to a single unfiltered value from the same experiment when unfiltered replicates were not conducted (and vice versa). Asterisks (*) indicate dates when the spiked batch incubation method was used rather than the isotope-tracer method. The error of P_{H2O2} and $k_{loss,H2O2}$ are discussed in the methods section (see also Table 2.1).

Table 2.2 Correlation (R^2) between cell counts per mL with dark P_{H2O2} and $k_{loss,H2O2}$. Data includes sampling from Mirror Lake 7/19/12 and Sloan's Lake 8/17/12 through 9/20/12 (N = 7)

Cells per mL of:	P_{H2O2} R^2 / p-value	$k_{loss,H2O2}$ R^2 / p-value
Bacteria	0.05 / >0.05	0.79 / <0.01
Algae	0.002 / >0.05	0.95 / <0.001
Cyanobacteria	0.14 / >0.05	0.51 / >0.05
Total Cells	0.003 / >0.05	0.91 / <0.001

In contrast to $k_{loss,H2O2}$, dark P_{H2O2} does not generally correlate well with microbial abundance determined by chlorophyll content (e.g. $R^2 = 0.03$, $p > 0.05$, N =10 in the spatial study, Figure 2.4c) and cell counts (e.g., $R^2 = 0.003$, $p > 0.05$, N =10, for total cell counts per mL) . This may be because some microorganisms are better producers than others. For example, John's Pond in MA (▲ in Figure 2.4a and 2.4c, highlighted with a solid black arrow) is considered to be oligotrophic, as shown by its low chlorophyll content (0.005 mg L^{-1}). It had a relatively high P_{H2O2} (57 nM h^{-1}) when compared to other oligotrophic sites with similar chlorophyll content, such as Boulder Creek where P_{H2O2} = 3 nM h^{-1} (◇ in Figure 2.4a and 2.4c highlighted with a dashed arrow). Meanwhile, the $k_{loss,H2O2}$ values of both John's Pond and Boulder Creek fall in line with the general trend of $k_{loss,H2O2}$ versus chlorophyll ($R^2 = 0.56$, $p < 0.05$, N=10, Figure 2.4a). These results suggest that the organism(s) present at John's Pond were higher producers of H_2O_2. However, given the high uncertainty in our P_{H2O2} measurements, we cannot rule out that the high value measured in John's Pond (which was not duplicated) was due to measurement error, and that a correlation between P_{H2O2} and chlorophyll was masked by measurement variability.

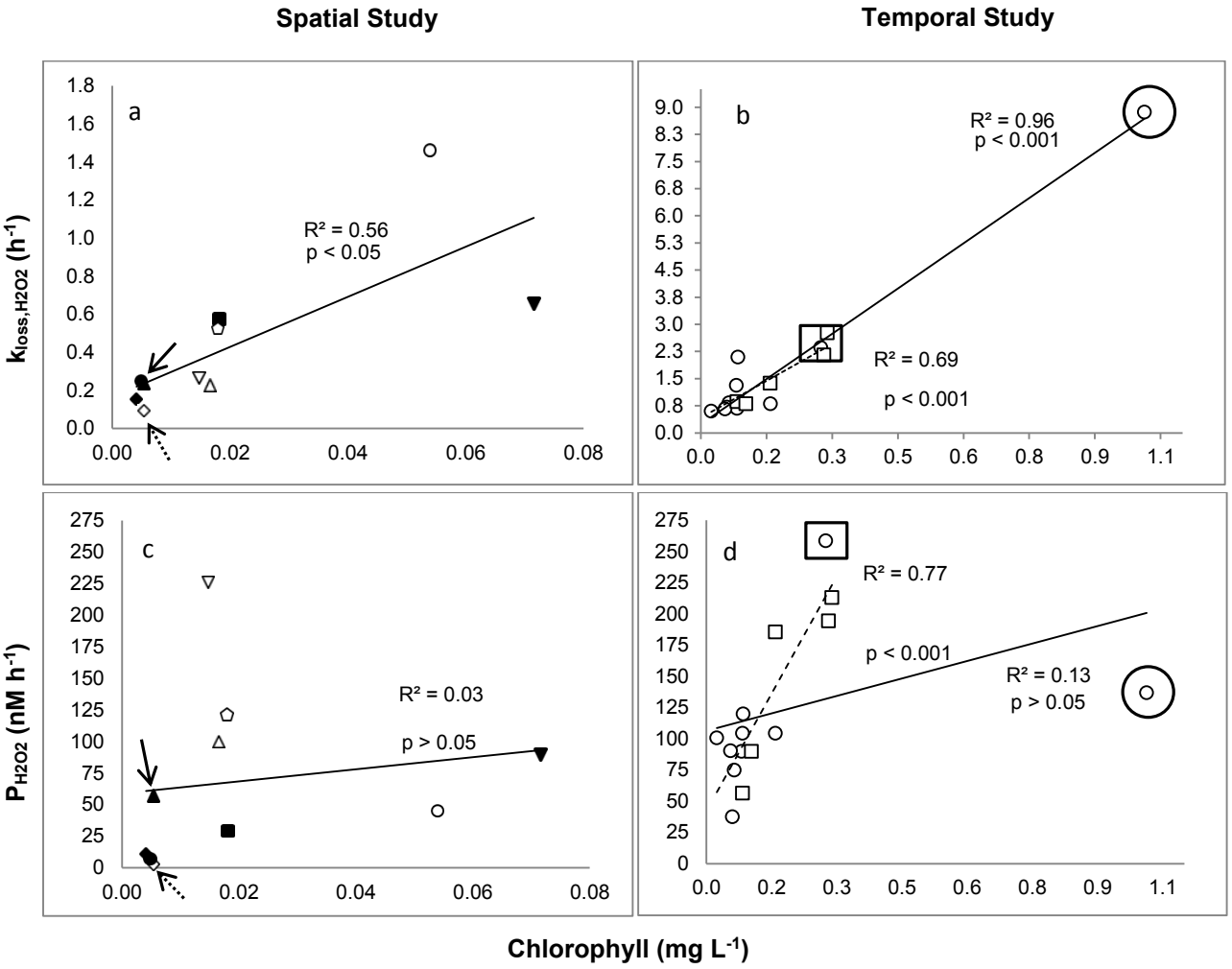

Fig. 2.4 Chlorophyll content correlations with dark $k_{loss,H2O2}$ from the a.) spatial, and b.) temporal variability studies. Parts c.) and d.) are the chlorophyll content correlations with the spatial, and temporal variability of dark P_{H2O2}, respectively. *Spatial study:* CO Sites (open symbols): Boulder Creek (◇), Crown Hill Lake 8/23 (△), Crown Hill Lake 9/29 (▽), Sloan's Lake (○), South Pawnee Creek (⬠). MA sites (black symbols): Ashumet Pond (◆), John's Pond (▲), Santuit Pond (▼), Assabet River (●), and Lake Boon (■). *Temporal study:* Sloan's Lake (○) and Mirror Lake (□). The solid trend lines are the correlation lines with all data included. The dashed lines in the temporal study are the trend lines with the unusually high chlorophyll (1.01 mg L^{-1} chlorophyll) data removed. Additional symbols (solid and dashed arrows / solid circles and squares) are data points discussed in the text. Average values of P_{H2O2} and $k_{loss,H2O2}$ were used on days where replicate measurements were made to correspond to only one chlorophyll value. The error bars of P_{H2O2}, $k_{loss,H2O2}$, and chlorophyll are discussed in the methods section (see also Table 2.1 and the Appendix A)

In the temporal variability study, Sloan's Lake 8/29 had unusually high chlorophyll content (1.01 mg L^{-1}), stemming from an algal bloom, but with a moderate P_{H2O2} (137 nM h^{-1}), highlighted with a black circle in Figure 2.4d. In contrast, another Sloan's Lake data point, highlighted with a black box, had lower chlorophyll content (0.27 mg L^{-1}), but a higher P_{H2O2} (259 nM h^{-1}) more in line with the rest of the observations in Figure 2.4d. Including the 8/29 data point with the unusually high chlorophyll content weakens the correlation between P_{H2O2} and chlorophyll for the Sloan's Lake samples ($R^2 = 0.12$, $p > 0.05$, $N = 10$, solid line in Figure 2.4d versus $R^2 = 0.74$, $p < 0.01$, $N = 9$ if the point is removed, dashed line in Figure 2.4d). A P_{H2O2} far outside the confidence interval of the 8/29 measurement would be required to fit the correlation implied by the dashed line in Figure 2.4d. In contrast, including the 8/29 data point improves the correlation between $k_{loss;H2O2}$ and chlorophyll ($R^2 = 0.96$, $p < 0.001$, $N = 10$, solid line in Figure 2.4b, versus $R^2 = 0.46$, $p < 0.05$, $N = 9$, dashed line in Figure 2.4b). These results suggest that the organism(s) blooming at that time were similar to other organisms in terms of their ability to break down H_2O_2, but far below average producers of H_2O_2. The Mirror Lake data points (squares in Figure 2.4b, d), which were not included in the correlations, show P_{H2O2} and $k_{loss;H2O2}$ values consistent with those measured in Sloan's Lake (Figure 2.4b, d).

Regardless of the natural settings and how well certain types of microorganisms can produce H_2O_2, dark P_{H2O2} did not exceed several hundred nM h^{-1}. Up to an order of magnitude faster dark P_{H2O2} was observed in closed-bottom mesocosms (lacking a sediment–water interface, and most closely corresponding to the conditions of the present study) in the agriculturally influenced Maple Creek in Nebraska (Dixon et al.2013). However, the rates in the Maple Creek study are not directly comparable to ours because they include possible effects of prior light exposure immediately before dark P_{H2O2} measurements were taken. In the Maple Creek

mesocosms, production rates appeared first to increase during exposure to 4 h of midday light, and then to decrease over several hours when the mesocosms werecovered to prevent further light exposure. These trends did not agree with expected photochemical production rates, which should have decreased as the light intensity decreased in the afternoon hours and ceased immediately after the mesocosms were covered. Therefore, it is possible that biological production of H_2O_2 increased gradually with increasing light exposure and then decreased after light exposure ceased. After 4 h in the dark, P_{H2O2} values in closed-bottom Maple Creek mesocosms were approximately 100–400 nM h^{-1} (Dixon et al. 2013) or similar to those observed in the present study.

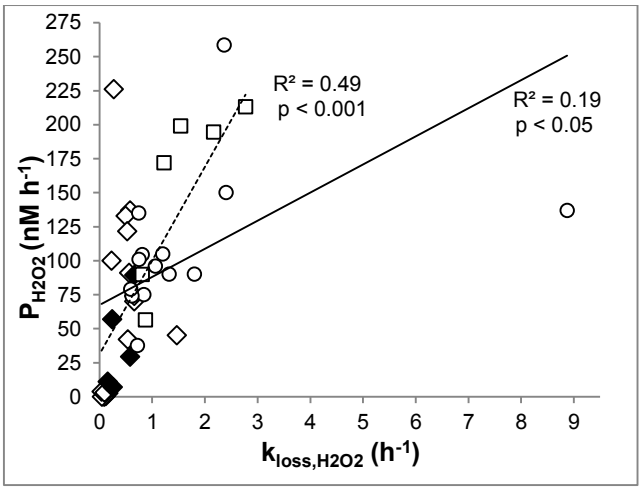

Fig. 2.5 Correlation of dark P_{H2O2} and dark $k_{loss,H2O2}$ for the 2011 and 2012 spatial and temporal variability studies. The solid line is the correlation line with all data included and the dashed line is the correlation line with the decay parameter (8.87 h^{-1}), from the unusually high chlorophyll day (algal bloom), excluded. *Spatial study:* CO (◇) and MA (◆). *Temporal study:* Sloan's Lake (○) and Mirror Lake (□).The error of P_{H2O2} and $k_{loss,H2O2}$ are discussed in the methods section (see also Table 2.1)

The production rates in the present study should have been minimally affected by prior light exposure, since all samples were incubated in the dark only, and all samples other than the 2012 Sloan's Lake samples had been stored in the dark for 14–15 h prior to incubation. The

Sloan's Lake samples did receive some light exposure close in time to being incubated, since they were collected after sunrise, and incubated within an hour or two after collection. However, because sampling took place at least 3 h before solar noon, the light exposure was much smaller than that received by the Maple Creek samples, and Sloan's Lake production rates looked very similar to those of Mirror Lake (Figure 2.2a). Decay rates in Dixon et al. (2013) closed-bottom mesocosms were 2.4–2.6 h^{-1}, similar to those observed in the hypereutrophic Sloan's and Mirror Lakes in the present study (Figure 2.2b). Faster decay rates were observed by Dixon et al. (2013) in the open-bottom mesocosms (4.6–9.0 h^{-1}), most likely due to interaction with biofilms or mineral surfaces (Richard et al. 2007).

The correlation between P_{H2O2} and $k_{lossH2O2}$ in the present study was weak with a R^2 of 0.19 ($p < 0.05$) or $R^2 = 0.49$ ($p < 0.001$) when the unusually high $k_{loss,H2O2}$ from the Sloan's Lake algal bloom is excluded (Figure 2.5). Excluding all of the 2012 Sloan's Lake data has little effect on this correlation ($R^2 = 0.47$, $p < 0.001$, $N = 28$), indicating that any variability introduced by using shorter storage times for these samples, and sometimes a different analytical technique (spiked batch incubations), was not a major factor. Due to the measurement uncertainty of P_{H2O2} and $k_{loss;H2O2}$ (see Table 2.1 and 95 % confidence limits), it is possible that the correlation could be improved with more precise measurements. We are not aware of any previous study correlating these parameters in freshwater systems. However, there was a good correlation ($R^2 = 0.74$) of P_{H2O2} with $k_{loss;H2O2}$ in relatively productive ocean waters during a 3-week cruise near the Gulf of Alaska (Vermilyea and Voelker 2009) using the spiked batch incubation method. The present study took place over much greater temporal and spatial scales, and included a much wider range of trophic states and geochemical conditions, than the marine study. We therefore

speculate that a greater diversity of different microorganisms was sampled in the present study, which could account for the difference.

2.4.3 P_{H2O2} and $k_{loss,H2O2}$ correlation with Geochemical Parameters

The correlations of geochemical parameters (dissolved metals, nutrients, DOM, etc) with P_{H2O2} and $k_{loss,H2O2}$ were generally weak (see Table A.3 of the supplementary Appendix A). A sufficiently large data set for multivariate data analysis would be required to determine more conclusively whether these parameters play a role in P_{H2O2} and $k_{loss,H2O2}$.

2.5 Conclusion

While hydrogen peroxide decay rate coefficients ($k_{loss;H2O2}$) were well correlated to measures of microbial abundance (e.g. chlorophyll and cell numbers), this was not the case for production rates. One possible explanation for this, as mentioned above, is that some species of microorganisms could be more active producers than others, while most microorganisms have similar ability to break down H_2O_2. In addition, there may be environmental or ecological triggers for biological H_2O_2 production by certain species. For example, Kim et al. (2007) observed that extracellular H_2O_2 production is correlated to intracellular levels in two marine raphidophyte species, perhaps indicating that the level of oxidative stress experienced by the cells plays a role in determining production rates. Ultimately, a better understanding of the mechanisms of biological H_2O_2 production will be key for understanding the wide variability in production rates observed in the present study.

2.6 Acknowledgements

The authors would like to thank Bob Siegrist of Civil and Environmental Engineering at the Colorado School of Mines for letting us use the GCMS and Ed Dempsey for his technical support with the GCMS. We would also like to thank Paul Flanagan and the residents of Big Elk

Meadows for allowing sampling at their private lake. This work was funded by the National Science Foundation Grant EAR-1025077/1245919 to BMV and CMH (Geobiology and Low-Temperature Geochemistry program).

CHAPTER 3

USE OF AMPLEX RED TO DETERMINE GROSS DARK HYDROGEN PEROXIDE PRODUCTION RATES IN FRESHWATER AND ALGAL CULTURES

A paper to be submitted to *Analytica Chimica Acta*

Ryan M. Marsico[1*], Shuichi Ushijima[2*], Bettina M. Voelker[3*], Colleen M. Hansel[4†]

[1] Graduate student, primary researcher and author
[2] Undergraduate student, contributing researcher
[3] Professor, Principal Investigator, and corresponding author
[4] Associate Scientist, co-Principal Investigator, and corresponding author
*Colorado School of Mines, Department of Chemistry & Geochemistry, 1500 Illinois St., Golden, CO 80401
†Woods Hole Oceanographic Institution, Marine Chemistry & Geochemistry, 266 Woods Hole Rd. MS# 52, Woods Hole, MA 02543-1050

3.1 Abstract

Hydrogen peroxide (H_2O_2) is an oxidant and reductant of redox active metals in natural waters, and recent studies have shown that dark production of H_2O_2, often attributed to microorganisms, is comparable to its photochemical production. Here, we validate the use of horseradish peroxidase (HRP) catalyzed oxidation of N-acetyl-3,7-dihydroxyphenoxazine (Amplex Red or AR) by H_2O_2 as a novel way to determine gross dark H_2O_2 production rates (P_{H2O2}) in natural freshwater and in cultures of *Chlamydomonas reinhardtii*, a model algal microorganism. Colorless AR is oxidized to the pink-colored compound resorufin and analyzed using visible spectroscopy at 570 nm. Both AR and resorufin were stable in our freshwater and culture incubations and laboratory control experiments for 3-7 hours. Manganese oxides produce false positive P_{H2O2} in laboratory experiments, indicating the importance of performing catalase-amended controls to confirm AR is oxidized by H_2O_2 in unfiltered freshwater samples. The apparent molar absorptivity (ε_{app}, absorbance measured per cm per M added H_2O_2) in laboratory experiments has a marginal dependence on pH, but appreciable dependence on the concentration

of natural organic matter isolates (Suwannee River Fulvic Acid, SRFA). ε_{app} also greatly deviated from $\varepsilon_{resorufin}$ (5.4-5.8x10^{-5} nM^{-1} cm^{-1}) in freshwater samples, but not in *C. reinhardtii* cultures or phosphate buffer controls, indicating that natural freshwater components (e.g.natural organic matter) can affect the AR/HRP/H_2O_2 reaction. Gross dark P_{H2O2} measured from freshwater incubations were of the same order of magnitude (nM h^{-1}) as those obtained at the same field sites using other techniques. Filtering suggests that particle-associated processes are the dominant source of gross dark P_{H2O2} in freshwater. In *C. reinhardtii* cultures, P_{H2O2} increased, but cell-normalized P_{H2O2} decreased, with increasing cell density.

3.2 Introduction

Hydrogen peroxide (H_2O_2), a reactive oxygen species (ROS), is important to natural water systems because of its ability to drive aquatic redox reactions. For example, freshwater H_2O_2 is known to be a reductant of manganese oxides, and in the Fenton reaction, H_2O_2 is known to be an oxidant of ferrous iron (Moffett & Zika 1987, Sunda & Huntsman 1994, Vermilyea & Voelker 2009). The Fenton reaction produces other strong oxidants including the hydroxyl radical (·OH) capable of breaking down environmentally relevant recalcitrant organic molecules (Pignatello et al. 2006, Vermilyea & Voelker 2009).

Freshwater ROS are generated from both light dependent and independent processes. A well-known light dependent pathway occurs via the photo-oxidation of chromophoric dissolved organic matter (CDOM), in which dissolved oxygen (DO) is reduced to superoxide (O_2^-), which can then be reduced or disproportionate to form H_2O_2 (Cooper et al. 1988, Scully et al. 1995, Andrews et al. 2000). The primary light independent or dark source of ROS in freshwater is postulated to be production by microorganisms. For example, some fungi (Aguirre et al. 2005, Silar 2005, Rose 2012), heterotrophic bacteria (Diaz et al. 2013), and phototrophs, including

algae, (Oda et al. 1997, Kim et al. 2000, Kim et al. 2005, Garg et al. 2007a, Kim et al. 2007, Liu et al. 2007) are known to produce extracellular ROS in the dark. Dark H_2O_2 production rates (P_{H2O2}) were previously measured in many freshwater lakes and streams where the dominant dark source is believed to be from microorganisms (Zhang et al. , Vermilyea et al. 2010a, Dixon et al. 2013, Marsico et al. 2015). Previously unknown non-biological sources including dissolved organic matter (DOM) may also contribute to dark H_2O_2 production. For example, it is known that oxidized moieties on DOM can act as terminal electron acceptors in microbial respiration (Lovley et al. 1996), and may shuttle electrons to DO producing O_2^- and H_2O_2 (Page et al. 2012).

Most of these past studies (Vermilyea et al. 2010a, Dixon et al. 2013, Marsico et al. 2015) have indirectly determined gross dark P_{H2O2} from dark decay rates of isotope labeled hydrogen peroxide ($H_2{}^{18}O_2$), a laborious method requiring multi-day analyses. In this study, gross dark P_{H2O2} was directly measured in less than 5 hours for freshwater and *C. reinhardtii* cultures using AR, the colorless form of a leuco dye. AR reacts with H_2O_2 stoichiometrically in the presence of HRP and forms the pink-colored dye resorufin. Resorufin's high extinction coefficient or molar absorptivity (e.g. 54,000 M^{-1} cm^{-1} at pH 7) at 570 nm (Zhou et al. 1997) makes it attractive for visible spectroscopy, and avoids the use of fluorescence spectroscopy. Additionally, the fluorescence of resorufin has been shown to decay in pH range of 6.2-7.7, a common range for natural water samples (Towne et al. 2004).

Due to its high sensitivity and specificity for H_2O_2, variations of the AR technique have been developed for natural and biological fluids (Rhee et al. 2010, Burns et al. 2012), in the presence of plant (Snyrychova et al. 2009) and animal cells (Zhou et al. 1997, Mishin et al. 2010), and in aqueous solution (Gajovic-Eichelmann & Bier 2005). HRP-catalyzed oxidation of

AR and its derivative Amplex UltraRed (AUR) have also been used to detect H_2O_2 production in algal cultures, in seawater, and in solutions of DOM isolates (Suggett et al. 2008, Rose et al. 2010, Sharpless et al. 2014). However, other studies have shown potential drawbacks of the AR/HRP method to detect H_2O_2 in biological systems. Negative interference by reduced forms of superoxide reductase (SOR), ascorbate, pyridine nucleotides (e.g. nicotinamide adenine dinucleotide or NADH), and glutathione can occur when these compounds scavenge AR radical intermediates produced in peroxidase-catalyzed reactions (Gorris & Walt 2009). Alternative HRP substrates like hydroquinone (QH_2) inhibit AR oxidation by competitively consuming H_2O_2 (Reszka et al. 2005) while another study (counterintuitively) suggests that anti-oxidants like ascorbic and gallic acid directly oxidize AR without H_2O_2 (Serrano et al. 2009). Positive interference may also occur when NADH and glutathione reduce O_2 to superoxide as an intermediate to H_2O_2 formation (Votyakova & Reynolds 2004). Perhaps more pertinent to this study is that aquatic humic substances are known to inhibit peroxidase activity including peroxidase-catalyzed oxidations of leuco dyes (Pflug 1980, Zepp et al. 1988, Wetzel 1992). Additionally, negative interferences may occur through the instability of the AR/HRP/H_2O_2 reaction product, resorufin. Two studies report the photobleaching of resorufin in visible light (Chang et al. 2011, Zhao et al. 2011) and suggest that it can be reduced back to its colorless form (or AR) in the presence of an electron donor (e.g. NADH) through radical intermediates (Zhao et al. 2011). The oxidation of resorufin to resazurin may also be catalyzed by HRP in the presence of high amounts of H_2O_2, after AR has been consumed (Zhao et al. 2012).

The goal of the present study was to develop an AR/HRP technique for determining gross dark P_{H2O2} for natural freshwater and algal cultures, with an emphasis on understanding and correcting for possible interferences that may affect measurements in waters of widely variable

composition. In particular, we examined a suite of common freshwater constituents to determine their effects on resorufin stability and their ability to cause positive and negative interferences, e.g. by directly oxidizing AR (without H_2O_2) or by interfering with the yield of resorufin, respectively. We also examined the variability in the method's sensitivity and determined gross H_2O_2 production rates in a variety of natural water samples as well as in cultures of the microalgae *C. reinhardtii*.

3.3 Materials and Methods

This section describes the methods used to measure true dark P_{H2O2} in freshwater, algal cultures, and fulvic acid isolate solutions using Amplex Red. It also describes the field sites and how methodological interference tests were conducted.

3.3.1 Field Sites

The field sites included freshwater lakes sampled in Colorado (CO). Mirror Lake at Big Elk Meadows (ML-BEM) was one of five lakes nestled in a catchment basin adjacent to a homeowners association. BEM lakes were hypertrophic due to being subjected to high amounts of nutrients leaking into the lake from septic tanks. These lakes ceased to exist when a flooding event in September 2013 destroyed the dams that created them. Crown Hill Lake (CHL) resides in the Denver suburb of Wheat Ridge, CO and is fed by storm drainage. Spring fed Sloan's Lake (SL) exists within Denver's city limits, the most densely populated area that was sampled. Bull Marsh (BM) is part of the Bull Reservoir area in the northern Denver suburb (Westminster, CO) and formed by the overflow of Big Dry Creek. BM's surface water is covered by duckweed in the summer, with dense vegetation year-round creating a lower dissolved oxygen environment.

3.3.2 Natural Water Sample Collection and Transfer

All freshwater samples were collected near the shore-line (littoral zone) during early to mid-day using a pole sampler and placed in 0.5 L amber Nalgene bottles. Once collected, all samples were kept on ice and transferred to the laboratory for analysis. Before sample collection, the Nalgene bottles were cleaned by soaking in 30% isopropyl alcohol overnight, rinsing with nanopure water (Milli-Q), soaking in 3% nitric acid overnight, and then rinsing again repeatedly with nanopure water.

3.3.3 Preparation of *C. reinhardtii* Cultures

C. reinhardtii (CC 125) cultures were grown in TAP medium at pH 7 and harvested at the mid-exponential phase. Cultures were then diluted ($1/5^{th}$, $1/10^{th}$, $1/20^{th}$, and $1/40^{th}$ dilutions) with fresh medium and allowed to sit for 30 minutes to acclimate before incubating. Dilution was necessary to prevent clogging of the syringe filter, which is undesirable since it can increase the pressure in the filter and lyse the cells, potentially contaminating the sample with intracellular H_2O_2 or H_2O_2-generating compounds. Cell densities were measured using a coulter counter (Z2 Beckman) before each experiment.

3.3.4 Buffer and reagent preparation

Phosphate and carbonate buffers were used as controls for freshwater and laboratory experiments, and prepared with 50 mM total phosphate and carbonate salts, respectively. The monobasic and dibasic sodium phosphate salts (Fischer Scientific) were adjusted to the targeted pH (from 6 - 9.5) while the sodium bicarbonate and sodium carbonate salts (Fischer Scientific) were adjusted to pH 9.5 using 1 M HCl and 1 M NaOH.

N-acetyl-3,7-dihydroxyphenoxazine (Amplex Red or AR, Sigma Aldrich) stock solutions were made by first adding 5-10 µL of DMSO to the 5 mg AR package vial and then diluting to

100 mL with nanopure water in a volumetric flask. HRP (Sigma Aldrich) stock solutions were made by adding 10 kU lyophilized HRP powder to nanopure water for a total volume of 100 mL. Both AR and HRP stock solutions were divided into daily portions and stored frozen until use.

A fresh 25 mL 5.1 µM H_2O_2 tertiary stock solution was prepared at each time point for the standard additions and stored in an amber glass vial for the duration of the time point. The tertiary stock was prepared with a 2.9 mM H_2O_2 secondary stock that was stored in an amber Nalgene bottle at 4℃ prepared from 30% w/w H_2O_2 (Sigma Aldrich). The secondary stock was stored for up to one year and the concentration was verified for accuracy once a month using a UV-visible spectrophotometer (Hewlett Packard 8453 with Chemstation Software) at 240 nm (ε_{H2O2} = 38.1 M^{-1}).

In laboratory experiments (see section 3.3.7), freshwater constituents were used to test the stability of AR and resorufin. These included dissolved metals, added as 1 µM aliquots, such as ferrous ammonium sulfate, ferric chloride, manganese (II) chloride, and copper (II) chloride (all from Fischer Scientific). 1 µM aliquots of laboratory synthesized (Appendix B.1) ferrihydrite (Zhao et al. 1994) and manganese dioxide (MnO_2) (Taujale & Zhang 2012) were also added to determine resorufin stability in the presence of metal oxides. Suwanee River River Fulvic Acid or SRFA (International Humic Substances Society) was added to final concentrations of 10 mg L^{-1}, with some experiments including the addition of 10 mg L^{-1} photo-oxidized SRFA. Photo-oxidation was conducted by exposing 10 mL of a 250 mg L^{-1} SRFA stock solution to direct sunlight in a capped quartz cuvette. SRFA and dissolved metal combinations, at the same concentrations described previously, were also used to determine resorufin's stability.

3.3.5 Freshwater and culture incubations for P_{H2O2}

Incubations were conducted in syringes to allow for easy sample withdrawal without introducing incubation solutions to room air. 18.0 mL of unfiltered or filtered (Pall Corp. 0.2 µm Acropak) freshwater or *C. reinhardtii* culture were placed into a sterile plastic 60 mL syringe (Fischer Scientific) with a plastic plunger and luer lock. A plastic stopcock was screwed into the luer lock with a syringe filter (Millipore 0.22 µm PES) placed on the end. To prevent background H_2O_2 signals from the syringe filter, it was cleaned before use by running 3 mL of 0.01 M HCl followed by 5 mL of nanopure water through the filter.

After the solutions were placed into the syringes, 6.75 mL of 194 µM AR stock was added (50 µM AR final) followed by 250 µL of 100 kilounit L^{-1} (kU L^{-1}) HRP (1 kU L^{-1} final). A stir bar was added to each syringe, which was then placed in the dark at room temperature on a stir plate (lowest setting) to ensure a well-mixed solution. Aliquots of the incubation solutions were then withdrawn through the filter periodically for spectrophotometric analysis (see section 3.3.6). The solutions were allowed to incubate for 10 minutes before the first measurement on the spectrometer.

3.3.6 Hydrogen peroxide analysis

The accumulation of resorufin versus time in the incubation solutions is a direct measurement of gross P_{H2O2} in the incubation samples, because any H_2O_2 produced in the incubation immediately reacts with excess AR/HRP rather than decaying away by reaction with other solution constituents (e.g. metals and anti-oxidant enzymes such as catalase). Solution absorbance was measured at 570 nm every hour up to 4 hours, and then background corrected with the subtraction of absorbance at 700 nm. To sample the incubation solution, approximately 0.5-1.0 mL of the incubation solution was withdrawn through the syringe, stopcock, and syringe

filter and discarded, and then approximately 1.5 mL was dispensed into a plastic beaker. Exactly 1.00 mL of the filtered solution was then pipetted into a small volume 1 cm path length cuvette and measured with a UV-visible spectrophotometer (Hewlett Packard 8453 with Chemstation Software).

3.3.6.1 Standard additions

After the first absorbance measurement described above, standard additions were conducted in the same cuvette, with an apparent molar absorptivity ε_{app} (absorbance per cm per M of H_2O_2 added) determined at each time point for each sample analyzed. The sample cuvette was spiked with 44 µL of 5.1 µM H_2O_2 stock solution for an initial spike of 200 nM H_2O_2, mixed with the pipet tip, and then measured on the spectrophotometer. A second spike of 44 µL 5.1 µM H_2O_2 stock was then added to the cuvette for a total spike of 400 nM H_2O_2, mixed, and then measured. ε_{app} was then determined from these standard additions after dilution correction. The relative percent accuracy of the 200 and 400 nM H_2O_2 spikes are -0.2 ± 26% and -5.4% ± 20% (N = 28), respectively, determined by standard additions in 50 mM pH 7 phosphate buffer.

Standard additions were also conducted in catalase amended natural water to determine the limit of detection (LOD) for H_2O_2 concentration. Catalase should eliminate background H_2O_2 and added H_2O_2 to yield negligible absorbance signals. The standard deviation of those absorbances (0.001 absorbance units, N = 24) was used to calculate the LOD of 57 nM. $\varepsilon_{resorufin}$ at pH 7 (5.4×10^{-5} nM^{-1} cm^{-1}) was applied as the representative sensitivity. Because catalase amended samples cannot yield a production rate, the LOD of P_{H2O2} (37 nM h^{-1}) was determined using measured P_{H2O2} values in 50 mM pH 7 phoshphate buffer controls (N = 8). See section 3.3.6.2 for the calculation of production rates.

3.3.6.2 Calculation of production rates (P_{H2O2})

Using the Beer-Lambert law, ($A = \varepsilon_{app}bc$, where A = absorbance, b = 1 cm pathlength, and c is concentration in nmol L^{-1}) H_2O_2 production rates were obtained. The change in absorbance (ΔA) of resorufin accumulation is measured over time (Δt) in the incubation where the slope of ΔA/Δt is determined by linear regression. ΔA/Δt isthen divided by ε_{app}, determined from H_2O_2 standard additions, to get P_{H2O2} in nanomolar per hour (nM h^{-1}) as shown in equation 3.1:

$$\frac{\Delta A/\Delta t}{\varepsilon_{app} b} = \frac{\Delta A}{\varepsilon_{app} b \Delta t} = \frac{\Delta c}{\Delta t} = P_{H2O2} \qquad \text{(Equation 3.1)}$$

The ε_{app} used in equation (3.1) is an average of four or more ε_{app} values measured by standard additions at four or more time points throughout the incubation. In AR experiments without HRP added, standard additions could not be done and therefore ε_{app} could not be measured. In this case, P_{H2O2} equivalents were calculated by dividing the slope of ΔA/Δtby the known molar absorptivity of resorufin at pH 7.0 ($\varepsilon_{resorufin}$), 5.4×10^{-5} nM^{-1} cm^{-1}.

The error reported for each P_{H2O2} value comes from the standard deviation of the regression slope of resorufin accumulation over time or ΔA/Δt, calculated using the LINEST function in Microsoft Excel. To test P_{H2O2} values for statistical significance the standard deviation of the linear regression was used, also calculated using the LINEST function. The error reported for any molar absorptivity (ε_{app}) value is a 95% confidence interval (see Figures 3.4 and 3.5 for N values).

3.3.7 Laboratory experiments and controls

Laboratory experiments were conducted in conjunction with measuring dark P_{H2O2} in freshwater, algal cultures, and fulvic acid isolate solutions. These included measuring the

stability of Amplex red and resorufin (the reaction production) in phosphate buffer containing freshwater constituents such as metals and fulvic acid.

3.3.7.1 Resorufin stability

Resorufin was added to 50 mM phosphate buffer at pH 6.0, 7.0, and 8.4 for final resorufin concentrations of 0, 10, and 40 µM in 50 mL Teflon bottles. Its absorbance signal at 570 nm was considered stable if it did not change more than ±10% for 3-7 hours (beyond the time needed for an incubation experiment). Resorufin stability was also determined in the presence of freshwater constituents (see section 3.4.1). Resorufin sodium salt was also used as a control in the freshwater incubation experiments. In this case, a 200 nM final concentration of the sodium salt was added to filtered fresh water or 50 mM pH 7 phosphate buffer, prepared, and analyzed as a sample as described in section 3.3.4.

3.3.7.2 Tests for positive interference

The same freshwater constituents were examined for their ability to give a false positive P_{H2O2}, or in other words, to cause AR oxidation without HRP and H_2O_2 present. 50 µM AR was added to 50 mM pH 7 phosphate buffer, and prepared the same way as that of the resorufin stability experiments including the same added amounts of freshwater constituents (section 3.3.7). The exception is that metal oxide concentrations (MnO_2 and ferrihydrite) were varied at 0.4, 1.0, and 10 µM once AR oxidation was observed with MnO_2. False positive P_{H2O2} was calculated using the Beer-Lambert law by dividing absorbance, over time at 570 nm, by $\varepsilon_{resorufin}$ instead of ε_{app} (see section 3.3.6.2 and equation 3.1). AR was considered stable when negligible signal at 570 nm was observed over time (i.e. no oxidation to resorufin was observed). 50 µM AR in 50 mM pH 7 phosphate buffer was also used alongside freshwater incubations as a blank

control for background P_{H2O2}, but in this case it was prepared and analyzed the same as a natural water sample as described in section 3.3.4.

3.3.7.3 Catalase and HRP controls

To determine if AR is oxidized to resorufin by something other than H_2O_2 in natural water samples, freshwater incubation experiments had unfiltered or filtered controls with added catalase (Sigma Aldrich) while others purposely did not have HRP added to the incubation, and were otherwise treated the same as the unamended samples. Catalase (150 kU L^{-1} final) was added to control incubation syringes immediately before AR and HRP were added to scavenge any H_2O_2 that was produced in the unfiltered or filtered freshwater.

3.3.7.4 P_{H2O2} by SRFA

P_{H2O2} was measured by 0, 10, 25, and 50 mg L^{-1} SRFA using 25 and 50 µM AR in 50 mM pH 7 phoshphate buffer, and 50 µM AR in 50 mM pH 9.5 carbonate buffer. Incubations of SRFA solutions were prepared and analyzed in the same manner as freshwater and culture samples (section 3.3.4).

3.3.7.5 ε_{app} and $\varepsilon_{resorufin}$ dependence on pH and SRFA

ε_{app} and $\varepsilon_{resorufin}$ dependence on pH and SRFA was also investigated. 50 mM phosphate and carbonate buffer solution pH was adjusted from 6.0 up to 9.5 followed by the addition of 50 µM AR and 1 kU L^{-1} HRP. ε_{app}, determined from H_2O_2 standard additions (section 3.3.6.1), and $\varepsilon_{resorufin}$, determined by1 µM resorufin sodium salt absorbance at 570 nm, were measured at 0.5 pH intervals. ε_{app} and $\varepsilon_{resorufin}$ were also determined with varied SRFA concentration (0 to 50 mg L^{-1}) in 50 mM pH 7 phosphate buffer with added 25 and 50 µM AR and 1 kU L^{-1} HRP L^{-1}. Half the normal AR concentration (25 µM) was used to determine if SRFA oxidation outcompeted AR oxidation by HRP, which would result in a lower ε_{app}.

3.4 Results and Discussion

This section shows the results of true dark P_{H2O2} measured in freshwater, algal cultures, and fulvic acid isolate solutions. Additionally, it describes potential positive interferences and the effect on the apparent molar absorptivity of the Amplex red reaction by pH, fulvic acid, and unknown freshwater constituents.

3.4.1 Resorufin stability

The absorbance signal of 1 µM resorufin sodium salt was stable for 3-7 hours at pH 6.0-8.4 (Figure B.2.1a., B.2.2a, and B2.3a in Appendix B). Both the absorbance signals of 10 and 40 µM resorufin signals were stable up to 6 hours at pH 8.4 (Figure B.2.3a), but both signals rapidly decayed at pH 6.0 (Figure B.2.1a.). Decay of the absorbance signal may be caused by the oxidation of resorufin to resazurin or from de-acetylation and polymerization of resorufin [23]. The limited stability of resorufin could clearly be an issue in some natural water incubations, depending on the pH of the water and the amount of resorufin accumulated. However, in our freshwater and *C. reinhardtii* samples, the pH was always above 7.0 and resorufin did not accumulate to above 1.2 µM (typically reached 1 µM or below) in 3-4 hours, suggesting stable conditions.

The absorbance signal of 1 µM resorufin also remained stable for 7 hours at pH 6.0-8.4 in the presence of typical freshwater constituents such as dissolved and particulate metals (see Figures B.2.1b-c, B.2.2a-b, and B.2.3b-c). Furthermore, 1 µM resorufin absorbance signal was also stable in solutions with added 10, 25, and 50 mg L^{-1} SRFA (Figure B.2.2c), up to 2-5 times higher than DOM concentrations observed at the field sites. These results suggest resorufin is not consumed or oxidized in waters with metals concentrations up to 1 µM, and fulvic acid concentrations up to 50 mg L^{-1}.

3.4.2 Laboratory experiments to test for positive interferences in measurement of P_{H2O2}

False positive P_{H2O2}, or AR oxidation in the absence of H_2O_2, was minimal in the presence of added dissolved metals, SRFA, and varied amounts of ferrihydrite particles (Figure 3.1). Therefore, dissolved constituents and ferrihydrite are most likely minor contributors to false positive P_{H2O2} in natural samples. However, added particulate manganese dioxide (δ-MnO_2) produced a substantial false positive P_{H2O2} (Figure 3.1). For example, the oxidation of AR by 10 µM MnO_2 resulted in a false positive P_{H2O2} equivalent to 251 ± 35 nM h^{-1}.

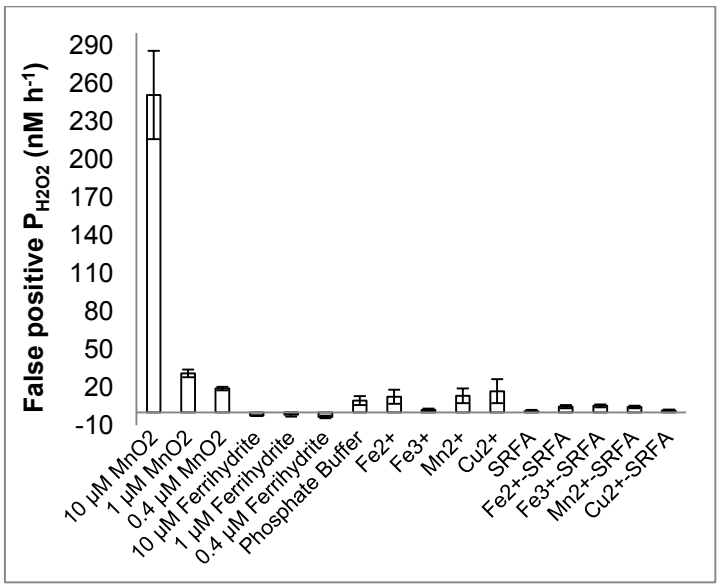

Fig. 3.1 False positive P_{H2O2} by MnO_2. In 50 mM pH 7 phosphate buffer, MnO_2 directly oxidizes AR to resorufin (without added HRP or H_2O_2) while ferrihydrite and dissolved constituents contribute minor to non-existent false positive P_{H2O2} (calculated with $\varepsilon_{resorufin}$).

Although SRFA did not cause a false positive P_{H2O2} (in the absence of HRP), a substantial true P_{H2O2} was measured in the presence of SRFA when HRP was added to phosphate and carbonate buffered solutions (Figure 3.2). The mechanism of H_2O_2 formation by SRFA is likely to be from oxidation of reduced moieties in the SRFA by oxygen. Studies have previously observed formation of hydroxyl radical by the rapid (time scale of hours) re-oxidation of

electrochemically reduced humic substances, and posited H_2O_2 as an intermediate in this process (Page et al. 2012, Page et al. 2013). In our experiments, SRFA stock solutions were made from the freeze-dried material and stored under air, so the continued presence of reducing moieties is somewhat surprising. One possibility is that oxidation is slow in the mildly acidic pH of the stock solutions and faster in the buffer solutions in which these experiments were conducted.

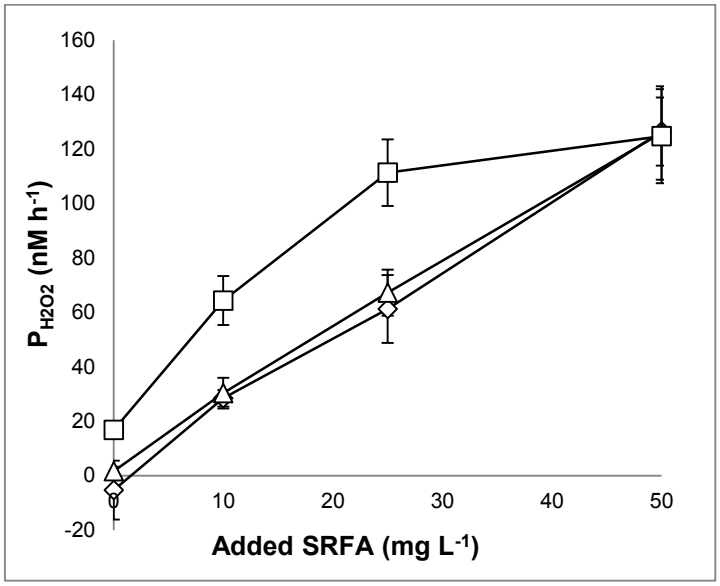

Fig. 3.2 True P_{H2O2} by SRFA. SRFA contributes to true P_{H2O2} in the presence of HRP with 50 µM AR (◇) and 25 µM AR (△) in 50 mM pH 7 phosphate buffer, and 50 µM AR in pH 9.5 50 mM carbonate buffer (□). SRFA appears to be a source of non-biological dark P_{H2O2}

3.4.3 Testing for positive interferences in natural water samples

Because catalase can catalytically destroy H_2O_2 in our incubations before it has a chance to oxidize AR, catalase controls can be used to test natural water samples for false positive P_{H2O2}, as shown by previous applications of the AR method in biological samples (Mohanty et al. 1997). At ML-BEM (7/10/13), P_{H2O2} of the unfiltered incubation amended with catalase was significantly ($p < 0.001$) lower (11 ± 6 nM h^{-1}) than P_{H2O2} of both the unamended unfiltered replicates at 105 ± 1 and 76 ± 4, nM h^{-1}, respectively (see Figure 3.3). Similar results were

obtained with CHL incubations from 7/19/13 (Figure 3.3) where P_{H2O2} (-8 ± 3 nM h^{-1}) of the unfiltered catalase control was significantly ($p < 0.001$) lower than the unamended unfiltered replicates (P_{H2O2} = 38 ± 8 and 37 ± 3 nM h^{-1}). The catalase controls demonstrate that the HRP-catalyzed oxidation of AR by H_2O_2 is responsible for forming resorufin in these samples.

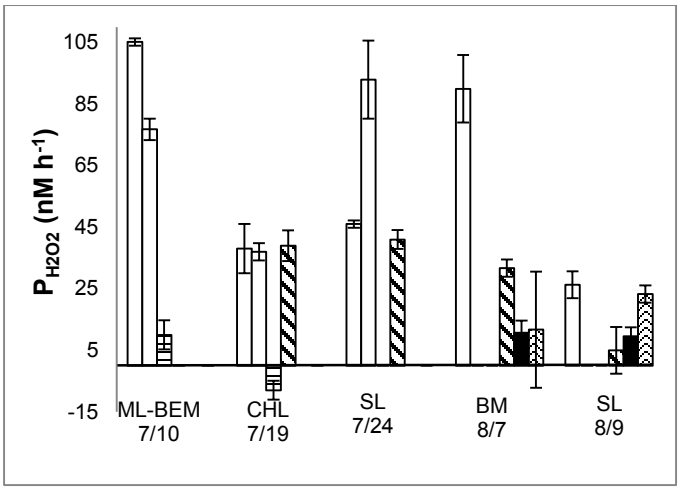

Fig. 3.3 Catalase and HRP P_{H2O2} controls in freshwater. Unfiltered (☐) and filtered(■) replicates of P_{H2O2} from freshwater incubations with amended controls: i. unfiltered samples with added catalase (▤), ii. unfiltered samples without HRP added (▨), and iii. filtered samples without HRP added (▨)

We also used unfiltered freshwater controls incubated *without* added HRP for determining false positive P_{H2O2}, but this strategy was partially ineffective. For example, P_{H2O2} (39 ± 5 nM h^{-1}) of the control *without* HRP from CHL (7/19/13) was not statistically ($p > 0.05$) different from the unfiltered incubation replicates *with* added HRP (P_{H2O2} = 38 ± 1 and 37 ± 1 nM h^{-1}, see Figure 3.3). However, all three measurements from CHL (7/19/13) are close to the LOD and may explain some of the statistical insignificance. At SL (7/24/13), only one replicate with HRP (P_{H2O2} = 94 ± 13 nM h^{-1}) was statistically significant ($p < 0.05$) from the sample without HRP (41 ± 3 nM h^{-1}) while the other replicate's P_{H2O2} (46 ± 1 nM h^{-1}) was not ($p > 0.05$).

At BM (8/7/13), P_{H2O2} of the unfiltered sample with HRP (90 ± 11 nM h^{-1}) was statistically significant ($p < 0.01$) from P_{H2O2} of the sample without HRP (26 ± 3 nM h^{-1}). However, there was measureable P_{H2O2} of all samples without HRP and may indicate either i. AR is oxidized by something other than H_2O_2 (e.g. MnO_2), but this was ruled out for CHL (7/19/13) by the catalase control (Figure 3.3), and/or ii. naturally existing peroxidases capable of catalyzing the reaction are present in these water samples. It is known that peroxidases other than HRP are capable of catalyzing the AR/H_2O_2 reaction (Serrano et al. 2009).

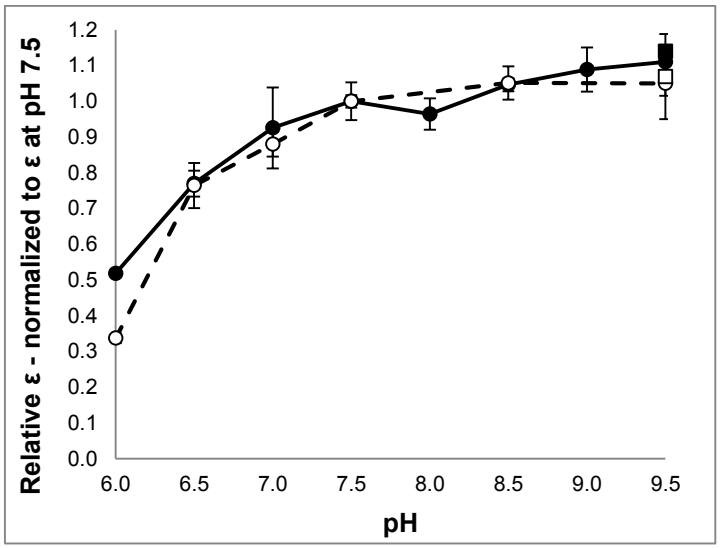

Fig. 3.4 Molar absorptivity dependence on pH. pH dependence of ε_{app} (50 mM phosphate buffer ○ and 50 mM carbonate buffer □) normalized to ε_{app} at pH 7.5, and $\varepsilon_{resorufin}$ in 50 mM phosphate buffer (●) and carbonate buffer (■) normalized to $\varepsilon_{resorufin}$ at pH 7.5. Error bars are 95% confidence intervals where N = 3 for $\varepsilon_{resorufin}$ at all pH values except pH 8.0 and 9.0 where N =2, and N = 4 for ε_{app} at all pH values except pH 6 and 7 where N = 3 and 26, respectively.

3.4.3 Apparent molar absorptivity, ε_{app}, dependence on pH and fulvic acid

It is known that leuco dyes including pink resorufin can become colorless under certain conditions such as an acidic pH, and may result in false absorbance and P_{H2O2} values. To our knowledge, resorufin's (i.e. the sodium salt) molar absorptivity ($\varepsilon_{resorufin}$) and the apparent molar absorptivity (ε_{app}) of resorufin, from AR's reaction with HRP/H_2O_2, have never been measured

systematically over the circumneutral pH range found in natural waters. AR/HRP solutions are commonly buffered to pH 7.4 with an $\varepsilon_{resorufin}$ around 54,000 M^{-1} cm^{-1} (Burns et al. 2012), but because ε_{app} is used to calculate P_{H2O2} (section 3.3.6.2) it is desirable to know the behavior of ε_{app} in the pH range of 6-9.5, or the range commonly found in natural water systems.

ε_{app}, determined via H_2O_2 standard additions, and $\varepsilon_{resorufin}$, determined via resorufin sodium salt additions in buffer, are marginally dependent upon pH above pH 7.5 (○ and ● in Figure 3.4, respectively). It is known that resorufin is colorless below pH 6.0, confirmed with a negligible ε_{app} measurement (via H_2O_2 standard additions) at pH 5.5 (not shown). However, measurable ε_{app} values are most dependent upon pH from 6.0 to 7.0 where its value ranged from 30% to 88% of ε_{app} at pH 7.5 (Figure 3.4). The lower ε_{app} values we observed in the pH range of 6.0-7.0 will ultimately result in a higher calculated P_{H2O2} when applied to natural waters. Similarly, $\varepsilon_{resorufin}$ values at pH 6.0-7.0 ranged from 50% to 90% of $\varepsilon_{resorufin}$ at pH 7.5. The fact that there is a similar pH dependence for $\varepsilon_{resorufin}$ as there is for ε_{app}, in the same range of pH 6.0-7.0, suggests it is in fact resorufin (the product) influenced by pH and not some process affecting the reaction between AR/HRP and H_2O_2.

Measuring true dark P_{H2O2} by SRFA (see section 3.4.2) revealed that SRFA influenced ε_{app} values, and again, affected the P_{H2O2} calculations. It is known that DOM, possibly containing SRFA-like compounds, can form complexes with extracellular enzymes resulting in decreased enzymatic activity in freshwater (Pflug 1980, Wetzel 1992), and may decrease product (i.e. resorufin) formation in peroxidase-catalyzed reactions (Zepp et al. 1988). Therefore, we tested the SRFA concentration dependence of both ε_{app} and $\varepsilon_{resorufin}$ to determine if SRFA had an influence on the HRP enzyme catalyst of the AR/ H_2O_2 reaction. ε_{app} has an appreciable

dependence on SRFA concentration (see Figure 3.5 for solutions containing 50 µM AR ◇ and 25 µM AR △ in 50 mM pH 7 phosphate buffer and 50 µM AR in 50 mM pH 9.5 carbonate buffer □). For example, the value of ε_{app} decreased 30-40% when SRFA concentration was increased from 0 to 10 mg L^{-1} (Figure 3.5). Likewise, solutions with the highest SRFA concentration (50 mg L^{-1}) had the lowest ε_{app} values (e.g 2.28 ± 0.05 x10^{-5} absorbance cm^{-1} nM^{-1} H_2O_2 added at pH 7 with 50 µM AR). SRFA had no observable influence on $\varepsilon_{resorufin}$ (●, Figure 3.5). Therefore, we believe that SRFA prevents AR oxidation, and lacks influence on the product, resorufin, after it forms, and may explain why SRFA concentration does not have the same effect on $\varepsilon_{resorufin}$ as it does on ε_{app} (Figure 3.5).

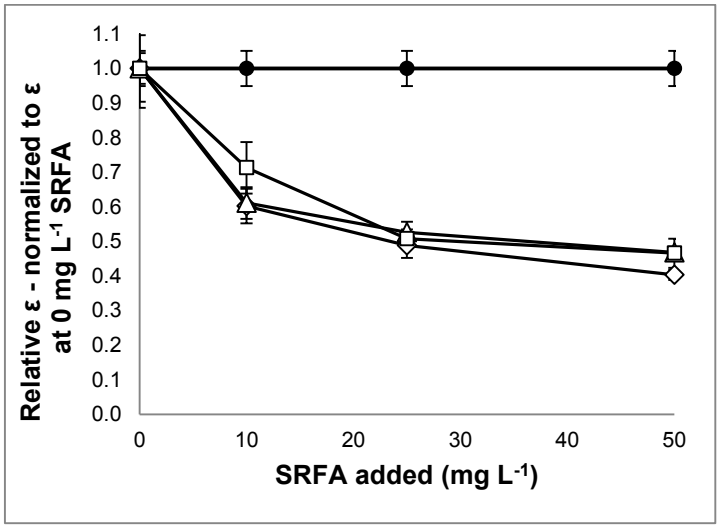

Fig. 3.5 Molar absorptivity dependence on SRFA. ε_{app} dependence on SRFA with 50 µM AR (◇) and 25 µM AR (△) in 50 mM pH 7 phosphate buffer SRFA, and 50 µM AR in pH 9.5 50 mM carbonate buffer (□) is normalized ε_{app} at 0 mg L^{-1}. There is no dependence of $\varepsilon_{resorufin}$, on SRFA (●). Error bars are 95% confidence intervals where N = 3 for $\varepsilon_{resorufin}$ and N = 4 for ε_{app} at all SRFA concentrations.

Quinone-like moieties present in SRFA, similar to QH_2, may be consuming H_2O_2 (Reszka et al. 2005) added in standard additions which would result in the loss of resorufin

formation and lower ε_{app}. However, if this were the case, SRFA should have a greater effect on ε_{app} in solutions with half the amount of AR (25 µM, Δ in Figure 3.5) since SRFA should outcompete AR for oxidation by H_2O_2, but this was not observed. However, the reactive intermediates produced by the HRP catalytic cycle may make a kinetic competition between AR and SRFA more complicated to elucidate. Alternatively, reduced organic compounds (e.g. ascorbate) (Rodrigues & Gomes 2010), and possibly reduced DOM, may scavenge AR radical intermediates also resulting in the loss of resorufin formation and lower ε_{app} (Gorris & Walt 2009). For example, Reszka et al. (2005) observed a similar result where ε_{app} was lowered to $2.4x10^{-5}$ cm^{-1} M^{-1} in ascorbate amended solutions containing cells.

3.4.4 Apparent molar absorptivity (ε_{app}) variation in freshwater and *C. reinhardtii* cultures

ε_{app} varied widely in unfiltered and filtered freshwater samples with mean values (◆, Figure 3.6) well above $\varepsilon_{resorufin}$ ($5.4x10^{-5}$ cm^{-1} nM^{-1} at pH 7.4, dashed line in Figure 3.6) at 6.94±0.4 and 7.43±0.4 $x10^{-5}$ absorbance cm^{-1} nM^{-1} H_2O_2 added, respectively. The largest ε_{app} values measured in this study were from unfiltered and filtered freshwater from SL on 8/30/13 at 15-18 $x10^{-5}$ and 8.6-13$x10^{-5}$ absorbance cm^{-1} nM^{-1} H_2O_2 added, respectively. They were subsequently removed as an outlier in Figure 3.6 (see Appendix B for all raw ε_{app} values). However, the majority of ε_{app} values measured in natural freshwater samples are considerably higher than $\varepsilon_{resorufin}$ even when taking into account minor variations of ε_{app} at higher pH (see section 3.4.3 and Figure 3.4). In fact, 76% and 79% of all unfiltered (N = 98) and filtered (N = 96) ε_{app} values, respectively, were above $5.6x10^{-5}$ absorbance cm^{-1} nM^{-1} H_2O_2 added, as shown in Figure 3.6. This upper threshold was determined from ε_{app} of 50 mM pH 7 phosphate buffer controls and laboratory samples that have a mean value of 5.4±0.2 $x10^{-5}$absorbance cm^{-1} nM^{-1}

H_2O_2 added (N = 26), and because of its relatively low variability when compared to natural water samples (Figure 3.6). Additionally, ε_{app} measured in *C. reinhardtii* cultures also did not vary as widely as natural water samples, but 75% of the measurements (N = 40) were above the upper threshold of 5.6 x10^{-5}absorbance cm^{-1} nM^{-1} H_2O_2 added. However, ε_{app} of *C. reinhardtii* cultures are more tightly clustered around a mean value of 5.7±0.2 x10^{-5}absorbance cm^{-1} nM^{-1} H_2O_2 added (Figure 3.6).

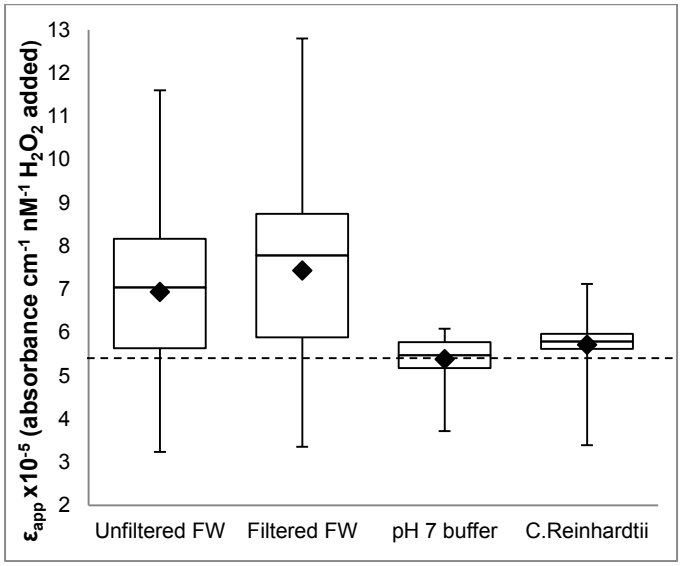

Fig. 3.6 Apparent molar absorptivity variability in freshwater. ε_{app} varies widely around $\varepsilon_{resorufin}$ (~5.4x10^{-5} cm^{-1} nM^{-1} at pH 7.4, dashed line) in natural unfiltered (N = 98) and filtered (N = 96) freshwater (FW) samples when compared to ε_{app} measured in 50 mM pH 7 phosphate buffer (N = 26) and cultures of *C. Reinhardtii* (N = 40). This suggests that natural water components influence the AR/HRP/H_2O_2 reaction and ε_{app}. Mean and median ε_{app} values are represented by ◆ and horitzontal lines within the boxes, respectively. The upper and lower range of ε_{app} values are represented by the "whiskers" of the box-whisker plot

The greater variability and higher mean ε_{app} values in the natural water samples, when compared to ε_{app} of the buffer controls and *C. reinhardtii* cultures, suggests that natural freshwater components affect the AR/HRP reaction when H_2O_2 is added for standard additions. The mechanism of peroxidase-catalyzed reactions for H_2O_2 assays produces two dye radicals

(i.e. AR radicals) per one H_2O_2 molecule added, and a 1:1 stoichiometry results when the two AR radicals disproportionate, yielding resorufin and AR (Gorris & Walt 2009). Therefore, ε_{app} values up to twice the expected value could potentially be observed if an oxidant present in natural fresh water oxidizes both AR radicals to resorufin after the reaction is initiated. There is potential for future studies to elucidate this mechanism further.

Conversely, 67% of all filtered (N = 15) and 71% of all unfiltered (N = 17) ε_{app} values measured below the lower threshold of $5.2x10^{-5}$ absorbance cm^{-1} nM^{-1} H_2O_2 added were from BM alone, with the remaining values spread among the 3 other field sites. BM is a shallow (<0.5 meter in depth) wetland that is covered in duckweed in the summer and thick vegetation year-round resulting in lower DO levels (2-4 mg L^{-1}). DOM at BM may contain more reduced moieties and could be responsible for more ε_{app} values falling below the 5.2 threshold. This is similar to ε_{app}'s dependence on SRFA in laboratory experiments (see section 3.4.3 and Figure 3.5) where ε_{app} was below $4x10^{-5}$ absorbance cm^{-1} nM^{-1} H_2O_2 added for all SRFA concentrations added. In fact, 100% of the ε_{app} values from BM were below $4x10^{-5}$ absorbance cm^{-1} nM^{-1} H_2O_2 added. The reduced moieties in this case may reduce more of the AR radicals back to AR resulting in less resorufin formation per H_2O_2 molecule added.

3.4.5 Dark P_{H2O2} from freshwater field sites and possible non-biological sources

The variability and magnitude of gross dark P_{H2O2} measured in unfiltered freshwater incubations from this study (Figure 3.7) is on the same order of magnitude (10's to 100's nM h^{-1}) as previous methods (Vermilyea et al. 2010a, Dixon et al. 2013, Marsico et al. 2015). For example, dark P_{H2O2} measured at Mirror Lake during a two week period in a July 2012 study

ranged from 56-212 nM h^{-1} while in this study (2013) dark P_{H2O2} measured at Mirror Lake during a one week period in July ranged from 76 – 234 nM h^{-1} (Marsico et al. 2015).

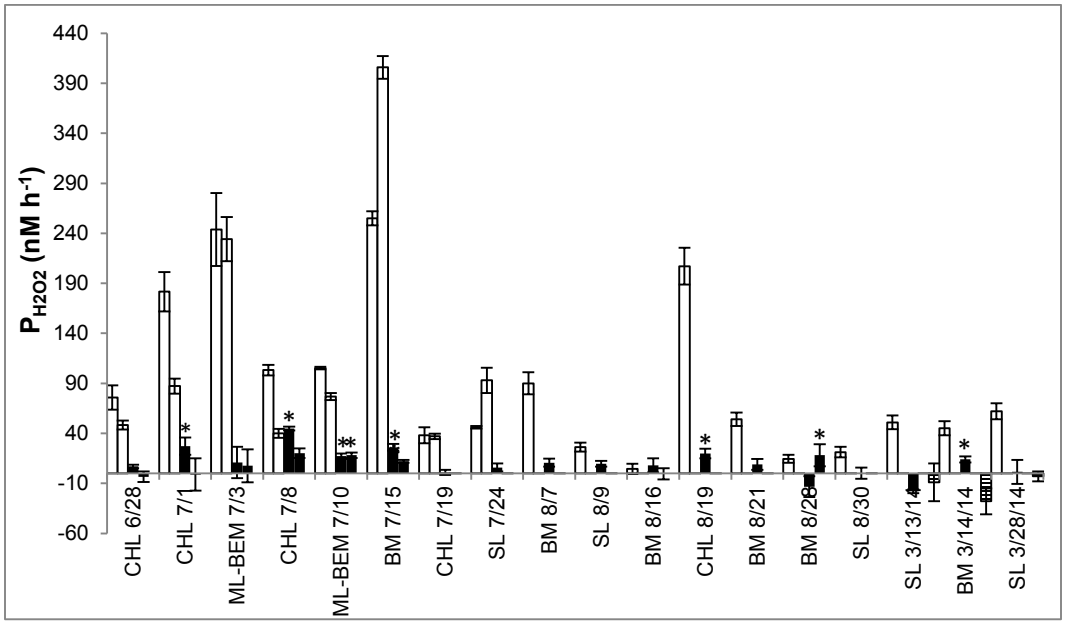

Fig. 3.7 Gross dark P_{H2O2} in freshwater. Unfiltered (□), filtered replicates (■), and 50 mM pH 7 phoshate buffer controls (▤). Asterisks indicate filtered P_{H2O2} values significantly different from zero

Unfortunately, lack of resources prevented an intercomparison study, but also consistent with previous studies (Marsico et al. 2015) is that filtering largely removed dark P_{H2O2} (black bars, Figure 3.7) when compared to the unfiltered samples (white bars, Figure 3.7). This implies that the majority of unfiltered P_{H2O2} comes from particle-associated (>0.2 µm) processes, most likely microorganisms. Additionally, several filtered incubations had dark P_{H2O2} significantly greater than zero: $p < 0.1$ for CHL 6/28, 7/1, 7/8,8/19/13 and SL 8/9/13; $p < 0.05$ for ML 7/10/13 and BM 7/15/13 and 3/14/14). Though, only one filtered sample (replicate 1 from CHL 7/8/13 at 45 ± 2 nM h^{-1}, $p < 0.01$) exceeded the limit of detection of 37 nM hr^{-1}. Dark P_{H2O2} may come from the dissolved portion of natural waters including moieties of DOM that can reduce DO to

superoxide eventually forming H_2O_2 (Page et al. 2012), as discussed in section 3.4.2. Direct oxidation of AR (i.e. not by H_2O_2) cannot be ruled out in all cases since a catalase control was not done for each experiment.

3.4.6 P_{H2O2} in *C. reinhardtii* cultures

Overall, dark P_{H2O2} values increased as the number of *C. reinhardtii* cells were increased per unit volume (open symbols in Figure 3.8). For example, the most diluted ($1/40^{th}$ dilution) cell culture had the lowest dark P_{H2O2} measurements at 138 ± 10 nM h^{-1} while the least diluted culture ($1/5^{th}$) had dark P_{H2O2} = 484 ± 17 nM h^{-1} (see Figure 3.8). When P_{H2O2} was normalized to cell density (Mcells mL^{-1}) dark P_{H2O2} decreased as cell density increased (black symbols, Figure 3.8). In other words, less H_2O_2 is produced per cell as cell density increases, but the overall production increases.

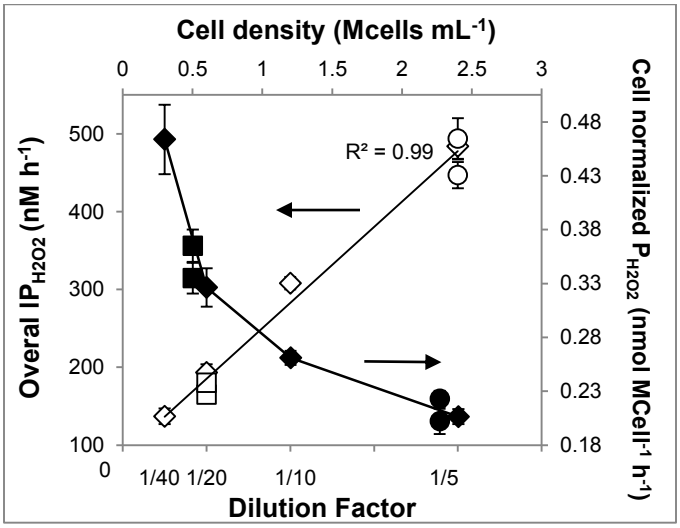

Fig. 3.8 Dark P_{H2O2} of *C. reinhardtii*. Dark P_{H2O2} (nM h^{-1}) increases when dilution with TAP media is decreased in *C.reinhardtii* cultures: from March 26^{th} (◇), April 2^{nd} (□) and April 9^{th} (○). However, when normalized with cell density (Mcells mL^{-1}), dark P_{H2O2} (nmol $Mcell^{-1}$ h^{-1}) decreases with increasing *C.reinhardtii* cell density: from March 26^{th} (◆), April 2^{nd} (■), and April 9^{th} (●) indicating less H_2O_2 is made per cell as cell density increases

3.5 Conclusion

In this study, we show that the AR method is capable of determining gross dark production rates of H_2O_2 in freshwater incubations and *C. reinhardtii* cultures using visible spectroscopy. Because we have shown the stability of 1 μM (but not 10-40 μM) resorufin at pH 6-8.4 we recommend keeping accumulated resorufin concentrations to 1 μM or lower (after AR/HRP has reacted with H_2O_2), and, if possible, keeping solutions above pH 7 to prevent resorufin signal decay (a 3-4 hour incubation should achieve this for a typical freshwater system). We also show that it is important to perform controls on resorufin stability under conditions identical to AR incubations to ensure that biological degradation of resorufin does not occur. Perhaps most importantly, we recommend to users of the AR method in freshwater to consistently utilize catalase controls to rule out false positive P_{H2O2}. Additionally, our study shows the variability of ε_{app} in natural freshwater, and therefore, it is critical to calibrate each sample with H_2O_2 standard additions to obtain ε_{app} for accurate P_{H2O2} calculations.

3.6 Acknowledgements

The authors would like to thank Paul Flanagan and the residents of Big Elk Meadows for allowing sampling at their private lake, and the Posewitz group at CSM for their help on culturing *C.reinhardtii*. This work was funded by the National Science Foundation Grant 1025077 (Geobiology and Low-Temperature Geochemistry program).

CHAPTER 4
DARK SUPEROXIDE OXIDATION AND REDUCTION OF MERCURY IN VINEYARD SOUND SEAWATER

Ryan M. Marsico[1*], Bettina M. Voelker[2*], Gretchen J. Swarr[3†],
Colleen M. Hansel[4†], Carl H. Lamborg[5^]

[1] Graduate student, primary researcher and author
[2] Professor, Principal Investigator, and corresponding author
[3] Laboratory technician, technical contributor
[4] Associate Scientist, co-Principal Investigator, and corresponding author
[5] Assistant Professor, co-Principal Investigator, and corresponding author
*Colorado School of Mines, Department of Chemistry & Geochemistry, 1500 Illinois St., Golden, CO 80401
†Woods Hole Oceanographic Institution, Marine Chemistry & Geochemistry, 266 Woods Hole Rd. MS# 52, Woods Hole, MA 02543-1050
^University of California Santa Cruz, Ocean Sciences Department, 1156 High St., Santa Cruz, CA 95064

4.1 Abstract

Superoxide (O_2^-) produced in the ocean is known to be an oxidant and reductant of redox active metals (e.g. Mn and Cu), and may also play a role in the dark biogeochemical cycling of inorganic mercury (Hg). In this study, filtered Vineyard Sound seawater (VSSW) samples were spiked with $^{202}Hg(II)$ or $^{202}Hg^0$ and an abiotic source of O_2^- (xanthine/xanthine oxidase or potassium superoxide) to determine if Hg is oxidized and/or reduced in the dark by O_2^-. The samples were sparged and trapped with gold-coated silica traps twice, thermally desorbed, and analyzed for Hg by inductively coupled plasma mass spectrometry (ICPMS). The first sparge step captured Hg^0 while the second sparge step captured Hg(II) after artificial reduction using bromine monochloride (BrCl) and stannous chloride ($SnCl_2$). A $^{202}Hg^0$ stock was created by sparge/trapping an artificially reduced $^{202}Hg(II)$ spike in MilliQ (MQ) water followed by thermal desorption into a Tedlar bag containing MQ water and argon gas. $^{202}Hg^0$ spikes were successfully recovered in VSSW. $^{202}Hg(II)$ spikes were successfully recovered in MQ water, but recoveries were more variable in VSSW, possibly due to increased organic complexation of

Hg(II). There was a statistical difference in oxidation of $^{202}Hg^0$ in samples with and without O_2^- added, but superoxide dismutase (SOD) controls for the oxidation experiments were similar to those with only O_2^- added, suggesting the oxidation of Hg^0 observed in the presence of O_2^- was an indirect process. $^{202}Hg(II)$ reduction by O_2^- was statistically different from one SOD control, and a second order rate constant ($k_{Hg(II)}$) was calculated to be 6.9 (3.1) x10^2 M^{-1} s^{-1}, possibly enough to achieve the dark, microbially induced Hg(II) reduction rate of ~1% day^{-1} that was observed in previous studies. Several secondary dark reactions of O_2^- were also investigated to determine if they oxidize or reduce Hg. For example, Mn(III/IV) and Cu(I), formed from O_2^- reactions with Mn(II) and Cu(II), may oxidize Hg^0 or reduce Hg(II), respectively. There was no evidence of Mn(II) and Cu(II) assisting O_2^- in Hg oxidation or reduction. Catalase added in Mn(II) supplemented experiments, to prevent H_2O_2 reduction of Mn(III/IV), oxidized ~70% of the $^{202}Hg^0$ spike. The coenzyme nicotinamide adenine dinucleotide (NADH), which could stimulate biological reduction of Hg(II), did not reduce significant $^{202}Hg(II)$ in filtered VSSW Ultimately, the direct Hg(II) reduction and indirect Hg^0 oxidation by O_2^- suggests that O_2^- could be an important factor in the dark biogeochemical cycle of Hg in the ocean.

4.2 Introduction

Recent marine studies report that dark particle-associated production of superoxide occurs in the ocean, and microorganisms are most likely a major source (Rose et al. 2008, Hansard et al. 2010). For example, dark superoxide production has been measured by many marine microorganisms including bacteria, diatoms, and algae (Kustka et al. 2005, Marshall et al. 2005, Learman et al. 2011, Rose 2012, Diaz et al. 2013). The reasons why marine microorganisms produce O_2^- still remains unclear, but some studies suggest ROS are produced for cell signaling and for manipulating metal bioavailability (Aguirre et al. 2005, Silar 2005,

Rose 2012). After O_2^- is produced, O_2^- can oxidize or reduce metals in seawater including Fe (Bielski et al. 1985, Kustka et al. 2005, Waite et al. 2006, Garg et al. 2007b, c, Fujii et al. 2008, Waite et al. 2009), Mn (Hansard et al. 2011, Learman et al. 2011, Learman et al. 2013), and Cu (Zafiriou et al. 1998, Voelker et al. 2000).

Hg is another important metal in the ocean, especially because of its toxicity to marine organisms. Hg from both natural (e.g. volcanic) and anthropogenic sources primarily enters the ocean through wet and dry atmospheric deposition as well as through erosion and watershed processes (Fitzgerald et al. 1991, Rolfhus & Fitzgerald 2004, Mason et al. 2012). The oxidized form of mercury, Hg(II), can work its way to depth (e.g. the O_2 minimum zone, ~200-1000 m deep), where it may become methylated by microorganisms such as sulfate-reducing bacteria (SRB) and possibly iron-reducing bacteria (Fitzgerald et al. 2007). The methylated forms of Hg (monomethyl mercury or MMHg and dimethyl mercury or DMHg) are highly toxic and bioaccumulative (Amyot et al. 1997, Monperrus et al. 2007). However, seasonally variable biogeochemical processes in the ocean can also reduce Hg(II) to Hg^0, a dissolved gaseous form of Hg, resulting in its partial removal from the surface aqueous phase by evasion to the atmosphere (Fitzgerald et al. 1991, Rolfhus & Fitzgerald 2004, Andersson et al. 2007). While photo-oxidation and photo-reduction primarily drive Hg cycling during daylight hours in the photic zone (Lalonde et al. 2001, Qureshi et al. 2010), dark redox cycling of Hg persists both during the night at the surface and at depth where sunlight is minimal (Amyot et al. 1997, Rolfhus & Fitzgerald 2004). Therefore, dark Hg(II) reduction processes are postulated to account for the production of Hg^0 at depth in the ocean, suggesting involvement of microorganisms and/or dark non-biological reactions (Kim & Fitzgerald 1988, Mason et al. 1995).

Microorganisms have been shown to reduce Hg(II) to Hg^0 in part to detoxify their environment (Ben-Bassat & Mayer 1977). For example, freshwater and marine bacteria (Barkay et al. 1991, Barkay & Schaefer 2001, Barkay et al. 2003, Barkay & Wagner-Dobler 2005, Fantozzi et al. 2009) as well as marine diatoms (Lanzillotta et al. 2004) were shown to play a fundamental role in dark Hg(II) reduction, revealing a resistance to the toxic metal. It also known that marine algae can oxidize dissolved Hg^0 via biogenic compounds (Poulain et al. 2007a, Poulain et al. 2007b). Little is known about the mechanism of dark Hg oxidation and reduction, but O_2^- could potentially be involved.

The main goal of this study was to determine if a dark abiotic source of O_2^- can oxidize or reduce Hg in filtered Vineyard Sound seawater (VSSW) using isotopically labeled ^{202}Hg additions (Whalin & Mason 2006, Whalin et al. 2007) and inductively coupled plasma mass spectrometry (ICPMS) analysis with gold traps (Hintelmann & Ogrinc 2003). In order to achieve this goal, we first needed to validate our method for recovering the entire ^{202}Hg spike to determine the portion of ^{202}Hg that is oxidized or reduced by O_2^-. Because trace metals can rapidly react with O_2^- and interfere with Hg oxidation/reduction, it was also important to show that traditional bottle cleaning procedures and laboratory practices for Hg analysis (Hammerschmidt et al. 2011) are viable for O_2^- experiments. We studied direct dark oxidation/reduction of Hg by two abiotic sources O_2^-: xanthine/xanthine oxidase (X/XO) and potassium superoxide (KO_2). Additionally, we determined whether secondary dark reactions involving O_2^- could drive Hg redox cycling in the dark. For example, O_2^- can oxidize Mn(II), and Mn(III/IV) produced from O_2^- may then be able to oxidize Hg^0. O_2^- can also reduce Cu(II) to Cu(I) in seawater (Zafiriou et al. 1998), which may then be able to reduce Hg(II). In addition, the coenzyme nicotinamide adenine dinucleotide (NADH), which has been used to stimulate

biological O_2^- production (Diaz et al. 2013), was tested for its ability to reduce Hg(II) in filtered VSSW without microorganisms present.

4.3 Materials and Methods

This section describes how Hg oxidation and reduction experiments were conducted using isotope labeled ^{202}Hg additions and inductively coupled plasma mass spectrometry (ICPMS). Superoxide production and decay rate methods are also described.

4.3.1 Reagent preparation

This subsection includes how Hg, O_2^-, and supplementary (e.g. Mn, Cu, catalase, and NADH) reagents were made. Additionally, it describes a novel way to create $^{202}Hg^0$ stock solutions.

4.3.1.1 Reagents for Hg analysis

A 40 mM acidified bromine monochloride (BrCl) reagent was prepared in a fume hood by dissolving 10.8 g of reagent grade KBr (Sigma Aldrich) in 1 L of 35% Instra-Analyzed HCl and stirred on a magnetic stir plate. Next, 15.2 g of $KBrO_3$ (Sigma Aldrich) was slowly added to the KBr / HCl mixture while stirring. Hydroxylamine hydrochloride was prepared by dissolving 300 g of $NH_2OH \cdot HCl$ (Sigma Aldrich) in 1L MQ water. Stannous chloride was prepared by dissolving 200 g of $SnCl_2 \cdot 2H_2O$ (Sigma Aldrich) in 100 mL of 35% Instra-Analyzed HCl and brought to 1 L with MQ water. The $SnCl_2$ solution was sparged with Hg-free N_2 gas to lower background Hg signals. All reagents were stored refrigerated in 100 mL glass bottles.

4.3.1.2 ^{202}Hg stock solutions

Isotope labeled $^{202}Hg(II)Cl_2$ (95 ± 4%), herein $^{202}Hg(II)$, was provided by Oak Ridge National Laboratory and used to prepare a secondary stock solution in 1% HCl (JT Baker

InstraAnalyzed). The secondary stock solution concentration (155 ± 9 nM) was verified by spiking ten 80 mL MQ water samples with 10-20 µL of the secondary stock, artificially reducing using stannous chloride, sparging, and trapping. After thermal desorption, ICPMS signals (in fmole) were measured for each MQ water standard spiked with $^{202}Hg(II)$ and calibrated using 0-500 fmole common Hg^0 gas spike standards with a known amount of ^{202}Hg. The common Hg^0 gas spike standards were spiked upstream of a gold trap, thermally desorbed, and analyzed by ICPMS the same way as the standards. $^{202}Hg(II)$ spiked standards in MQ were conducted again before each experiment to ensure that the secondary stock solution concentration did not change.

To make stock solutions of $^{202}Hg^0$, 3.4 nM $^{202}Hg(II)$ solutions in MQ water were artificially reduced (with Sn), sparged, and trapped. The gold trap was subsequently thermally desorbed, using Ar gas passing through the trap at 500℃, into a 0.5 L Tedlar bag containing 0.25 L of MQ water and 0.25 L available headspace. The Ar carrier gas, now containing $^{202}Hg^0$, filled the headspace of the Tedlar bag with approximately $2.7x10^{-10}$ mol of $^{202}Hg^0$. The Tedlar bag was then shaken vigorously for approximately 5-10 minutes to equilibrate $^{202}Hg^0$ into the gas and aqueous phases. Via a Henry's law calculation (Hg^0 dimensionless $K_H = 0.362$, T = 22 ℃), approximately $2x10^{-10}$ mol of the $^{202}Hg^0$ should be in the aqueous phase, giving 0.8 nM concentration with 0.25 L aqueous phase volume (USEPA 2014). However, a 0.3-0.5 nM range of $^{202}Hg^0$ stock solutions was observed. This was determined by spiking 1.5 mL of the $^{202}Hg^0$ stock into 80 mL of MQ water, sparging, trapping, and calibrating the same way as the $^{202}Hg(II)$ stock solution standards (discussed above). The $^{202}Hg^0$ stock solution standards were conducted before and after the oxidation experiments to verify that the concentration of the $^{202}Hg^0$ stock solutions in the Tedlar bag had not changed over time.

4.3.1.3 Superoxide reagents

Primary stock solutions of O_2^- were made by dissolving a small amount (unmeasured) of KO_2 (Fisher scientific) in approximately 25 mL of a 0.032 M NaOH (pH 12.5) solution containing 30 µM diethylene triamine pentaacetic acid (DTPA, Fisher Scientific). The O_2^- concentration was then calculated by first measuring the absorbance at 240 nm (Cary 500 UV-Visible spectrometer) and subtracting the absorbance at 240 nm after SOD was added (as a correction for the absorbance by H_2O_2 at 240 nm) and dividing by 2183 M^{-1} cm^{-1} (effective molar absorptivity). An aliquot of the primary KO_2 stock was added to seawater samples (1000 - 1200 nM superoxide final) within seconds of the first absorbance measurement. A new primary KO_2 stock was made before spiking each sample.

A 3 mM stock solution of xanthine (Sigma Aldrich) was made by dissolving 46 mg in 1 mL of 1 M NaOH and bringing the volume to 100 mL with MQ water. This solution was stored in the refrigerator before use. A 100 U L^{-1} xanthine oxidase stock solution was made by dissolving in 5 U (Sigma Aldrich) in 50 mL of MQ water. 5 mL aliquots were placed in falcon tubes and stored frozen. A 3.6 kU mL^{-1} stock solution of superoxide dismutase or SOD (≥3000 U mg^{-1}, Sigma Aldrich) was made by adding 1.0 mg per 1.0 mL of MQ. 10 mL aliquots were placed in falcon tubes and stored frozen.

4.3.1.4 Mn, Cu, Catalase, and NADH Supplements

A 100 µM secondary stock solution of Mn(II) chloride (Fisher Scientific) and Cu(II) chloride dihydrate (JT Baker) were made from 10 mM stock solutions in MQ water. Both the primary and secondary stock were adjusted to pH 4.0 using 10% Instra-Analyzed HCl. A catalase (Sigma Aldrich, 11000 U mg^{-1}) stock solution was made by dissolving 1 mg per 1 mL of

MQ and stored frozen. A 20 mM NADH (beta disodium salt, MP Biomedical LLC) stock solution was made by dissolving 0.14 g in 10 mL of MQ water.

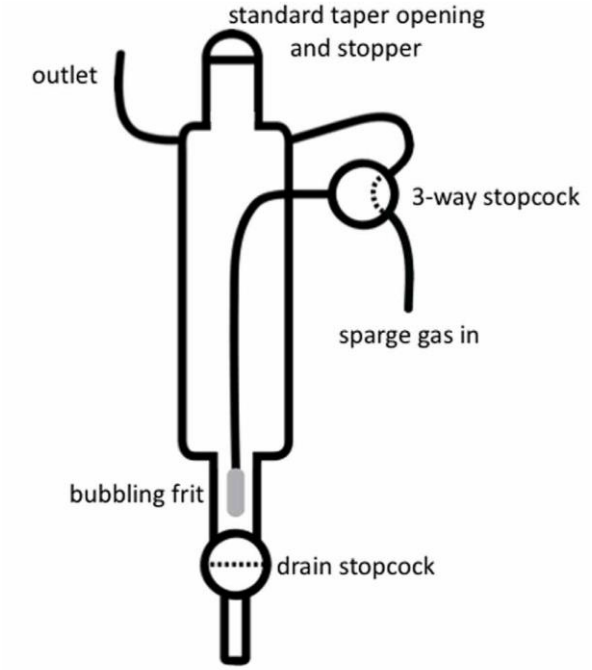

Fig. 4.1 Schematic of the glass bubbler (courtesy of Lamborg et al. 2012)

4.3.2 Bottle and glass bubbler cleaning

The Nalgene bottles used for seawater storage and the pyrex glass bottles used for experiments were cleaned by first rinsing with MilliQ (MQ, Millipore) water three times followed by a 1-3 day soak in 1% citranox (Sigma Aldrich) followed by another three time rinse with MQ water. The bottles then soaked for 1-3 days in 10% HCl (Instra-analyzed, JT Baker) followed by three more rinses with MQ water. Glass bubblers (University of Connecticut, see Figure 4.1) were cleaned by filling with MQ, adding 5-10 pellets of potassium hydroxide (KOH, Fischer Scientific), and soaking overnight. After the KOH soak, the bubblers were rinsed twice with MQ water, filled with filtered seawater and sparged for 1 minute with Hg free N_2 gas, and finally rinsed a third time with MQ water. Two glass bubblers were reused for sample replicates

and rinsed between replicates in the same manner as the rinses following the KOH soak. All bottle/glass bubbler cleaning was done in a Class 100 clean room laboratory.

Table 4.1 List of Hg oxidation/reduction experiments. Seawater was sampled on numerous days

Experiment Date	Description	^{202}Hg spike (fmole)	[O_2^-] nM	[SOD] Control (kU L^{-1})	Seawater sample
May 5 (Day 1)	Hg(II) reduction with KO_2 in glass bottles	1550	1000	5	May 5 (Day 1)
May 6 (Day 2)	Hg^0 oxidation with KO_2 in glass bottles	705	1000	5	May 6 (Day 2)
May 8 (Day 3)	Hg(II) reduction with X/XO in glass bottles	1550	NA	5	May 8 (Day 3)
June 11 (Day 4)	Hg(II) reduction with X/XO in glass bubblers	3100	780	1.5	May 8 (Day 3)
June 12 (Day 5)	Hg^0 oxidation with X/XO in glass bubblers	525	780	1.5	May 8 (Day 3)
June 13 (Day 6)	Hg(II) reduction with X/XO in glass bubblers (24 hour equilibration)	3100	795	3	June 13 (Day 6)
June 14 (Day 7)	Hg^0 oxidation with X/XO active in glass bubblers	585	810	3	June 13 (Day 6)
June 15 (Day 8)	Hg^0 oxidation with X/XO and Mn(II) in glass bubblers	690	795	3	June 13 (Day 6)
June 16 (Day 9)	Hg(II) reduction with X/XO and NADH in glass bubblers	3100	1245	3	June 16 (Day 9)
June 17 (Day 10)	Hg(II) reduction with X/XO and Cu(II)	3100	1050	3	June 16 (Day 9)
June 19 (Day 11)	Hg(II) reduction with NADH and X/XO in glass bubblers	3100	1245	3	June 16 (Day 9)
June 19 (Day 11)	Hg^0 oxidation with Mn(II), catalase, and X/XO in glass bubblers	420	1245	3	June 16 (Day 9)
May 20	Superoxide decay rate constant (k_{O2-}) determination	-	1000	-	May 8 (Day 3)
June 1	Superoxide decay rate constant (k_{O2-}) determination	-	1000	-	May 8 (Day 3)
August 6	Superoxide decay rate constant (k_{O2-}) determination	-	1000	-	June 19 (Day 11)

4.3.3 Site and seawater sampling

Seawater was collected offshore between 7:00 and 8:00 am in the Vineyard Sound near the Shore Lab (Quissett Campus) of Woods Hole Oceanographic Institution by submerging a 3 L white translucent Nalgene bottle. The 3 L bottle was rinsed three times with seawater before it

was filled. It was placed into a brown plastic Ziploc bag immediately after filling to minimize light exposure. The seawater was then brought to the lab and filtered (0.2 µm Acropak) into an identical 3 L Nalgene bottle using a peristaltic pump. The filter was rinsed with 0.01 M HCl followed by ~250 mL of MQ water. Table 4.1 summarizes the dates on which different seawater samples were obtained and the experiments that were conducted with each seawater sample.

4.3.4 Hg(II) reduction by superoxide

Experiments involving Hg(II) reduction by two sources of O_2^- are described in this section.

4.3.4.1 Reduction by superoxide from KO_2

Pyrex glass bottles (100 mL graduated) were filled with 80 mL of filtered seawater. 1550 fmol ^{202}Hg(II) was spiked into the seawater samples (approximately 5x the natural total ^{202}Hg concentration). The samples were tightly capped and allowed to equilibrate at room temperature for 1 hour in the dark using a photography bag and were never removed from the dark unless a reagent was added. Next, 5 kU L^{-1} SOD was added to the SOD controls (Experiment Days 1-3, Table 4.1). Samples were then spiked with 1000 - 1200 nM (final concentration) potassium superoxide and allowed to react for a minimum of 15 minutes. Each of the bottles was then equipped with a solvent cap (Omnifit) containing gas entry and exit ports and sparged in the dark for 5 minutes with Hg-free N_2 gas with a flow rate of 0.5 L min^{-1}. The N_2 gas carried gaseous Hg^0 (both natural and from reduction of the ^{202}Hg(II) spike) from the samples to gold-coated beaded silica traps (Tekran), herein gold trap. The N_2 gas was made free of Hg by placing a gold trap upstream of the gas entering the samples.

4.3.4.2 Reduction by superoxide from Xanthine/Xanthine Oxidase

Xanthine/xanthine oxidase (X/XO) was also used as a superoxide source in lieu of a KO_2 spike (see Table 4.1). In this case, filtered seawater (80 mL) was first added to a pyrex glass

bottle followed by a 3100 fmol spike of ^{202}Hg(II). The bottle was then capped and allowed to equilibrate in the dark for 1 or 24 hours. The equilibrated seawater was then transferred to a 300 mL glass bubbler (Figure 4.1). Next, 5 µM xanthine was added to the seawater followed by 0.2 U L^{-1} xanthine oxidase. See section 4.3.8 for calibration of X/XO superoxide production rate. SOD (1.5-3.0 kU L^{-1}, see Table 4.1 for specific details) was added to SOD controls in the glass bubbler before X/XO was added. The samples were allowed to react in the dark for 10-15 minutes in the glass bubbler (sealed with a 20.5 mm Luba Seal septum) followed by 5 minutes of sparging to gold traps, to capture natural Hg(II) and ^{202}Hg(II) reduced to Hg^0, in the dark at 0.5 L min^{-1}. One set of samples was sparged and trapped beginning immediately after addition of X/XO and continuing for the duration that X/XO was still expected to be active (about 15 minutes).

4.3.4.3 Capturing the remaining ^{202}Hg(II) spike

The filtered seawater samples were sparged a second time after a Hg(II) reduction treatment to capture the remaining natural Hg(II) and ^{202}Hg(II) spike that did not get reduced. If glass bottles were used as the first sparging vessel, the seawater remained in their respective capped glass bottles until the second sparge. If seawater samples were sparged in a glass bubbler, as described for the X/XO experiments, they were transferred to glass bottles after sparging and capped. 300 µL of acidified 40 mM bromine monochloride (BrCl) reagent was then added and the solution was allowed to sit for a minimum of 1 hour to free Hg(II) from organic complexes. This was followed by the addition of 300 µL of 70 mM of hydroxylamine hydrochloride ($HONH_2 \cdot HCl$) to scavenge any free halogens from the BrCl capable of destroying the gold traps. The sample was then transferred to a separate 200 mL glass bubbler dedicated for artificial reduction where 100 µL of 20 mM stannous chloride ($SnCl_2$), a reductant, was added. The glass

bubbler was capped with a 19.0 mm Suba Seal septum and the treated seawater was then sparged with Hg-free N_2 gas, capturing the Hg^0 formed by this treatment.

4.3.4.4 Sparge, trapping, and analysis

During each sparge, Hg^0 exits the sparging vessel through low-porosity chemically resistant PFA-Teflon tubing attached to two successive traps: i. a soda lime trap that captures any moisture exiting the sparging vessel (which could damage the sample gold traps) and ii. the sample gold trap (pre-blanked by heating to 500℃ using a Nichrome wire coil) that collects any Hg^0 sparged out of the seawater. Once the sparging is finished, plastic end caps are placed on each end of the Au traps to prevent contamination by Hg in the air.

Hg sorbed to the gold traps from sparging is then thermally (500℃) desorbed using a Nichrome wire coil in line with the Ar carrier gas of an ICAPq inductively coupled plasma mass spectrometer (ICPMS) where the fmole quantities of Hg are measured including all stable isotopes. Following the thermal desorption of the sample trap, a standard curve is created by injecting known volumes of common gaseous Hg^0 standard into the carrier gas upstream of the sample trap and thermally desorbing (see section 4.3.1.2). Instrumental drift was tested using quality control gas standards after each sample and standard run by injecting a known volume of the gaseous Hg^0 standard into the carrier gas downstream of the gold trap.

All ^{202}Hg signals measured by the ICPMS (natural plus spiked ^{202}Hg) were corrected to obtain the ^{202}Hg signal from the spike only by using the natural ratio of ^{202}Hg to ^{200}Hg. The natural abundances of ^{202}Hg and ^{200}Hg is 29.86% and 23.10%, respectively, with a known ratio of 1.2926 (de Laeter et al. 2009). The natural signal of ^{200}Hg is multiplied by 1.2926 to calculate the natural amount of ^{202}Hg present in the seawater samples. The calculated natural ^{202}Hg amount is then subtracted from the total measured ^{202}Hg ICPMS signal and calculates the amount

of ^{202}Hg signal from the spike. All data presented in this paper is the ^{202}Hg signal from the spike corrected in this way for natural amounts of ^{202}Hg.

4.3.5 Hg^0 oxidation by superoxide

Experiments involving Hg^0 oxidation by two sources of O_2^- are described.

4.3.5.1 Oxidation by superoxide from KO_2

$^{202}Hg^0$ oxidation experiments were conducted in a similar manner to the KO_2 $^{202}Hg(II)$ reduction experiments. However, a 1.5 mL aliquot (705 fmole of $^{202}Hg^0$, see Table 4.1) was removed from the Tedlar bag stock solution with a 3 mL plastic syringe and then carefully injected near the surface of an 80 mL seawater sample in a glass bottle, which was then capped. The $^{202}Hg^0$ spiked samples were then shaken to equilibrate the gas spike to the aqueous and gas phases as otherwise an inconsistent amount of $^{202}Hg^0$ spike escapes whenever the sample cap was opened to add a reagent. Once equilibrated, each sample was opened the same number of times for the addition of reagents (e.g. KO_2 and SOD). After allowing a minimum of 15 min for reaction, the samples were sparged for the first time to capture any natural Hg^0 or spiked $^{202}Hg^0$ not oxidized to Hg(II).

4.3.5.2 Oxidation by superoxide from X/XO

80 mL of filtered seawater was added directly to the 300 mL glass bubbler followed by X, XO, and SOD (for controls). A 1.5 mL aliquot of the $^{202}Hg^0$ stock solution (420-690 fmole, see Table 4.1) was then drawn up into a 3 mL plastic syringe and injected by needle through a 20.5 mm Suba Seal septum covering the opening of the glass bubbler. The samples were allowed to react in the dark for 10-15 minutes in the glass bubbler followed by 5 minutes of sparging in the dark at 0.5 L min^{-1} to trap Hg^0.

4.3.5.3 Capturing the remaining $^{202}Hg^0$ spike oxidized to $^{202}Hg(II)$

The samples were sparged a second time after a reducing treatment to capture the Hg(II) or $^{202}Hg(II)$ formed from natural or superoxide oxidation of Hg^0. Seawater in glass bottles used as the first sparging vessel remained in their respective capped glass bottles until the second sparge. If seawater samples were sparged in a glass bubbler, as in the X/XO experiments, they were transferred to glass bottles and capped. The same reduction procedure was used as in section 4.3.4.3 above.

4.3.6 Mn, Cu, Catalase, and NADH supplemented experiments

Filtered seawater samples were amended with 100 nM Mn(II) and 150 kU L^{-1} catalase for oxidation experiments and 100 nM Cu(II) and 0.2 mM NADH for reduction experiments when X/XO was used as a O_2^- source. Mn(II) and catalase were added prior to the addition of $^{202}Hg^0$, X/XO, and SOD. Cu(II) and NADH were added after $^{202}Hg(II)$ equilibrated for 1 hour, but prior to the additions of X/XO and SOD. After all supplements and reagents were added, the samples were sparged/trapped/analyzed according to their respective reduction and oxidation protocols (sections 4.3.4 and 4.3.5, respectively).

4.3.7 Superoxide decay rate measurements

Pseudo-first-order decay rates constants of superoxide (k_{O2-}) were measured in VSSW because these are needed to determine the second order rate constants (k_{Hg}) for O_2^- reactions with Hg. Additionally, k_{O2-} measurements also indicate whether contamination of seawater samples by trace metals, which could consume O_2^- before it can react with Hg, is a problem. The k_{O2-} measurements were done by spiking 1000-1200 nM KO_2 into glass bottles containing 80 mL VSSW. These bottles had been subjected to the same cleaning protocols as those described above for the Hg redox experiments. k_{O2-} measurements were also conducted after exposing

seawater to glass bubblers that were cleaned by the KOH cleaning procedure (section 4.3.2), and then transferred to glass bottles for the KO_2 spike. The relative concentration of O_2^- versus time was then measured using flow injection analysis (FIA) and the chemiluminescence reagent MCLA (2-methyl-6-(4 methoxyphenyl)-3,7-dihydroimidazo[1,2-a]pyrazin-3-one) until the signal decayed to a steady state. The decaying O_2^- signal was fitted to a pseudo-first-order kinetic model using the solver function in Microsoft Excel to obtain k_{O2-}; all nonlinear fits had R^2 values 0.98 or greater. To make the MCLA reagent, a 200 µM stock of MCLA was prepared by adding 10 mg to 170 mL of MQ water, and stored frozen as 12.5 mL aliquots. A 12.5 mL aliquot is added to a 500 mL MQ solution containing 30 µM DTPA and 0.2 M 2-(*N*-morpholino)ethanesulfonic acid (MES) buffer.

4.3.8 Measurement of rate of superoxide production by X/XO and NADH

Xanthine/Xanthine oxidase production of O_2^- was measured via the reduction of ferricytochrome c (FC). A 4 mM FC (Sigma Aldrich) solution was made by dissolving 50 mg in 1 mL of MQ water. 0.2 mL aliquots were put in 0.5 mL centrifuge tubes and stored frozen. 10 mL of filtered VSSW was placed into a 15 mL Falcon tube followed by the addition of 5 µM xanthine and 0.2 U L^{-1} xanthine oxidase. Exactly 1 mL of the solution was placed into a small volume cuvette and 12.5 µL of FC (50 µM final) was added. The solution's absorbance was measured over time (6-15 minutes) at 550 nm where the peak of FC is observed after reduction using the molar absorptivity of 19,600 M^{-1} cm^{-1} (Heller & Croot 2010). The absorbance at 700 nm was subtracted as background. The slope of the linear regression was then used to calculate the reduction rate of ferricytochrome by superoxide. The production rate of superoxide by 0.2 mM NADH was also measured in the same manner.

4.4. Results and Discussion

This section shows the results of O_2^- oxidation/reduction of Hg and O_2^- decay rates in Vineyard Sound seawater. It includes the recoveries of added ^{202}Hg that are important for determining the oxidation/reduction of Hg by O_2^-.

4.4.1 Superoxide decay rates (k_{O2-})

The pseudo-first order decay rate constant (k_{O2-}) of O_2^- was determined to be 0.036 ± 0.006 s^{-1} (N = 11) from three filtered VSSW sample days (see Table 4.1), and used in the estimation of the second order rate constant for O_2^- reaction with Hg(II) (see section 4.4.4). Coastal VSSW most likely has higher trace metal concentrations, which may explain why k_{O2-} is higher than k_{O2-} values of the open ocean, e.g. 0.002-0.02 s^{-1} (Hansard et al. 2010). Another reason we measured k_{O2-} was to check for trace metal contamination that could speed up the decay rate of O_2^- and prevent reaction with Hg. For example, k_{O2-} increased to nearly 0.1 s^{-1} when nM Mn was added to open ocean water (Hansard et al. 2011) and µM levels of Cu have been shown to increase k_{O2-} a few orders of magnitude (10^3-10^4 s^{-1}) (Zafiriou et al. 1998). The good reproducibility of our k_{O2-} measurements indicates that trace metal contamination of the glass bottles did not interfere with our measurements.

4.4.2 Total Hg recoveries

Figure 4.2 shows the total (Hg^0 + Hg(II)) percent recoveries from the ^{202}Hg spikes in glass bubblers. For the oxidation experiments, multiple $^{202}Hg^0$ aliquots were spiked into MQ water, sparged, and trapped on each experiment day to standardize the $^{202}Hg^0$ Tedlar stock (section 4.3.1.2), and were defined as 100% recovery signals. Recoveries of $^{202}Hg^0$ spikes in filtered VSSW (black circles, Figure 4.2) were compared to the $^{202}Hg^0$ spiked MQ water standards, and had an average recovery of 98 ± 3% (α = 0.05, N = 29) which includes all

experiments with $^{202}Hg^0$ added to VSSW with the exception of catalase amended solutions on Day 11 (46 ± 15%, N = 10, black square, Figure 4.2). The low recoveries with the catalase-amended solutions on that day were due to a visually observed seafoam build up during the second sparge step that clogged the glass wool stopper in the soda lime trap, preventing a full recovery of Hg. However, the foam build-up was not observed in the first sparge step (because of the larger volume bubbler) on day 11, and good recoveries were observed in two $^{202}Hg^0$ standards spiked in VSSW without catalase (96 ± 7%, last black circle, Figure 4.2). In fact, except for the catalase-amended solutions on Day 11, almost all added $^{202}Hg^0$ was recovered in the first sparge step (93 ± 10%, N =30) in all the Hg oxidation experiments (excluding any with added catalase), indicating that i. little oxidation of $^{202}Hg^0$ occurred (see below) and ii. Hg^0 recoveries can be assumed to be excellent in all experiments.

Our technique for conducting experiments with isotope-labeled Hg^0 is similar to a previous method that was developed to measure Hg oxidation over a time scale of hours. In that method, $^{202}Hg^0$ stock solutions were generated by inserting an elemental $^{202}Hg^0$ droplet into permeable tubing that allowed diffusion of $^{202}Hg^0$ into aqueous solution, and subsequent secondary stock solutions were made through serial dilution. Although minimized in that study, Hg^0 is allowed to evade to the atmosphere after opening, possibly changing the stock solution concentration. Their Teflon bags were then spiked with $^{202}Hg^0$ using a HDPE syringe and the bag was subsampled into glass bottles (Whalin and Mason 2006; Whalin and Mason 2007). In our study, $^{202}Hg^0$ stocks were generated by thermally desorbing a gold trap via artificial $^{202}Hg(II)$ reduction (see section 4.3.1.2). Our $^{202}Hg^0$ stock solutions were freshly made before each oxidation experiment, but were repeatedly reliable from day to day with an average $^{202}Hg^0$ concentration of 0.40 ± 0.02 nM (N = 5). Additionally, we spiked $^{202}Hg^0$ directly into a glass

bubbler through a SubaSeal septum to prevent the Hg^0 spike from escaping the sample while the $^{202}Hg^0$ stock remained sealed in a Tedlar bag in MQ water.

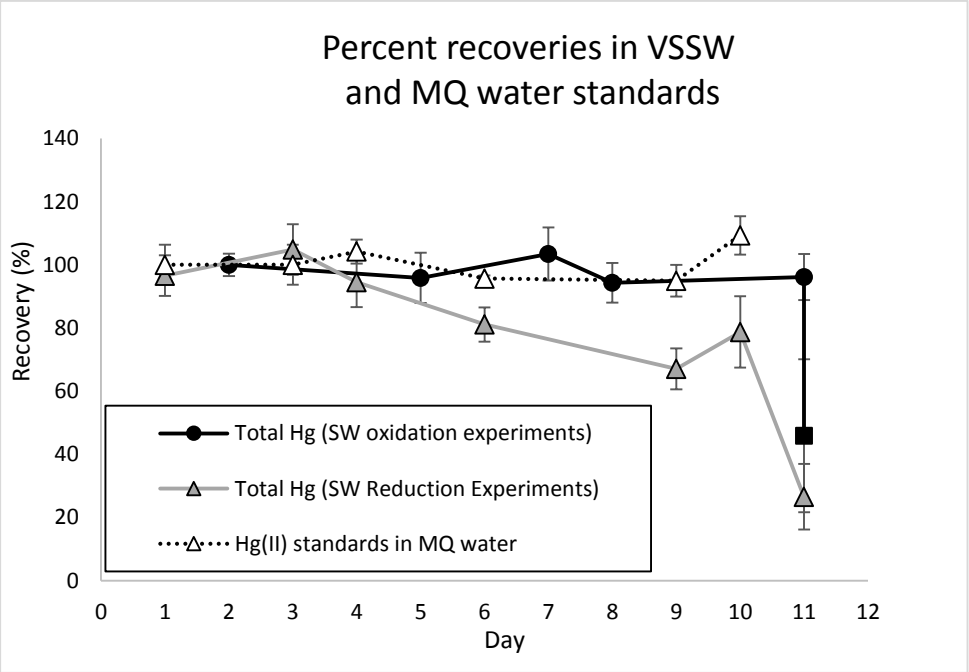

Fig. 4.2 Recoveries for total ^{202}Hg spikes in VSSW (black circles, black line) for the oxidation experiments. The black square represents $^{202}Hg^0$ recoveries in VSSW for Day 11, when visually observed sea foam clogged the glass wool stopper in the soda lime trap preventing full recovery during the second sparge step. Recoveries of total ^{202}Hg spikes in VSSW (grey triangles, grey line) and $^{202}Hg(II)$ standards in MQ water (open triangle, dotted line) for the reduction experiments.

The total (Hg^0 + Hg(II)) percent recoveries from $^{202}Hg(II)$ standard spikes in high purity MQ water (white triangles, Figure 4.2) also had excellent recoveries averaging 101 ± 5% (α = 0.05, N = 12), indicating no change in the stock solution concentration over time. However, total (Hg^0 + Hg(II)) percent recoveries from the $^{202}Hg(II)$ spike were not as good in the filtered VSSW. Daily averages and 95% confidence intervals (α = 0.05 and N = 9 for each day) are shown on Figure 4.2 (grey triangles). Averages ranged from 95 ± 5% to 105 ± 8% (Day 1-4, Figure 4.2) and fell to 81 ± 4% (Day 6), 68 ± 5% (Day 9), and 79 ± 7% (Day 10). As mentioned

above, we believe that the poorest recovery, observed on Day 11, was primarily due to a gas leak during the second sparge step.

We observed sea foam accumulation in our coastal seawater samples from Day 6 to Day 11 during the second sparging step, which sometimes filled the smaller volume glass bubblers. Sea foam is known to have variable organic composition from phenolics to carbohydrates to proteins (Barlocher et al. 1988, Craig et al. 1989, Schilling & Zessner 2011), including compounds that could act as Hg(II) ligands. In addition, the sea foam may simply have been an indication of samples with higher content of other organic ligands. The 1-hour exposure of natural water samples to BrCl used here is typically considered sufficient to break the Hg(II)-organic ligand bonds before reduction and analysis, even in waters with high dissolved organic carbon content (Lamborg et al. 2012). However, some studies suggest that a 24-hour exposure to BrCl may be required for full quantitation of Hg(II) (Parker & Bloom 2005). The combination of high organic content and only a 1-hour BrCl exposure may have been enough to have cause a decrease in our percent recoveries of the ^{202}Hg(II) spike in the reduction experiments in some of the VSSW samples, compared to those in MQ water.

The poor ^{202}Hg(II) recoveries have implications for both the oxidation experiments (section 4.4.3) and reduction experiments (section 4.4.4). For example, in the second sparge step of the oxidation experiments, ^{202}Hg(II) formed by $^{202}Hg^0$ oxidation would also have poor relative recoveries in seawater days with higher organic complexation of Hg(II) (6-11, Table 4.1). However, as discussed above, the recoveries were excellent in the first sparge step of $^{202}Hg^0$ oxidation experiments in VSSW indicating that little ^{202}Hg(II) was formed from oxidation and that therefore the effect on total recoveries was negligible in the oxidation experiments. In the reduction experiments, the poor ^{202}Hg(II) recoveries in VSSW may also mean that ^{202}Hg(II)

bound to strong organic complexes may be inaccessible to reduction by O_2^-. The exception is on Day 4 when sea foam was not visually observed, with excellent ^{202}Hg recoveries in VSSW (Day 4, grey triangles, Figure 4.2). However, as mentioned above, $^{202}Hg^0$ standards had excellent recoveries in the first sparge step for in both MQ water and VSSW implying $^{202}Hg^0$ formed from $^{202}Hg(II)$ reduction also had excellent recoveries.

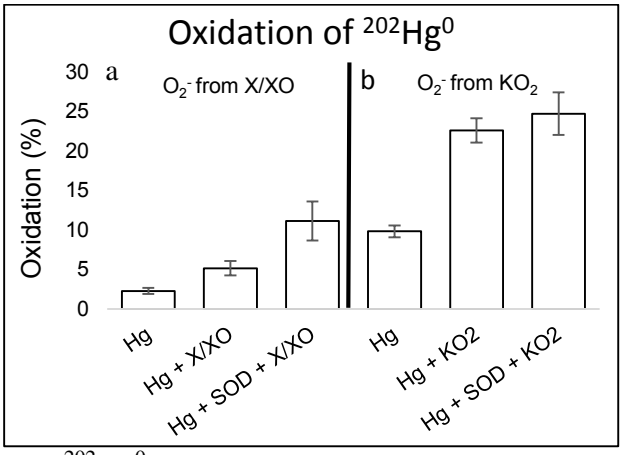

Fig. 4.3 Percent oxidation of $^{202}Hg^0$ is significant by superoxide from X/XO and KO_2 when compared to natural oxidation (i.e Hg only) where $p < 0.01$ and $p < 0.001$, respectfully, but not significant when compared to the the SOD control.

4.4.3 Hg^0 oxidation by superoxide

A small amount of dark $^{202}Hg^0$ oxidation was observed with X/XO and KO_2 added (Figure 4.3) when compared to the samples without a O_2^- source. For example, 0.19 ± 0.06 pM of a 6.6 pM $^{202}Hg^0$ spike (or ~3% of the total) was oxidized to $^{202}Hg(II)$ when X/XO was used as a O_2^- source. The 0.19 ± 0.06 pM signal is calculated as the difference between the oxidation measured by X/XO added and natural oxidation (i.e. no X/XO present) which has a statistical difference of $p < 0.01$ (Figure 4.3a). Similarly, 1.1 ± 0.15 pM of an 8.8 pM spike of $^{202}Hg^0$ (~13% of the total) was oxidized to $^{202}Hg(II)$ when KO_2 was used as the O_2^- source. 1.1 ± 0.15

pM is also calculated from the difference between oxidation when KO_2 is added and natural oxidation ($p < 0.01$, Figure 4.3b).

Similar levels of O_2^- were added to the system in the KO_2 and X/XO experiments. The production of O_2^- by X/XO (or $(P_{O2-})_{X/XO, FC}$) was calibrated with ferricytochrome c (FC) and had a reduction at a rate of 52 ± 5 nM min^{-1} (Day 5). After 15 minutes there was a total O_2^- concentration of 780 ± 75 nM while KO_2 was spiked in at 1000 -1200 nM (see Table 4.1). This calculation assumes that all of the FC reduction is by O_2^-. However, the calibration of the X/XO plus SOD control for O_2^- production (or $(P_{O2-})_{X/XO + SOD, FC}$) on Day 5 revealed a rate of 40 ± 4 nM min^{-1}. Therefore, either O_2^- was only produced at 12 ± 6 nM min^{-1} or 1.5 kU L^{-1} SOD (about $1.5x10^{-8}$ M, assuming a pure enzyme) scavenged only 23% of the O_2^- that could have otherwise reduced FC in the calibration assay.

The superoxide dismutase (SOD) controls appeared to be ineffective at preventing O_2^- from oxidizing even small amounts of Hg^0 (Figure 4.3). We observed this phenomenon in experiments with two different O_2^- sources, X/XO and KO_2 (Figure 4.3) We can use the SOD effect on FC reduction in the presence of X/XO to determine whether or not there was enough SOD to scavenge O_2^- in the Hg^0 oxidation experiments. Assuming that the FC reduction rate observed in the absence of SOD, 50 nM hr^{-1}, was due entirely to reaction with O_2^-, the fraction of O_2^- that reacted with FC in the presence of SOD is shown by equation 4.1:

$$Fraction(O_2^- rxn)_{FC} = \frac{\left(P_{O_2^-}\right)_{X/XO+SOD,FC}}{\left(P_{O_2^-}\right)_{X/XO,FC}} \qquad \text{(Equation 4.1)}$$

This fraction is equal to the ratio of the rate of reaction of O_2^- with FC to the rate of reaction of O_2^- with both FC and SOD::

$$Fraction(O_2^- rxn)_{FC} = \frac{k_{FC}[FC]}{k_{FC}[FC]+k_{SOD}[SOD]} \qquad \text{(Equation 4.2)}$$

Inserting for k_{FC} is the reduction rate constant of FC ($3x10^5$ M^{-1} s^{-1} at pH 7.8 Heller & Croot 2010) and an [FC] and [SOD] of $5.0x10^{-5}$ M and $1.5x10^{-8}$ M, respectively, we obtain a value of $2.9x10^8$ M^{-1} s^{-1} for k_{SOD}. Therefore, 1.5 kU L^{-1} SOD is enough to scavenge a large fraction of O_2^- produced by X/XO in the Hg^0 oxidation experiments since there is enough SOD to outcompete O_2^- reaction with other seawater sinks (i.e. $k_{O2-} = 0.036$ s^{-1}, see section 4.4.1).

Because the SOD control was ineffective at preventing Hg^0 oxidation (Figure 4.3), but there was enough SOD to scavenge O_2^-, O_2^- must not have oxidized Hg^0 directly. One possible explanation of this finding is that H_2O_2, the product of O_2^- dismutation both in the presence and absence of SOD, is responsible for the observed oxidation. While H_2O_2 is not a strong oxidant of Hg^0 in aqueous solution (Wigfield & Perkins 1985), it can produce the strongly oxidizing hydroxyl radical (Munthe & McElroy 1992, Lin & Pehkonen 1999, Gardfeldt et al. 2001, Lalonde et al. 2004) via H_2O_2 reaction with Fe(II) in natural waters (Lin & Pehkonen 1997). It is possible that there are reductants in the water that maintain enough Fe(II) for this process. Another possibility is that there are other oxidants in the superoxide reagents causing secondary Hg^0 oxidation reactions, but because we saw the same trend with very different reagents (X/XO and KO_2) we think that it is most likely oxidation by reactions involving H_2O_2.

Additionally, the X/XO and KO_2 $^{202}Hg^0$ oxidation experiments were conducted with two different seawater samples from different days. It appears that there is more natural oxidation on the day when KO_2 was used (Figure 4.3) suggesting the seawater chemistry of that day was different.

4.4.4 Hg(II) reduction by superoxide

Four different seawater samples were measured for $^{202}Hg(II)$ reduction by O_2^-, one with KO_2 (Day 1, Figure 4.4a) and three with X/XO as a O_2^- source (Days 3, 4, and 6, Figures 4.4b, c

and d, respectively). In one of these samples (Figure 4.4b), we observed a small amount of dark $^{202}Hg(II)$ reduction by O_2^- (or $[Hg^0]_{produced}$) that was statistically different from a SOD control ($p < 0.05$, Figure 4.4b) where the difference accounts for <2% (0.37 ± 0.14 pM) reduction of the 19.4 pM $^{202}Hg(II)$ spike (time and resources did not permit for natural reduction of $^{202}Hg(II)$ to be measured in Figure 4.4b).

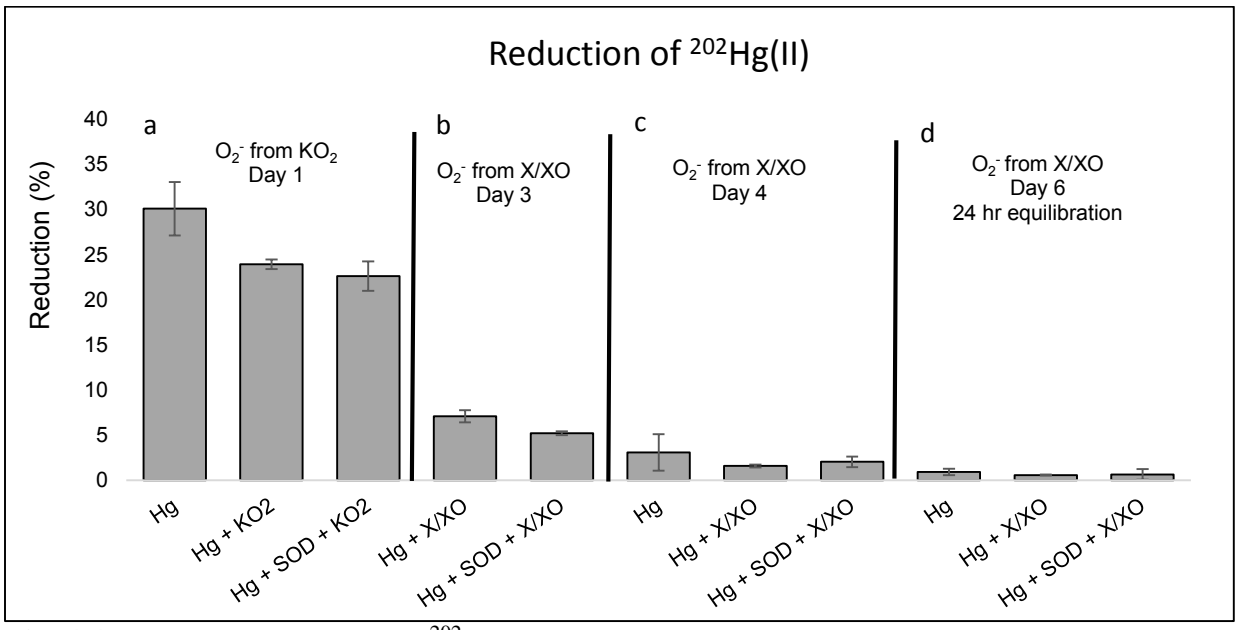

Fig. 4.4 a.) Percent reduction of $^{202}Hg(II)$ is not significant by superoxide from KO_2 on Day 1, but b.) significant ($p < 0.01$) on Day 3 with superoxide from X/XO when compared to an SOD control. c.) There was no significant reduction by superoxide with X/XO on Day 4 or d.) after 24 hr equilibration of $^{202}Hg(II)$ on Day 6

The production of Hg^0 (via Hg(II) reduction) by O_2^- can be used to estimate the second order reduction rate constant ($k_{Hg(II)}$), shown by equations 4.3a-d:

$$[Hg^0]_{produced} = \left(Fraction\ of\ [O_2^-]\ reacting\ with\ Hg(II)\right)[O_2^-]_{added} \qquad \text{(Equation 4.3a)}$$

$$[Hg^0]_{produced} = \left(\frac{k_{Hg(II)}[Hg(II)]}{k_{Hg(II)}[Hg(II)] + k_{Hg^0}[Hg^0] + k_{O_2^-}}\right)[O_2^-]_{added} \qquad \text{(Equation 4.3b)}$$

If one assumes that the Hg terms in the denominator are negligible, that no oxidation occurs to consume any Hg^0 produced, and that most of the Hg remains Hg(II), so that the value of the numerator does not change with time, this simplifies to:

$$[Hg^0]_{produced} = \left(\frac{k_{Hg(II)}[Hg(II)]}{k_{O_2^-}}\right)[O_2^-]_{added} \qquad \text{(Equation 4.3c)}$$

Rearranging Equation 4.3, we obtain:

$$k_{Hg(II)} = \frac{[Hg^0]_{produced} k_{O_2^-}}{[Hg(II)][O_2^-]_{added}} \qquad \text{(Equation 4.3d)}$$

Inserting values for $[Hg^0]_{produced}$ (0.37 ± 0.14 pM, section 4.4.4), k_{O2-} (0.036 ± 0.006 s^{-1}, section 4.4.1), the spiked [Hg(II)] amount (19.4 ± 1.5 nM), and $[O_2^-]$added (1000 ± 100 nM), we calculate $k_{Hg(II)}$ equal to 6.9x10^2 M^{-1} s^{-1} (s = 3.1 x10^2 M^{-1} s^{-1}).

Assuming a 0.1-1 nM natural steady concentration of O_2^- and a 10 pM concentration of Hg(II) in VSSW, a dark reduction rate of Hg(II) by O_2^- is estimated to be 0.7-7x10^{-18} M s^{-1}.This may be enough to account for at least part of the dark reduction of Hg(II) observed in other studies where a reduction rate of ~1% day^{-1} (or ~1x10^{-18} M s^{-1} for 10 pM Hg(II)) was measured in the coastal northern Atlantic Ocean (Rolfhus & Fitzgerald 2004).

There was no dark O_2^- reduction of ^{202}Hg(II) after it had been equilibrated for 24 hours (Figure 4.4d) as opposed to 1 hour (all other reduction experiments, Figures 4.4a, b, and c). In addition, natural reduction of ^{202}Hg(II) after 24-hour equilibration (Figure 4.4d) was lower compared to the natural reduction in the 1-hour equilibrated samples (Figures 4.4a, b, and c. Although, there was not any dark reduction of ^{202}Hg(II) by O_2^- from a KO_2 source (Figure 4.4a), but in that experiment there was substantial natural reduction of the ^{202}Hg(II) spike. It is not clear whether these difference are due to differences in the equilibration times or to differences

in the organic matter content of the four different water samples used to conduct the experiments in Figures 4.4 a, b, c and d.

4.4.5 Hg oxidation/reduction secondary reactions

Secondary dark reactions of O_2^- were also investigated to determine if they influence the oxidation/reduction of Hg in VSSW. For example, O_2^- is known to oxidize Mn(II) to Mn(III/IV) in seawater (Hansard et al. 2011, Learman et al. 2011, Learman et al. 2013), and it is possible that Mn(III/IV) could then oxidize Hg^0. Catalase is needed to scavenge the hydrogen peroxide (H_2O_2) produced from O_2^- oxidizing Mn(II) because H_2O_2 can re-reduce the newly formed Mn(III/IV) back to Mn(II) (Hansard et al. 2011, Learman et al. 2013) .

Mn(II) additions (100 nM) well above sub nM-nM North Atlantic Ocean Mn concentrations (Wu et al. 2014) did not assist in oxidizing $^{202}Hg^0$ in the presence of the X/XO O_2^- source (Figure 4.5a). Therefore, Mn(III/IV) formed by Mn(II) oxidation via O_2^- does not oxidize Hg^0 in filtered VSSW. Note that Figure 4.5a shows the remaining Hg^0 after oxidation because this experiment was conducted on Day 11 when noticeable leaking was observed in the second sparge step (see section 4.4.2 for more detail), and therefore only the Hg^0 measurements (obtained from the first sparge) were considered reliable. Catalase amended filtered VSSW solutions oxidized ~70% of the $^{202}Hg^0$ spike with and without Mn(II) added (Figure 4.5a). It is well known that catalase in the presence of H_2O_2 is capable of oxidizing Hg^0 to Hg(II) in blood cells, most likely by the formation of O_2 (Magos et al. 1978). However, others suggest that catalases of microorganism like *E. Coli* and soil bacteria *Bacillus* and *Streptomyces* can also oxidize Hg^0 to Hg(II) with and without elevated H_2O_2 depending on the type of catalase (Smith et al. 1998). Additional studies postulate that catalase-like enzymes are the cause of decreasing

Hg^0 in the water column of freshwater lakes (Siciliano et al. 2002), and in this study we report that adding catalase to filtered VSSW can oxidize Hg^0 (Figure 4.5).

We also supplemented our Hg(II) reduction experiments with 100 nM Cu(II). O_2^- is known to reduce Cu(II) in seawater (Zafiriou et al. 1998, Voelker et al. 2000), and Cu(I) may then reduce Hg(II). We did not observe any increase in dark $^{202}Hg(II)$ reduction by O_2^- in Cu(II) supplemented filtered VSSW solutions (Figure 4.5b).

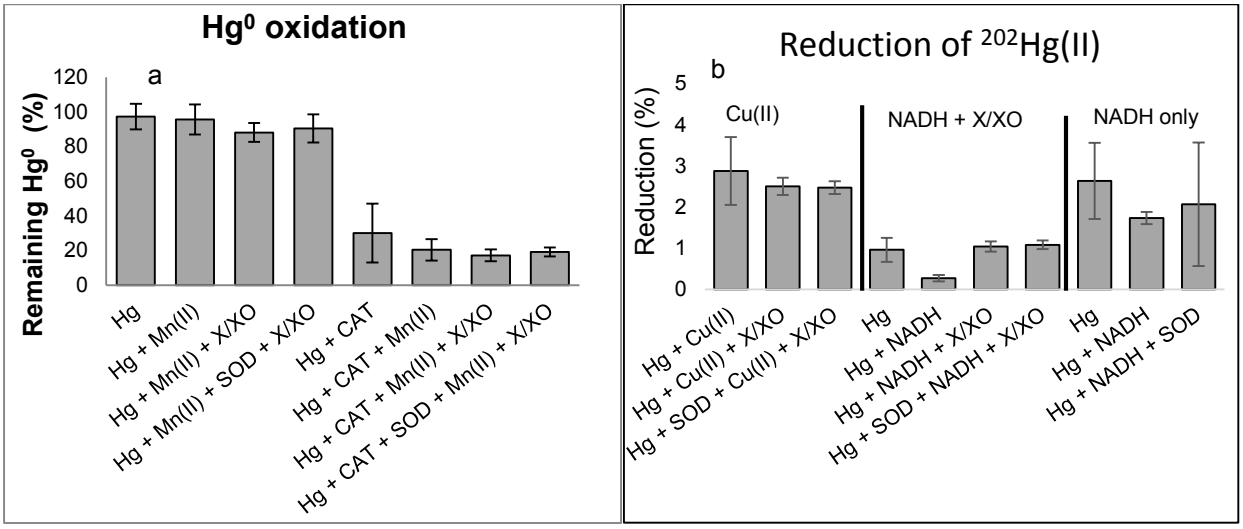

Fig. 4.5 a.) Remaining $^{202}Hg^0$ spike after oxidation: catalase oxidizes a significant portion of the $^{202}Hg^0$ spike when compared to samples without catalase. X/XO and Mn(II) did not appear to oxidize $^{202}Hg^0$ on this day. b.) $^{202}Hg^0$ formed after reduction of $^{202}Hg(II)$: Cu(II) and NADH do not appear to increase the reduction of $^{202}Hg(II)$ when superoxide is added.

NADH (nicotinamide adenine dinucleotide) was also added as a supplement to filtered VSSW samples. NADH can act as a reductant and is also known to produce O_2^- via autoxidation (Diaz et al. 2013), but reduction of $^{202}Hg(II)$ in our NADH amended samples (with and without O_2^- from X/XO) was not statistically significant from natural reduction or SOD controls in filtered VSSW (Figure 4.5b). This could shed light on the mechanisms of dark Hg(II) reduction stimulation by NADH supplements observed when microorganisms were present (Hansel and

Lamborg et al. unpublished data). Exogenous NADH is known to stimulate O_2^- production in microorganisms (Kim et al. 2000, Kustka et al. 2005, Diaz et al. 2013) because of the presence of the membrane-bound enzyme family of NAD(P)H oxidases. Our samples were sterilized by filtering at 0.2 µm, and while filtering could solubilize loosely bound enzymes we did not observe a stimulation of Hg(II) reduction with added NADH. This suggests that the proximity of NADH supplements to cells is important and could increase Hg(II) reduction either through direct reduction or by O_2^- production when microorganisms are present.

4.5 Conclusion

We show that O_2^- can indirectly oxidize a small amount of Hg^0 in VSSW and that O_2^- can sometimes reduce Hg(II) in the dark. The dark reduction rate constant that we measured in one VSSW sample (6.9 ± 3.1 M^{-1} s^{-1}) may be enough to account for the ~1% day^{-1} dark Hg(II) reduction rates observed in other coastal seawater studies. This potentially indicates that O_2^- produced by microorganisms can influence dark Hg cycling in seawater. Future work is needed to determine if additional indirect abiotic reactions of O_2^- can oxidize or reduce Hg outside of our Mn(II) and Cu(II) additions. For example, photoreduction and oxidation of Hg, via they hydroxyl radical (·OH), has been shown in the presence of iron oxides (Lin & Pehkonen 1997). This is most likely through the formation of H_2O_2 via a O_2^- intermediate. H_2O_2 can then react with Fe(II) (formed from other reductants near the oxide surface) to form ·OH. The biological mechanisms of NADH additions in unfiltered seawater is also important to determine if NADH stimulates both biological O_2^- and Hg^0 production simultaneously. Additionally, our study was limited to the coastal Atlantic Ocean which is likely to have higher levels of Hg(II)-organic ligand complexation compared to the open ocean. Lower levels of Hg(II)-organic complexes may allow more dark reduction of Hg(II) by O_2^- in the open ocean.

CHAPTER 5
CONCLUSIONS

ROS are important to natural aquatic environments for many reasons including the breakdown of recalcitrant organic pollutants (Pignatello et al. 2006, Vermilyea & Voelker 2009), microbial cell signaling (Aguirre et al. 2005, Silar 2005, Rose 2012), and oxidizing/reducing biologically important metals like Fe, Cu, and Mn (Moffett & Zika 1987, Sunda & Huntsman 1994, Zafiriou et al. 1998, Voelker et al. 2000, Hansard et al. 2011). ROS may even have influences on regional and global scales, such as when they have been linked to harmful algal bloom fish kills (Oda et al. 1997, Kim et al. 2000, Kim et al. 2004, 2005, Kim et al. 2007) and coral bleaching (Saragosti et al. 2010, Shaked & Armoza-Zvuloni 2013, Armoza-Zvuloni & Shaked 2014). Another globally relevant topic is the dark redox cycling of Hg and how it contributes to the accumulation of the toxic element along the food chain (Amyot et al. 1997, Fitzgerald et al. 2007, Monperrus et al. 2007). Because dark Hg cycling in the ocean is an enigma it is important to determine if ROS production contributes to Hg bioaccumulation. All of these factors make it crucial to understand why and how microorganisms and abiotic processes produce and decompose ROS. Perhaps just as critical is determining the ecological and geochemical stress factors that lead to ROS production and decomposition in natural waters.

We suspect that many of these factors lead to variability of ROS in freshwater. Therefore, one of the first steps in recognizing the environmental implications of ROS was to measure dark production and decay of H_2O_2 in different aquatic systems including oligotrophic and eutrophic waters. Chapter 2 of this thesis establishes, for the first time in freshwater, the variability of both dark H_2O_2 production and decay rates on temporal and spatial scales. A strong correlation of decay with microbial abundance indicators (chlorophyll and microbial cell

numbers) suggests microorganisms are generally good at decomposing H_2O_2 in freshwater. In fact, algal cell counts correlated very well with decay, agreeing with previous studies that suggest algal species are important for keeping oxidative stress levels (e.g. H_2O_2) low in freshwater (Zepp et al. 1992).

However, an excess of nutrients (e.g. phosphorus) often leads to algal blooms and associated microorganisms (Conley et al. 2009). It is possible that changes in microbial consortia associated with blooms are responsible for the variability of P_{H2O2} and weak correlation with biological abundance indicators (chlorophyll and microbial cell numbers). For example, unpublished Voelker group data reveal that some axenic phytoplankton cultures produce less H_2O_2 than those with invasive bacterial cells. However, the nutrients we measured, potentially responsible for algal blooms, generally showed weak correlation with H_2O_2 production and decay, indicating a minor to no influence on biological H_2O_2 processes in freshwater. Given time and resources I would conduct a more in-depth multi-variate analysis to determine if there is a correlation between variations in nutrients and P_{H2O2}. Additionally, I would add killed controls (i.e. autoclaving or inhibitors) to the experiments to help determine whether or not microorganisms or abiotic particles are the true source of ROS. In general, we need to better understand the mechanisms related to biological H_2O_2 production and if ROS are produced as a result of accidental electron transfer reactions or intentionally to obtain biologically important metals or for cell signaling and defense.

The mechanisms of abiotic production of ROS also need to be understood. Both chapters 2 and 3 show evidence of dissolved sources (i.e. free of microorganisms) of H_2O_2 in filtered freshwater. We also show that Suwannee River fulvic acid isolates (SRFA) can produce H_2O_2, most likely through reduced quinone moieties that transfer electrons to dissolved O_2 forming

H_2O_2 via a O_2^- intermediate. Other studies have shown that the hydroxyl radical is produced from humic substances from redox active moieties like hydroquinones (Page et al. 2012, Page et al. 2013), and we suspect it is most likely formed via Fenton-like reactions through an H_2O_2 intermediate. Therefore, I would study the sources of H_2O_2 from reduced humic substances in freshwater. Reduced humic substances may originate in anoxic to suboxic waters and sediments of freshwater lakes and may oxidize, through upwelling to oxic layers, by transferring electrons to O_2 forming ROS (Page et al. 2012, Page et al. 2013). Ultimately, humic substances maybe prove to be an important abiotic source of ROS because of its ability to undergo redox cycling at anoxic/oxic water interfaces.

Many of the dark oxidation and reduction mechanisms of Hg cycling in the ocean remain ambiguous. The redox cycling of Hg is important for various reasons, but one important reason is the production of methylated Hg compounds after Hg(II) is formed (Fitzgerald et al. 2007). It has been shown that the hydroxyl radical (a type of ROS) can oxidize Hg^0 (Gardfeldt et al. 2001), but before this study it was not known if other ROS like O_2^- can also influence the dark redox cycle of Hg. In Chapter 4, we show that, via filtered seawater experiments, dark abiotic O_2^- reduction of Hg(II) and indirect oxidation of Hg^0 may be an important factor for Hg cycling in the ocean. However, unpublished data (Hansel and Lamborg) show that unfiltered NADH amended samples show an increase in O_2^- production and increased Hg(II) reduction. This possibly indicates that a key microbiological component was removed during the filtering process that aids in Hg(II) reduction. A future study is needed to determine the biological mechanism of microbial interactions with NADH and Hg reactions. For example, NADH can be oxidized by cell surface enzymes resulting in O_2^- production that can potentially reduce Hg(II), or NADH close to the cell can potentially directly reduce Hg(II).

REFERENCES CITED

1. Aguirre J, Rios-Momberg M, Hewitt D, Hansberg W (2005) Reactive oxygen species and development in microbial eukaryotes. *Trends in Microbiology* 13:111-118

2. Amyot M, Gill GA, Morel FMM (1997) Production and loss of dissolved gaseous mercury in coastal seawater. *Environmental Science & Technology* 31:3606-3611

3. Andersson ME, Gardfeldt K, Wangberg I, Sprovieri F, Pirrone N, Lindqvist O (2007) Seasonal and daily variation of mercury evasion at coastal and off-shore sites at the Mediterranean Sea. *Marine Chemistry* 107:103-116

4. Andrews SS, Caron S, Zafiriou OC (2000) Photochemical oxygen consumption in marine waters: A major sink for colored dissolved organic matter? *Limnology and Oceanography* 45:267-277

5. Armoza-Zvuloni R, Shaked Y (2014) Release of hydrogen peroxide and antioxidants by the coral Stylophora pistillata to its external milieu. *Biogeosciences* 11:4587-4598

6. Barkay T, Miller SM, Summers AO (2003) Bacterial mercury resistance from atoms to ecosystems. *Fems Microbiology Reviews* 27:355-384

7. Barkay T, Schaefer J (2001) Metal and radionuclide bioremediation: issues, considerations and potentials. *Current Opinion in Microbiology* 4:318-323

8. Barkay T, Turner RR, Vandenbrook A, Liebert C (1991) The relationships of Hg(II) volatilization from a fresh-water pond to the abundance of MER-genes in the gene pool of the indigenous microbial community. *Microbial Ecology* 21:151-161

9. Barkay T, Wagner-Dobler I (2005) Microbial transformations of mercury: Potentials, challenges, and achievements in controlling mercury toxicity in the environment. *Advances in Applied Microbiology* 57:1-52

10. Barlocher F, Gordon J, Ireland RJ (1988) Organic composition of seafoam and its digestion by Corophium volutator (Pallas). *Journal of Experimental Marine Biology and Ecology* 115:179-186

11. Ben-Bassat D, Mayer AM (1977) Reduction of mercury chloride by Chlorella: Evidence for a reducing factor. *Physiologa Plantarum* 40:157-162

12. Bielski BHJ, Cabelli DE, Arudi RL, Ross AB (1985) Reactivity of HO2/O-2 radicals in aqueous solution. *Journal of Physical and Chemical Reference Data* 14:1041-1100

13. Burns JM, Cooper WJ, Ferry JL, King DW, DiMento BP, McNeill K, Miller CJ, Miller WL, Peake BM, Rusak SA, Rose AL, Waite TD (2012) Methods for reactive oxygen species (ROS) detection in aqueous environments. *Aquatic Sciences* 74:683-734

14. Chang C-P, Nagel DJ, Zaghloul ME (2011) Irradiance dependence of photobleaching of resorufin. *Journal of Photochemistry and Photobiology a-Chemistry* 217:430-432

15. Conley DJ, Paerl HW, Howarth RW, Boesch DF, Seitzinger SP, Havens KE, Lancelot C, Likens GE (2009) ECOLOGY Controlling Eutrophication: Nitrogen and Phosphorus. *Science* 323:1014-1015

16. Cooper WJ, Lean DRS (1989) Hydrogen-peroxide concentration in a northern lake – photochemical formation and diel variability. *Environmental Science & Technology* 23:1425-1428

17. Cooper WJ, Moegling JK, Kieber RJ, Kiddle JJ (2000) A chemiluminescence method for the analysis of H_2O_2 in natural waters. *Marine Chemistry* 70:191-200

18. Cooper WJ, Shao CW, Lean DRS, Gordon AS, Scully FE (1994) Factors affecting the distribution of H_2O_2 in surface waters. *Environmental Chemistry of Lakes and Reservoirs* 237:391-422

19. Cooper WJ, Zepp RG (1990) Hydrogen-peroxide decay in waters with suspended soils – evidence for biologically mediated processes. *Canadian Journal of Fisheries and Aquatic Sciences* 47:888-893

20. Cooper WJ, Zika RG, Petasne RG, Plane JMC (1988) Photochemical formation of H_2O_2 in natural-waters exposed to sunlight. *Environmental Science & Technology* 22:1156-1160

21. Craig D, Ireland RJ, Barlocher FJ (1989) Seasonal variation in the organic composition of seafoam. *Journal of Experimental Marine Biology and Ecology* 130:71-80

22. de Laeter JR, Boehlke JK, De Bievre P, Hidaka H, Peiser HS, Rosman KJR, Taylor PDP (2009) Atomic weights of the elements. *Pure and Applied Chemistry* 81:1535-1536

23. Diaz JM, Hansel CM, Voelker BM, Mendes CM, Andeer PF, Zhang T (2013) Widespread Production of Extracellular Superoxide by Heterotrophic Bacteria. *Science* 340:1223-1226

24. Dixon TC, Vermilyea AW, Scott DT, Voelker BM (2013) Hydrogen peroxide dynamics in an agricultural headwater stream: Evidence for significant nonphotochemical production. *Limnology and Oceanography* 58:2133-2144

25. Fantozzi L, Ferrarac R, Frontini FP, Dini F (2009) Dissolved gaseous mercury production in the dark: Evidence for the fundamental role of bacteria in different types of Mediterranean water bodies. *Science of the Total Environment* 407:917-924

26. Fitzgerald WF, Lamborg CH, Hammerschmidt CR (2007) Marine biogeochemical cycling of mercury. *Chemical Reviews* 107:641-662

27. Fitzgerald WF, Mason RP, Vandal GM (1991) Atmospheric cycling and air-water exchange of mercury over midcontinental lacustrine regions. *Water Air and Soil Pollution* 56:745-767

28. Fujii M, Ito H, Rose AL, Waite TD, Omura T (2008) Superoxide-mediated Fe(II) formation from organically complexed Fe(III) in coastal waters. *Geochimica Et Cosmochimica Acta* 72:6079-6089

29. Gajovic-Eichelmann N, Bier FF (2005) Novel electrochemical assay for H2O2 determination in aqueous solutions: A non time-critical method for H2O2 trace level detection. *Electroanalysis* 17:1043-1050

30. Gardfeldt K, Sommar J, Stromberg D, Feng XB (2001) Oxidation of atomic mercury by hydroxyl radicals and photoinduced decomposition of methylmercury in the aqueous phase. *Atmospheric Environment* 35:3039-3047

31. Garg S, Rose AL, Godrant A, Waite TD (2007a) Iron uptake by the ichthyotoxic Chattonella marina (Raphidophyceae): Impact of superoxide generation. *Journal of Phycology* 43:978-991

32. Garg S, Rose AL, Waite TD (2007b) Superoxide mediated reduction of organically complexed Iron(III): Comparison of non-dissociative and dissociative reduction pathways. *Environmental Science & Technology* 41:3205-3212

33. Garg S, Rose AL, Waite TD (2007c) Superoxide-mediated reduction of organically complexed iron(III): Impact of pH and competing cations (Ca2+). *Geochimica Et Cosmochimica Acta* 71:5620-5634

34. Gorris HH, Walt DR (2009) Mechanistic Aspects of Horseradish Peroxidase Elucidated through Single-Molecule Studies. *Journal of the American Chemical Society* 131:6277-6282

35. Hammerschmidt CR, Bowman KL, Tabatchnick MD, Lamborg CH (2011) Storage bottle material and cleaning for determination of total mercury in seawater. *Limnology and Oceanography-Methods* 9:426-431

36. Hansard PS, Easter HD, Voelker BM (2011) Rapid reaction of nanomolar Mn(II) with superoxide radical in seawater and simulated freshwater. *Environmental Science and Technology* 45:2811-2817

37. Hansard SP, Vermilyea AW, Voelker BM (2010) Measurements of superoxide radical concentration and decay kinetics in the Gulf of Alaska. *Deep-Sea Research Part I-Oceanographic Research Papers* 57:1111-1119

38. Heller MI, Croot PL (2010) Application of a superoxide (O-2(-)) thermal source (SOTS-1) for the determination and calibration of O-2(-) fluxes in seawater. *Analytica Chimica Acta* 667:1-13

39. Hintelmann H, Ogrinc N (2003) Determination of stable mercury isotopes by ICP/MS and their application in environmental studies. *Biogeochemistry of Environmentally Important Trace Elements* 835:321-338

40. Kim D, Nakamura A, Okamoto T, Komatsu N, Oda T, Iida T, Ishimatsu A, Muramatsu T (2000) Mechanism of superoxide anion generation in the toxic red tide phytoplankton Chattonella marina: possible involvement of NAD(P)H oxidase. *Biochimica Et Biophysica Acta-General Subjects* 1524:220-227

41. Kim D, Nakashima T, Matsuyama Y, Niwano Y, Yamaguchi K, Oda T (2007) Presence of the distinct systems responsible for superoxide anion and hydrogen peroxide generation in red tide phytoplankton Chattonella marina and Chattonella ovata. *Journal of Plankton Research* 29:241-247

42. Kim D, Watanabe M, Nakayasu Y, Kohata K (2004) Production of superoxide anion and hydrogen peroxide associated with cell growth of Chattonella antiqua. *Aquatic Microbial Ecology* 35:57-64

43. Kim D, Watanabe M, Nakayasu Y, Kohata K (2005) Changes in O-2(-) and H2O2 production by Chattonella antiqua during diel vertical migration under nutrient stratification. *Aquatic Microbial Ecology* 39:183-191

44. Kim J, Fitzgerald W (1988) Gaseous mercury profiles in the tropical Pacific-ocean. *Geophysical Research Letters* 15:40-43

45. Kustka AB, Shaked Y, Milligan AJ, King DW, Morel FMM (2005) Extracellular production of superoxide by marine diatoms: Contrasting effects on iron redox chemistry and bioavailability. *Limnology and Oceanography* 50:1172-1180

46. Lalonde JD, Amyot M, Kraepiel AML, Morel FMM (2001) Photooxidation of Hg(0) in artificial and natural waters (vol 35, pg 1372, 2001). *Environmental Science & Technology* 35:4961-4961

47. Lalonde JD, Amyot M, Orvoine J, Morel FMM, Auclair JC, Ariya PA (2004) Photoinduced oxidation of Hg-0 (aq) in the waters from the St. Lawrence estuary. *Environmental Science & Technology* 38:508-514

48. Lamborg CH, Hammerschmidt CR, Gill GA, Mason RP, Gichuki S (2012) An intercomparison of procedures for the determination of total mercury in seawater and recommendations regarding mercury speciation during GEOTRACES cruises. *Limnology and Oceanography-Methods* 10:90-100

49. Lanzillotta E, Ceccarini C, Ferrara R, Dini F, Frontini E, Banchetti R (2004) Importance of the biogenic organic matter in photo-formation of dissolved gaseous mercury in a culture of the marine diatom Chaetoceros sp. *Science of the Total Environment* 318:211-221

50. Learman DR, Voelker BM, Madden AS, Hansel CM (2013) Constraints on superoxide mediated formation of manganese oxides. *Frontiers in Microbiology* 4

51. Learman DR, Voelker BM, Vazquez-Rodriguez AI, Hansel CM (2011) Formation of manganese oxides by bacterially generated superoxide. *Nature Geos*cience 4:95-98

52. Lin CJ, Pehkonen SO (1997) Aqueous free radical chemistry of mercury in the presence of iron oxides and ambient aerosol. *Atmospheric Environment* 31:4125-4137

53. Lin CJ, Pehkonen SO (1999) Aqueous phase reactions of mercury with free radicals and chlorine: Implications for atmospheric mercury chemistry. *Chemosphere* 38:1253-1263

54. Liu W, Au DWT, Anderson DM, Lam PKS, Wu RSS (2007) Effects of nutrients, salinity, pH and light : dark cycle on the production of reactive oxygen species in the alga Chattonella marina. *Journal of Experimental Marine Biology and Ecology* 346:76-86

55. Lovley DR, Coates JD, BluntHarris EL, Phillips EJP, Woodward JC (1996) Humic substances as electron acceptors for microbial respiration. *Nature* 382:445-448

56. Magos L, Halbach S, Clarkson TW (1978) Role of catalase in the oxidation of mercury vapor. *Biochemical Pharmacology* 27:1373-1377

57. Marshall JA, de Salas M, Oda T, Hallegraeff G (2005) Superoxide production by marine microalgae. *Marine Biology* 147:533-540

58. Marsico RM, Schneider RJ, Voelker BM, Zhang T, Diaz JM, Hansel CM, Ushijima S (2015) Spatial and temporal variability of widespread dark production and decay of hydrogen peroxide in freshwater. *Aquatic Sciences* DOI 10.1007/s00027-015-0399-2

59. Mason RP, Choi AL, Fitzgerald WF, Hammerschmidt CR, Lamborg CH, Soerensen AL, Sunderland EM (2012) Mercury biogeochemical cycling in the ocean and policy implications. *Environmental Research* 119:101-117

60. Mason RP, Morel FMM, Hemond HF (1995) The role of microorganisms in elemental mercury formation in natural. *Water Air and Soil Pollution* 80:775-787

61. Mishin V, Gray JP, Heck DE, Laskin DL, Laskin JD (2010) Application of the Amplex red/horseradish peroxidase assay to measure hydrogen peroxide generation by recombinant microsomal enzymes. *Free Radical Biology and Medicine* 48:1485-1491

62. Moffett JW, Zika RG (1987) Reaction-kinetics of hydrogen-peroxide with copper and iron in seawater. *Environmental Science & Technology* 21:804-810

63. Mohanty JG, Jaffe JS, Schulman ES, Raible DG (1997) A highly sensitive fluorescent micro-assay of H_2O_2 release from activated human leukocytes using a dihydroxyphenoxazine derivative. *Journal of Immunological Methods* 202:133-141

64. Monperrus M, Tessier E, Amouroux D, Leynaert A, Huonnic P, Donard OFX (2007) Mercury methylation, demethylation and reduction rates in coastal and marine surface waters of the Mediterranean Sea. *Marine Chemistry* 107:49-63

65. Munthe J, McElroy WJ (1992) Some aqueous reactions of potential importance in the atmospheric chemistry of mercury. *Atmospheric Environment Part a-General Topics* 26:553-557

66. Oda T, Nakamura A, Shikayama M, Kawano I, Ishimatsu A, Muramatsu T (1997) Generation of reactive oxygen species by raphidophycean phytoplankton. *Bioscience Biotechnology and Biochemistry* 61:1658-1662

67. Page SE, Kling GW, Sander M, Harrold KH, Logan JR, McNeill K, Cory RM (2013) Dark Formation of Hydroxyl Radical in Arctic Soil and Surface Waters. *Environmental Science & Technology* 47:12860-12867

68. Page SE, Sander M, Arnold WA, McNeill K (2012) Hydroxyl Radical Formation upon Oxidation of Reduced Humic Acids by Oxygen in the Dark. *Environmental Science & Technology* 46:1590-1597

69. Parker JL, Bloom NS (2005) Preservation and storage techniques for low-level aqueous mercury speciation. *Science of the Total Environment* 337:253-263

70. Pflug W (1980) Effect of humica acids on the activity of 2 peroxidases. *Zeitschrift Fur Pflanzenernahrung Und Bodenkunde* 143:432-440

71. Pignatello JJ, Oliveros E, MacKay A (2006) Advanced oxidation processes for organic contaminant destruction based on the Fenton reaction and related chemistry. *Critical Reviews in Environmental Science and Technology* 36:1-84

72. Poulain AJ, Garcia E, Amyot M, Campbell PGC, Raofie F, Ariya PA (2007a) Biological and chemical redox transformations of mercury in fresh and salt waters of the high arctic during spring and summer. *Environmental Science & Technology* 41:1883-1888

73. Poulain AJ, Ni Chadhain SM, Ariya PA, Amyot M, Garcia E, Campbell PGC, Zylstra GJ, Barkay T (2007b) Potential for mercury reduction by microbes in the high arctic. *Applied and Environmental Microbiology* 73:2230-2238

74. Qureshi A, O'Driscoll NJ, MacLeod M, Neuhold YM, Hungerbuhler K (2010) Photoreactions of Mercury in Surface Ocean Water: Gross Reaction Kinetics and Possible Pathways. *Environmental Science & Technology* 44:644-649

75. Reszka KJ, Wagner BA, Burns CP, Britigan BE (2005) Effects of peroxidase substrates on the Amplex red/peroxidase assay: Antioxidant properties of anthracyclines. *Analytical Biochemistry* 342:327-337

76. Rhee SG, Chang TS, Jeong W, Kang D (2010) Methods for detection and measurement of hydrogen peroxide inside and outside of cells. *Molecules and Cells* 29:539-549

77. Richard LE, Peake BM, Rusak SA, Cooper WJ, Burritt DJ (2007) Production and decomposition dynamics of hydrogen peroxide in freshwater. *Environmental Chemistry* 4:49-54

78. Rodrigues JV, Gomes CM (2010) Enhanced superoxide and hydrogen peroxide detection in biological assays. *Free Radical Biology and Medicine* 49:61-66

79. Rolfhus KR, Fitzgerald WF (2004) Mechanisms and temporal variability of dissolved gaseous mercury production in coastal seawater. *Marine Chemistry* 90:125-136

80. Rose AL (2012) The influence of extracellular superoxide on iron redox chemistry and bioavailability to aquatic microorganisms. *Frontiers in Microbiology* 3:1-21

81. Rose AL, Godrant A, Furnas M, Waite TD (2010) Dynamics of nonphotochemical superoxide production and decay in the Great Barrier Reef lagoon. *Limnology and Oceanography* 55:1521-1536

82. Saragosti E, Tchernov D, Katsir A, Shaked Y (2010) Extracellular Production and Degradation of Superoxide in the Coral Stylophora pistillata and Cultured Symbiodinium. *Plos One* 5:1-10

83. Schilling K, Zessner M (2011) Foam in the aquatic environment. *Water Research* 45:4355-4366

84. Scully NM, Lean DRS, McQueen DJ, Cooper WJ (1995) Photochemical formation of hydrogen peroxide in lakes: Effects of dissolved organic carbon and ultraviolet radiation. *Canadian Journal of Fisheries and Aquatic Sciences* 52:2675-2681

85. Serrano J, Jove M, Boada J, Bellmunt MJ, Pamplona R, Portero-Otin M (2009) Dietary antioxidants interfere with Amplex Red-coupled-fluorescence assays. *Biochemical and Biophysical Research Communications* 388:443-449

86. Shaked Y, Armoza-Zvuloni R (2013) Dynamics of hydrogen peroxide in a coral reef: Sources and sinks. *Journal of Geophysical Research-Biogeosciences* 118:1793-1801

87. Sharpless CM, Aeschbacher M, Page SE, Wank J, Sander M, McNeill K (2014) Photo-oxidation induced changes in optical, electrochemical, and photochemical properties of humic substances. *Environmental Science & Technology* 48:2688-2696

88. Siciliano SD, O'Driscoll NJ, Learn DRS (2002) Microbial reduction and oxidation of mercury in freshwater lakes. *Environmental Science & Technology* 36:3064-3068

89. Silar P (2005) Peroxide accumulation and cell death in filamentous fungi induced by contact with a contestant. *Mycological Research* 109:137-149

90. Smith T, Pitts K, McGarvey JA, Summers AO (1998) Bacterial oxidation of mercury metal vapor, Hg(0). *Applied and environmental microbiology* 64:1328-1332

91. Snyrychova I, Ayaydin F, Hideg E (2009) Detecting hydrogen peroxide in leaves in vivo - a comparison of methods. *Physiologia Plantarum* 135:1-18

92. Suggett DJ, Warner ME, Smith DJ, Davey P, Hennige S, Baker NR (2008) Photosynthesis and production of hydrogen peroxide by Symbiodinium (Pyrrhophyta) phylotypes with different thermal tolerances. *Journal of Phycology* 44:948-956

93. Sunda WG, Huntsman SA (1994) Photoreduction of manganese oxides in seawater. *Marine Chemistry* 46:133-152

94. Taujale S, Zhang HC (2012) Impact of Interactions between Metal Oxides to Oxidative Reactivity of Manganese Dioxide. *Environmental Science & Technology* 46:2764-2771

95. Towne V, Will M, Oswald B, Zhao QJ (2004) Complexities in horseradish peroxidase-catalyzed oxidation of dihydroxyphenoxazine derivatives: appropriate ranges for pH values and hydrogen peroxide concentrations in quantitative analysis. *Analytical Biochemistry* 334:290-296

96. USEPA (2014) EPA On-line Tools for Site Assessment Calculation. Accessed August 3, 2015. www.epa.gov/athens/learn2model/part-two/onsite/esthenry.html

97. Vermilyea AW, Dixon TC, Voelker BM (2010a) Use of (H2O2)-O-18 to measure absolute rates of dark H_2O_2 production in freshwater systems. *Environmental Science & Technology* 44:3066-3072

98. Vermilyea AW, Hansard SP, Voelker BM (2010b) Dark production of hydrogen peroxide in the Gulf of Alaska. *Limnology and Oceanography* 55:580-588

99. Vermilyea AW, Voelker BM (2009) Photo-Fenton Reaction at Near Neutral pH. *Environmental Science & Technology* 43:6927-6933

100. Voelker BM, Sedlak DL, Zafiriou OC (2000) Chemistry of superoxide radical in seawater: Reactions with organic Cu complexes. *Environmental Science & Technology* 34:1036-1042

101. Votyakova TV, Reynolds IJ (2004) Detection of hydrogen peroxide with Amplex Red: interference by NADH and reduced glutathione auto-oxidation. *Archives of Biochemistry and Biophysics* 431:138-144

102. Waite TD, Godrant A, Fujii M, Rose AL (2009) Superoxide-mediated transformations of iron by cyanobacterial prokaryotes. *Geochimica Et Cosmochimica A*cta 73:A1400-A1400

103. Waite TD, Rose AL, Garg S, Fujii M (2006) Superoxide-mediated reduction of ferric iron in natural aquatic systems. *Geochimica Et Cosmochimica Acta* 70:A681-A681

104. Wetzel RG (1992) Gradient-dominated ecosystems – Sources and regulatory functions of dissolved organic-matter in fresh-water. *Hydrobiologia* 229:181-198

105. Whalin L, Kim EH, Mason R (2007) Factors influencing the oxidation, reduction, methylation and demethylation of mercury species in coastal waters. *Marine Chemistry* 107:278-294

106. Whalin LM, Mason RP (2006) A new method for the investigation of mercury redox chemistry in natural waters utilizing deflatable Teflon (R) bags and additions of isotopically labeled mercury. *Analytica Chimica Acta* 558:211-221

107. Wigfield DC, Perkins SL (1985) Oxidation of elemental mercury by hydroperoxides in aqueous solutions. *Canadian Journal of Chemistry-Revue Canadienne De Chimie* 63:275-277

108. Wu JF, Roshan S, Chen G (2014) The distribution of dissolved manganese in the tropical-subtropical North Atlantic during US GEOTRACES 2010 and 2011 cruises. *Marine Chemistry* 166:9-24

109. Zafiriou OC, Voelker BM, Sedlak DL (1998) Chemistry of the superoxide radical (O-2(-)) in seawater: Reactions with inorganic copper complexes. *Journal of Physical Chemistry A* 102:5693-5700

110. Zepp RG, Skurlatov YI, Ritmiller LF (1988) Effects of aquatic humic substances on analysis for hydrogen-peroxide using peroxidase-catalyzed oxidations of triarylmethanes or para-hydroxyphenylacetic acid. *Environmental Technology Letters* 9:287-298

111. Zhang T, Hansel CM, Voelker BM, Lamborg CH Extensive dark biological production of reactive oxygen species in brackish and freshwater ponds. *Under review: Global Biogeochemical Cycles*

112. Zhao B, Ranguelova K, Jiang J, Mason RP (2011) Studies on the photosensitized reduction of resorufin and implications for the detection of oxidative stress with Amplex Red. *Free Radical Biology and Medicine* 51:153-159

113. Zhao BZ, Summers FA, Mason RP (2012) Photooxidation of Amplex red to resorufin: Implications of exposing the Amplex red assay to light. *Free Radical Biology and Medicine* 53:1080-1087

114. Zhao JM, Huggins FE, Feng Z, Huffman GP (1994) Ferrihydrite-surface-structure and its effects on phase-transformation. *Clays and Clay Minerals* 42:737-746

115. Zhou MJ, Diwu ZJ, PanchukVoloshina N, Haugland RP (1997) A stable nonfluorescent derivative of resorufin for the fluorometric determination of trace hydrogen peroxide: Applications in detecting the activity of phagocyte NADPH oxidase and other oxidases. *Analytical Biochemistry* 253:162-168

APPENDIX A
SUPPLEMENTARY DATA FOR CHAPTER 2:
SPATIAL AND TEMPORAL VARIABILITY OF WIDESPREAD DARK PRODUCTION AND DECAY OF HYDROGEN PEROXIDE IN FRESHWATER

A.1 – Description of Appendix A

Appendix A is an electronic supplementary material file submitted with the journal article "Spatial and Temporal Variability of Widespread Dark Production and Decay of Hydrogen Peroxide in Freshwater" accepted by *Aquatic Sciences* (Chapter 2 of this Thesis). It includes pH, water temperature, and conductivity (Table A.1) as well as the auxiliary geochemical data (Table A.2). Table A.3 contains correlation values (R) of the auxiliary geochemical data with P_{H2O2} and $k_{loss,H2O2}$. Figure A.1 contains microbial cell counts per mL from unfiltered freshwater while Table A.4 lists cell counts per mL of filtered freshwater from select field sites. Figures A.2 and A.3 are maps of the field sites with listed coordinates.

Table A.1 pH, water temperature (T_w), and conductivity (µS, microsiemens) for field sites analyzed for dark production and dark decay rates of hydrogen peroxide

Site	Date	pH	T_w (°C)	Conductivity (µS)
Badger Creek	7/25/2011	N/A	N/A	N/A
Bijou Creek	7/25/2011	N/A	N/A	N/A
Box Elder Creek	7/25/2011	N/A	N/A	N/A
Cold Spring, (N. Boulder Creek)	8/03/2011	N/A	N/A	N/A
Barker Reservoir	8/03/2011	N/A	N/A	N/A
Clear Creek UP	8/10/2011	N/A	N/A	N/A
Clear Creek DOWN	8/10/2011	N/A	N/A	N/A
Crown Hill Lake	8/23/2011	N/A	27.0	N/A
Crown Hill Lake	9/29/2011	9.75	22.0	210
Sloan's Lake	10/06/2011	9.20	N/A	960
S. Pawnee Creek	10/09/2011	9.38	11.5	3200
Boulder Creek	10/17/2011	8.70	8.6	70
Assabet River	10/18/2011	5.32	13.7	431
Lake Boon	10/18/2011	4.55	16.5	237
Santuit Pond	11/01/2011	3.44	9.3	58
John's Pond	11/01/2011	5.21	13.1	63
Ashumet Pond	11/04/2011	5.47	12.1	67
Sloan's Lake	5/23/2012	8.80	22.0	710
Sloan's Lake	6/14/2012	8.90	25.3	670
Sloan's Lake	6/20/2012	8.55	23.5	670
Sloan's Lake	7/11/2012	8.26	24.0	660
Crown Hill Lake	7/16/2012	9.42	27.7	240
Mirror Lake	7/18/2012	8.80	21.2	90
Sloan's Lake	7/25/2012	9.20	26.8	620
Mirror Lake	8/01/2012	10.20	26.2	90
Mirror Lake	8/10/2012	10.00	23.9	100
Mirror Lake	8/17/2012	8.55	22.6	100
Mirror Lake	8/24/2012	8.69	20.3	100
Sloan’s Lake	8/29/2012	N/A	N/A	N/A
Sloan's Lake	9/04/2012	9.06	22.0	660
Sloan's Lake	9/11/2012	9.16	28.2	660
Sloan's Lake	9/20/2012	8.90	24.3	690
Sloan's Lake	9/11/2012	9.01	23.5	730
Sloan's Lake	9/20/2012	9.01	19.8	680

Table A.2 Geochemical parameters (all in ppm) measured at each field site at the date shown. Metals with an asterisk next to them are dissolved metals measured by ICP-AES. † symbol means measurement by a V2000 spectrometer and ^ symbol means measurement by ion chromatography. DOC is dissolved organic carbon. DO is dissolved oxygen. BDL is below detection limit. Nitrogen species concentrations are in ppm N of the particular species (ex. NO_2^--N ppm = parts per million nitrogen, N, of nitrate)

Site	Date	Fe*	Mn*	Al*	Cu*	Fe(II)†	Chl (SD)
*Dissolved metals measured by ICP-AES; †Measured by 2000 Spectrometer (^) Measured by Ion Chromatography SD = standard deviation							
Badger Creek	7/25/2011	N/A	N/A	N/A	N/A	N/A	N/A
Bijou Creek	7/25/2011	N/A	N/A	N/A	N/A	N/A	N/A
Box Elder Creek	7/25/2011	N/A	N/A	N/A	N/A	N/A	N/A
Cold Spring, N. Boulder Creek	8/03/2011	N/A	N/A	N/A	N/A	N/A	N/A
Barker Reservoir	8/03/2011	N/A	N/A	N/A	N/A	N/A	N/A
Clear Creek UP	8/10/2011	N/A	N/A	N/A	N/A	N/A	N/A
Clear Creek DOWN	8/10/2011	N/A	N/A	N/A	N/A	N/A	N/A
Crown Hill Lake	8/23/2011	N/A	N/A	N/A	N/A	N/A	0.017 (0.004)
Crown Hill Lake	9/29/2011	N/A	N/A	N/A	N/A	0.04	0.015 (0.0002)
Sloan's Lake	10/06/2011	N/A	0.001	N/A	N/A	0.22	0.054 (0.004)
S. Pawnee Creek	10/09/2011	N/A	0.005	N/A	N/A	N/A	0.018 (0.002)
Boulder Creek	10/17/2011	0.079	0.003	N/A	N/A	0.07	0.005 (0.002)
Assabet River	10/18/2011	0.363	0.053	N/A	0.003	0.02	0.005 (0.003)
Lake Boon	10/18/2011	0.058	0.041	N/A	0.009	BDL	0.018 (0.002)
Santuit Pond	11/01/2011	0.062	0.011	N/A	0.002	BDL	0.072 (0.002)
John's Pond	11/01/2011	0.023	0.003	N/A	0.002	BDL	0.005 (0.002)
Ashumet Pond	11/04/2011	0.036	0.141	N/A	0.003	BDL	0.004 (0.003)
Sloan's Lake	5/23/2012	N/A	0.004	0.152	0.005	0.47	0.064 (0.008)
Sloan's Lake	6/14/2012	N/A	0.058	0.005	0.006	0.58	0.060 (0.006)
Sloan's Lake	6/20/2012	N/A	0.010	0.006	0.004	0.92	0.081 (0.014)
Mirror Lake	7/11/2012	1.270	0.260	0.090	0.001	0.18	0.083 (0.006)
Sloan's Lake	7/16/2012	N/A	0.003	0.014	0.003	0.59	0.159 (0.009)
Mirror Lake	7/18/2012	1.19	0.210	0.050	0.001	0.28	0.289 (0.005)
Mirror Lake	7/25/2012	1.71	0.240	0.060	0.002	0.55	0.281 (0.003)
Mirror Lake	8/01/2012	1.82	0.200	0.140	0.003	0.31	0.104 (0.004)
Mirror Lake	8/10/2012	2.86	0.350	0.090	0.001	0.47	0.159 (0.013)
Sloan's Lake	8/17/2012	N/A	0.004	0.036	0.003	N/A	0.274 (0.096)
Sloan's Lake	8/24/2012	N/A	0.003	0.035	0.003	0.34	0.083 (0.014)
Sloan's Lake	8/29/2012	N/A	0.003	0.032	0.002	1.36	1.01 (0.043)

Table A.2 Continued

Sloan's Lake	9/04/2012	N/A	0.002	0.033	0.002	0.70	0.085 (0.008)
Sloan's Lake	9/11/2012	N/A	N/A	N/A	N/A	0.31	0.024 (0.006)
Sloan's Lake	9/20/2012	N/A	N/A	N/A	N/A	0.33	0.056 (.002)
Site	**Date**	**DOC**	**DO†**	**NO_2^--N †**	**NO_3^--N †**	**NH_3-N †**	**PO_4^{3-} †**
Badger Creek	7/25/2011	N/A	N/A	N/A	N/A	N/A	N/A
Bijou Creek	7/25/2011	N/A	N/A	N/A	N/A	N/A	N/A
Box Elder Creek	7/25/2011	N/A	N/A	N/A	N/A	N/A	N/A
Cold Spring, N. Boulder Creek	8/03/2011	N/A	N/A	N/A	N/A	N/A	N/A
Barker Reservoir	8/03/2011	N/A	N/A	N/A	N/A	N/A	N/A
Clear Creek UP	8/10/2011	N/A	N/A	N/A	N/A	N/A	N/A
Clear Creek DOWN	8/10/2011	N/A	N/A	N/A	N/A	N/A	N/A
Crown Hill Lake	8/23/2011	N/A	N/A	0.04	0.12	0.32	0.077
Crown Hill Lake	9/29/2011	3.01	9.14	0.05	N/A	N/A	0.06
Sloan's Lake	10/06/2011	7.83	6.14	0.05	0.09	0.47	0.23
S. Pawnee Creek	10/09/2011	12.71	9.40	0.02	0.12	0.38	0.00
Assabet River	10/18/2011	7.25	10.00	0.02	0.32	2.89	0.05
Boulder Creek	10/17/2011	2.43	8.61	0.01	0.00	N/A	0.17
Lake Boon	10/18/2011	3.09	8.90	0.02	0.08	3.82	0.00
Santuit Pond	11/01/2011	3.32	11.00	0.02	0.28	N/A	0.02
John's Pond	11/01/2011	1.53	10.10	0.01	0.15	0.07	0.01
Ashumet Pond	11/04/2011	1.51	9.50	0.01	0.15	0.46	0.00
Sloan's Lake	5/23/2012	9.18	9.13	0.08	0.00	0.50	0.40
Sloan's Lake	6/14/2012	8.78	7.02	0.08	0.08	0.52	1.15
Sloan's Lake	6/20/2012	8.51	6.93	0.12	0.11	1.27	0.84
Mirror Lake	7/11/2012	11.86	7.43	0.04	0.03	0.64	0.29
Sloan's Lake	7/16/2012	9.29	10.12	0.12	0.25	1.19	0.57
Mirror Lake	7/18/2012	12.83	8.99	0.05	0.10	1.03	0.34
Mirror Lake	7/25/2012	13.57	10.78	0.08	0.00	0.99	1.03
Mirror Lake	8/01/2012	13.87	6.64	0.08	0.05	1.01	0.45
Mirror Lake	8/10/2012	13.51	7.57	0.07	0.01	0.69	0.49
Sloan's Lake	8/17/2012	N/A	N/A	N/A	N/A	N/A	N/A
Sloan's Lake	8/24/2012	8.69	7.39	0.07	0.12	0.44	0.50
Sloan's Lake	8/29/2012	8.85	9.77	0.12	0.16	1.18	1.33
Sloan's Lake	9/04/2012	6.73	9.21	0.08	0.15	1.08	0.61
Sloan's Lake	9/11/2012	4.13	8.38	0.05	0.13	0.79	0.18
Sloan's Lake	9/20/2012	9.13	9.65	0.08	0.07	0.36	0.30
Site	**Date**	**F^- ^**	**Cl^- ^**	**Br^- ^**	**NO_3^--N ^**	**PO_4^{3-} ^**	**SO_4^{2-} ^**
Badger Creek	7/25/2011	N/A	N/A	N/A	N/A	N/A	N/A
Bijou Creek	7/25/2011	N/A	N/A	N/A	N/A	N/A	N/A

Table A.2 Continued

Box Elder Creek	7/25/2011	N/A	N/A	N/A	N/A	N/A	N/A
Cold Spring, N. Boulder Creek	8/03/2011	N/A	N/A	N/A	N/A	N/A	N/A
Barker Reservoir	8/03/2011	N/A	N/A	N/A	N/A	N/A	N/A
Clear Creek UP	8/10/2011	N/A	N/A	N/A	N/A	N/A	N/A
Clear Creek DOWN	8/10/2011	N/A	N/A	N/A	N/A	N/A	N/A
Crown Hill Lake	8/23/2011	0.56	12.53	BDL	0.08	BDL	32.84
Crown Hill Lake	9/29/2011	0.43	10.74	BDL	BDL	BDL	35.47
Sloan's Lake	10/06/2011	BDL	12.40	0.1	0.05	BDL	64.58
S. Pawnee Creek	10/09/2011	0.41	56.00	0.3	0.02	1.9	BDL
Assabet River	10/18/2011	0.07	61.00	BDL	0.60	BDL	5.80
Boulder Creek	10/17/2011	0.09	0.52	BDL	0.07	BDL	7.04
Lake Boon	10/18/2011	BDL	25.70	BDL	0.10	BDL	3.30
Santuit Pond	11/01/2011	BDL	14.27	BDL	0.27	BDL	4.38
John's Pond	11/01/2011	BDL	13.80	BDL	0.07	BDL	5.55
Ashumet Pond	11/04/2011	BDL	16.60	BDL	0.07	BDL	7.63
Sloan's Lake	5/23/2012	0.71	74.69	0.1	0.04	BDL	92.81
Sloan's Lake	6/14/2012	0.69	69.00	0.1	0.14	BDL	87.63
Sloan's Lake	6/20/2012	0.77	67.18	0.1	0.16	BDL	86.25
Mirror Lake	7/11/2012	0.28	2.88	BDL	0.05	BDL	2.37
Sloan's Lake	7/16/2012	0.74	61.29	BDL	0.22	BDL	74.52
Mirror Lake	7/18/2012	0.27	2.79	BDL	0.03	BDL	2.83
Mirror Lake	7/25/2012	0.27	3.22	BDL	BDL	BDL	2.73
Mirror Lake	8/01/2012	0.29	3.20	BDL	BDL	BDL	2.42
Mirror Lake	8/10/2012	0.29	3.41	BDL	BDL	BDL	2.24
Sloan’s Lake	8/17/2012	0.83	67.85	BDL	BDL	BDL	86.16
Sloan's Lake	8/24/2012	0.80	69.11	0.15	0.03	BDL	88.61
Sloan's Lake	8/29/2012	0.86	70.10	0.01	BDL	BDL	91.95
Sloan’s Lake	9/04/2012	0.88	73.68	BDL	BDL	BDL	96.96
Sloan’s Lake	9/11/2012	N/A	N/A	N/A	N/A	N/A	N/A
Sloan’s Lake	9/20/2012	N/A	N/A	N/A	N/A	N/A	N/A

Table A.3 Correlation values (R) computed by Excel for the dark production rates of H_2O_2 (P_{H2O2}) and dark decay rates ($k_{loss,H2O2}$) with geochemical parameters. The metals are of dissolved species. DOC is dissolved organic carbon. DO is dissolved oxygen. Any correlation reported as N/A either had insufficient data or a portion of the data was reported as below detection limit (BDL) and therefore a correlation value could not be established. Exceptions for N values: N =7 for P and k with F^-, Cl^-, and SO_4^{2-} at Sloan's Lake

*Dissolved metals measured by ICP-AES;
†Measured by 2000 Spectrometer
(^) Measured by Ion Chromatography

	Colorado 2011 (N = 5)		Massachusetts 2011 (N = 5)		Sloan's Lake 2012 (N =9)		Mirror Lake 2012 (N = 5)	
Parameter	**P**	**k**	**P**	**k**	**P**	**k**	**P**	**k**
Chl	-0.18	0.98	0.82	-0.23	0.35	0.98	0.89	0.97
Fe*	-0.77	-0.27	-0.48	-0.21	N/A	N/A	0.23	-0.28
Mn*	-0.42	0.97	-0.71	-0.54	-0.48	-0.21	0.16	-0.21
Al*	N/A	N/A	N/A	N/A	-0.14	-0.2	-0.71	-0.85
Cu*	N/A	N/A	-0.28	0.41	-0.63	-0.43	-0.3	-0.37
DOC	0.01	0.45	-0.32	0.05	0.32	0.09	0.39	0.06
NO_2^- (†)	0.52	0.52	0.13	0.73	0.27	0.46	0.26	-0.06
NO_3^- (†)	0.92	0.32	0.13	0.02	0.56	0.26	0.11	0.4
NH_3 (†)	-0.77	0.98	-0.38	0.79	0.54	0.47	0.41	0.54
PO_4^{3-} (†)	-0.68	0.54	-0.14	-0.1	-0.01	0.66	0.43	0.3
Fe(II) (†)	-0.48	0.96	-0.51	-0.31	0.43	0.85	0.65	0.31
DO (†)	0.5	-0.87	0.71	0.23	0.53	0.35	0.67	0.78
F^- (^)	N/A	N/A	N/A	N/A	0.62	0.59	-0.47	-0.81
Cl^- (^)	0.26	0.26	-0.56	-0.21	-0.12	0.14	0.16	-0.32
Br^- (^)	N/A	N/A	N/A	N/A	-0.48	-0.92	N/A	N/A
N-NO_3 (^)	N/A	N/A	-0.11	-0.02	0.02	0.34	N/A	N/A
PO_4^{3-} (^)	N/A	N/A	N/A	N/A	N/A	N/A	N/A	N/A
SO_4^{2-} (^)	N/A	N/A	-0.04	-0.75	-0.04	0.3	0.55	0.86

Table A.4 Microbial cell counts per mL of filtered samples. The 'percent (%) cells retentate' column reflect the percentage of cells that were removed by the filtering process

Organism	Filtered Cell Count	% Cells (retentate)	Date / Site
Bacteria	6.1E+03	99	7/19/2012
Algae	0.0E+00	100	Mirror Lake
Cyanobacteria	0.0E+00	100	
Bacteria	3.1E+04	96	8/17/2012
Algae	0.0E+00	100	Sloan's Lake
Cyanobacteria	0.0E+00	100	
Bacteria	2.0E+03	>99	8/24/2012
Algae	0.0E+00	100	Sloan's Lake
Cyanobacteria	0.0E+00	100	
Bacteria	2.0E+03	>99	8/30/2012
Algae	0.0E+00	100	Sloan's Lake
Cyanobacteria	0.0E+00	100	
Bacteria	3.1E+03	>99	9/4/2012
Algae	0.0E+00	100	Sloan's Lake
Cyanobacteria	0.0E+00	100	
Total bacteria	3.1E+03	>99	9/11/2012
Algae	0.0E+00	100	Sloan's Lake
Cyanobacteria	0.0E+00	100	
Bacteria	3.1E+03	>99	9/20/2012
Algae	0.0E+00	100	Sloan's Lake
Cyanobacteria	0.0E+00	100	

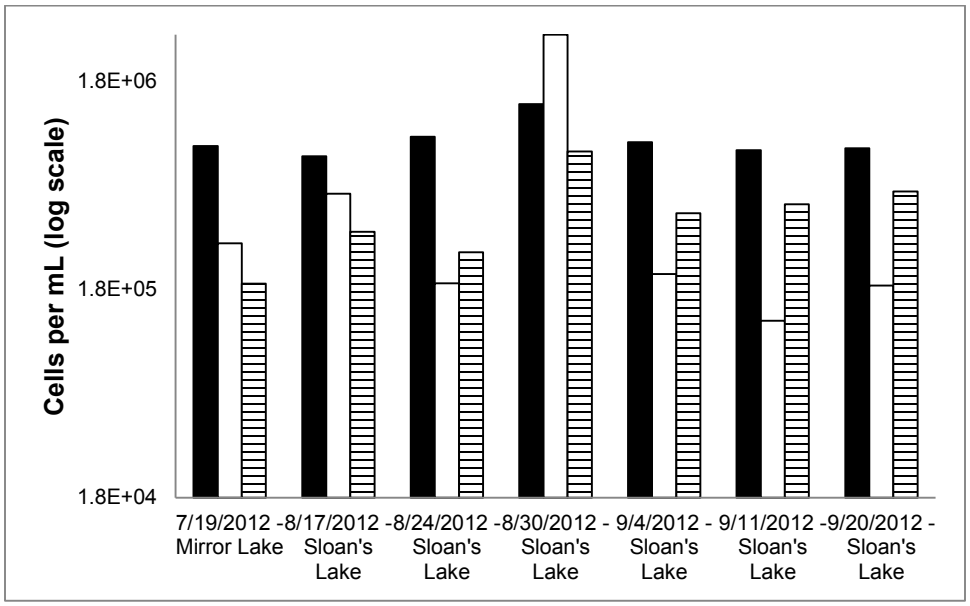

Fig. A.1 Microbial cell counts per mL of unfiltered samples: bacteria (black bars), algae (white bars), and cyanobacteria (striped bars).

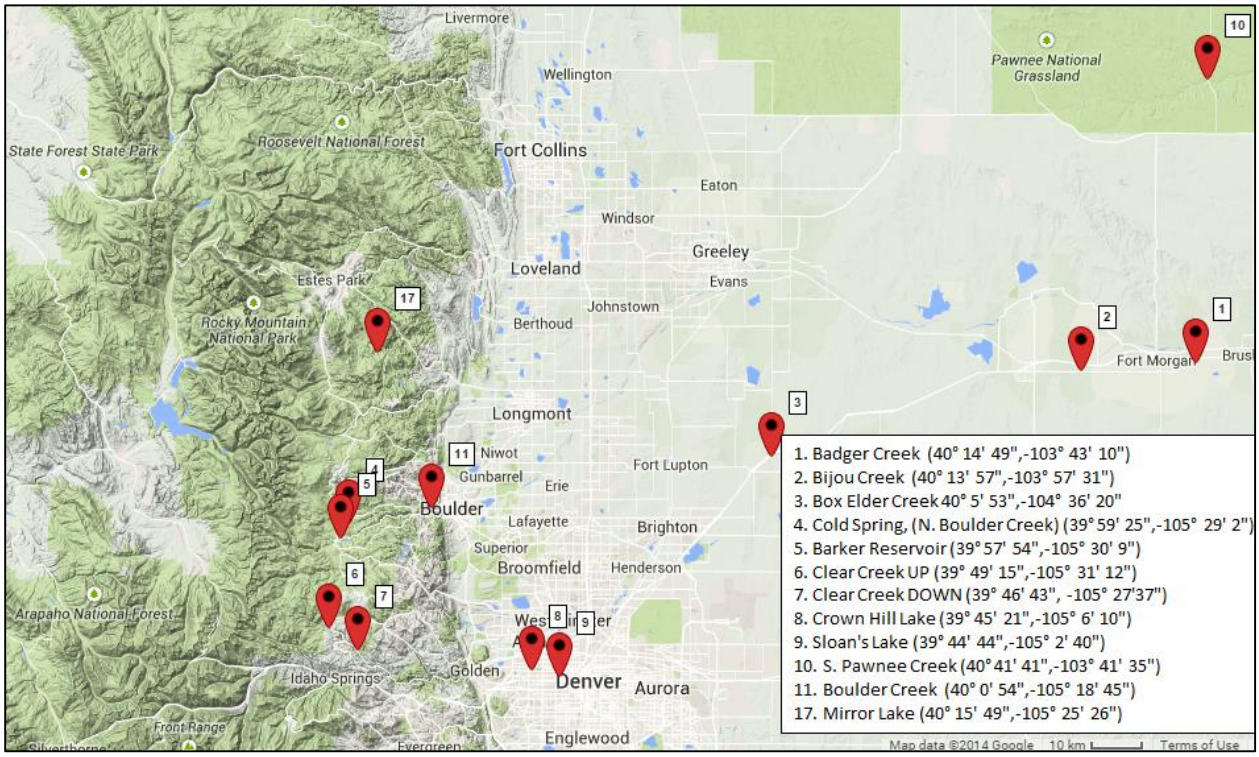

Fig. A.2 Colorado (CO) field site relative locations and coordinates. Partially created using a Google maps application (http://multiplottr.com/)

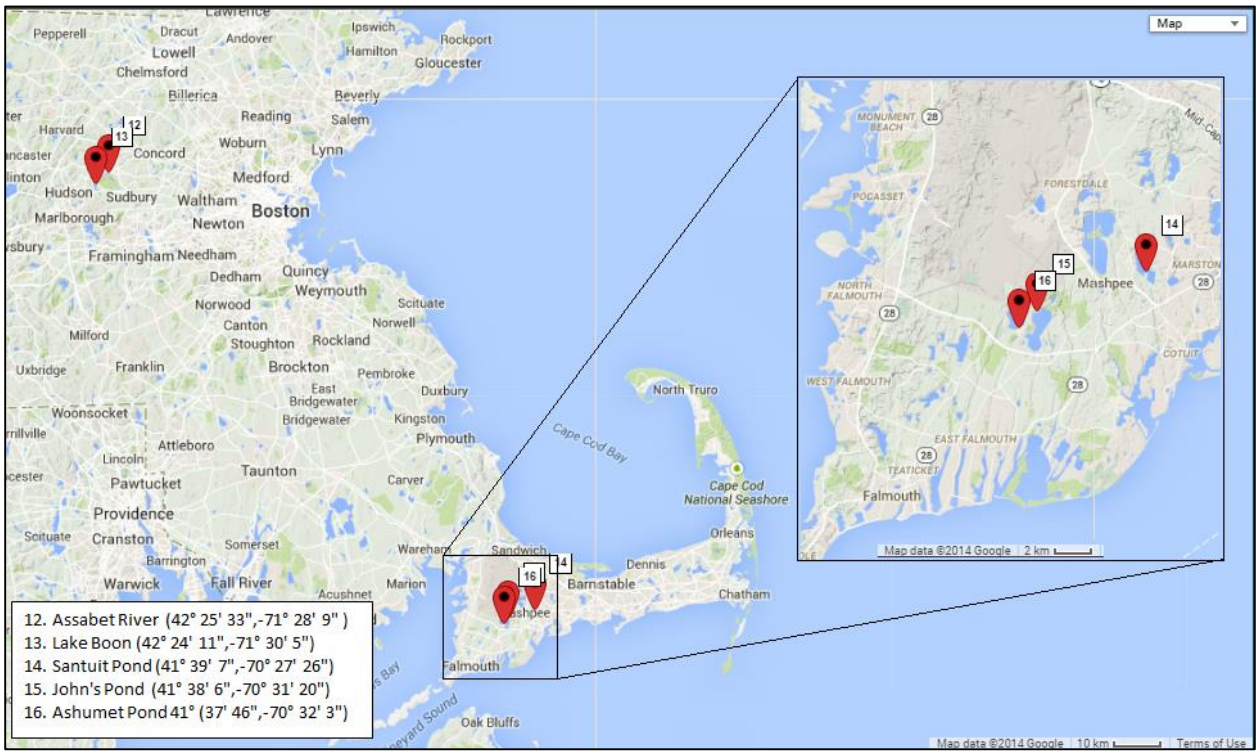

Fig. A.3 Massachusetts (MA) field site relative locations and coordinates. Partially created using a Google maps application (http://multiplottr.com/)

APPENDIX B

SUPPLEMENTARY DATA FOR CHAPTER 3:

USE OF AMPLEX RED TO DETERMINE GROSS DARK HYDROGEN PEROXIDE

PRODUCTION RATES IN FRESHWATER AND ALGAL CULTURES

Ryan M. Marsico[a], Shuichi Ushijima[a,1], Bettina M. Voelker[a,2], Colleen M. Hansel[b],

[a]Colorado School of Mines, Department of Chemistry & Geochemistry, 1500 Illinois St., Golden, CO, USA 80401
[b]Woods Hole Oceanographic Institution, Marine Chemistry & Geochemistry, 266 Woods Hole Rd. MS# 52, Woods Hole, MA, USA 02543-1050

B.1 - Synthesizing metal oxides

Metal oxides were synthesized in the laboratory and used in Amplex red and resorufin stability experiments.

B.1.1. Ferrihydrite

Ferrihydrite was synthesized based on a 2-line ferrihydrite synthesis (Zhao et al. 1994). The exception here is that once the pH was brought to 7 the ferrihydrite was kept in solution rather than decanted and dried. A 0.1M ferrihydrite stock solution resulted from this procedure.

B.1.2. Manganese dioxide (δ-MnO_2)

δ-MnO_2 was synthesized based on a procedure using potassium permanganate and $MnCl_2$ (supplementary material from Taujale and Zhang 2012). A 0.02 M δ-MnO_2 stock solution resulted from this procedure.

B.2 – Resorufin stability figures

All B.2 figures are referenced in the main text (see section 3.4.1) and describe resorufin's stability at various pH and freshwater constituents.

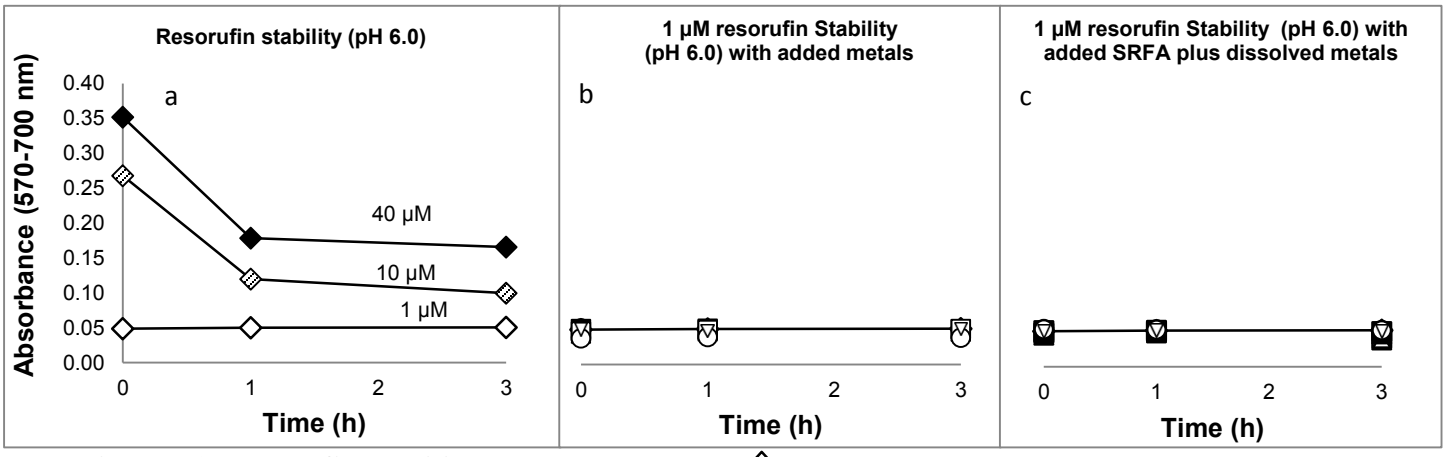

Fig. B.2.1. Resorufin stability at pH 6.0 *a.)* 1 µM (◇) resorufin was stable for 3 hours, but 10 (◈) and 40 µM (◆) resorufin decayed significantly after 1 hour. Based off the expected molar absorptivity of $5.8x10^{-5}$ L $nmol^{-1}$ cm^{-1}, the initial aborbances are even lower than expected for 10 µM resorufin (should be 0.58) and 40 µM resorufin (should be 2.32). *b.)* 1 µM resorufin was stable for 3 hours in presence of 1 µM dissolved and particulate metals: Fe^{2+} (■), Fe^{3+}(▲), ferrihydrite (●), Cu^{2+} (△), Mn^{2+} (□), MnO_2 (○), Potassium superoxide or KO_2 (▽). *c.)* 1 µM resorufin was stable for 3 hours in presence of 10 mg L^{-1} SRFA and 10 mg L^{-1} SRFA plus 1 µM dissolved metals: SRFA+Fe^{2+} (■), SRFA+Fe^{3+}(▲), SRF+Cu^{2+} (△), SRFA+Mn^{2+} (□), SRFA only (○), photo-oxidized SRFA (▽)

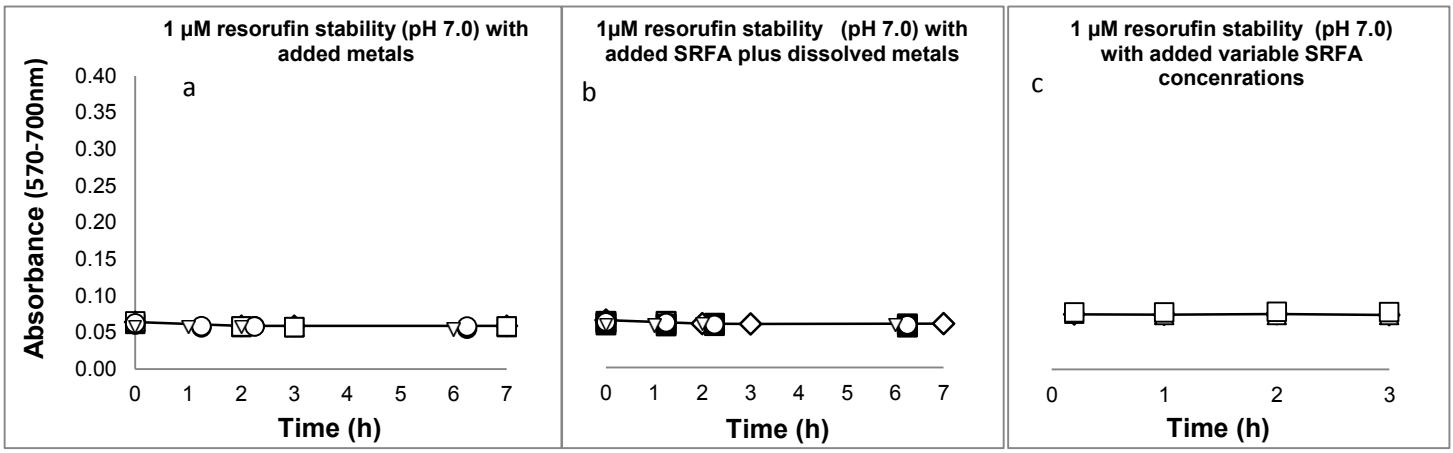

Fig. B.2.2. Resorufin stability at pH 7.0, *a.)* 1 µM (◇) resorufin was stable for 7 hours in presence of 1 µM dissolved and particulate metals: Fe^{2+} (■), Fe^{3+}(▲), ferrihydrite (●), Cu^{2+} (△), Mn^{2+} (□), MnO_2 (○), Potassium superoxide or KO_2 (▽). *b.)* 1 µM resorufin was stable for 7 hours in presence of 10 mg L^{-1} SRFA and 10 mg L^{-1} SRFA plus 1 µM dissolved metals: SRFA+Fe^{2+} (■), SRFA+Fe^{3+}(▲), SRF+Cu^{2+} (△), SRFA+Mn^{2+} (□), SRFA only (○), photo-oxidized SRFA (▽) *c.)* 1 µM resorufin was stable for 3 hours in the presence of varied SRFA at 0 (◇), 10(○), 25(△), and 50 (□) mg L^{-1}

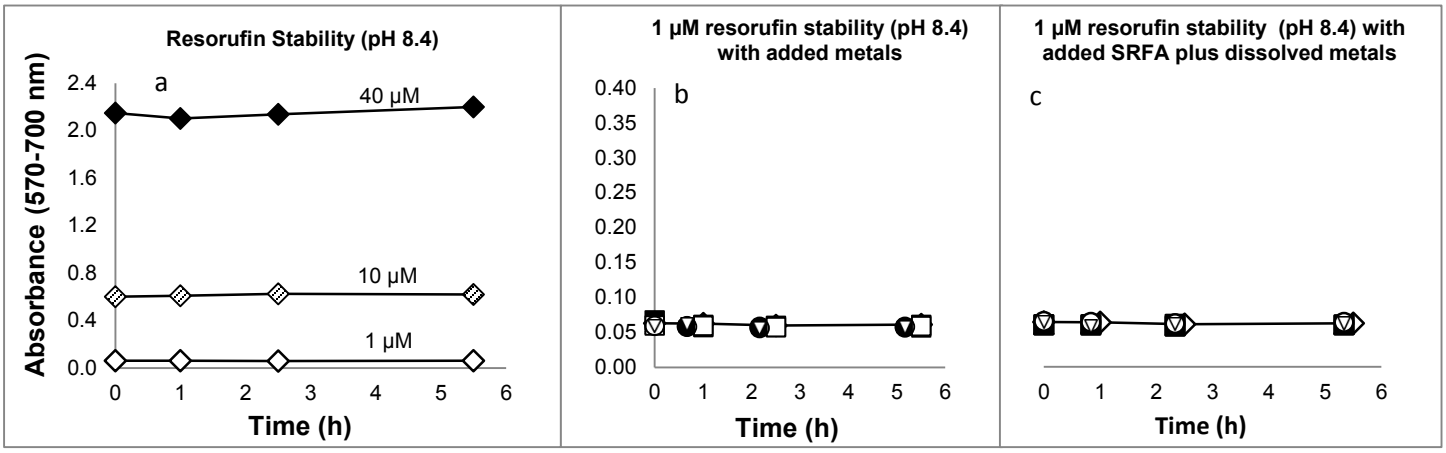

Fig. B.2.3 Resorufin stability at pH 8.5 *a.)* 1 (◇), 10 (◈), and 40 µM (◆) µM resorufin was stable for 7 hours. Based off the expected molar absorptivity of $5.8x10^{-5}$ L $nmol^{-1}$ cm^{-1}, the initial aborbances are at their expected values unlike at pH 6.0. *b.)* 1 µM resorufin was stable for 7 hours in presence of 1 µM dissolved and particulate metals: Fe^{2+} (■), Fe^{3+}(▲), ferrihydrite (●), Cu^{2+} (△), Mn^{2+} (□), MnO_2 (○), Potassium superoxide or KO_2 (▽). *c.)* 1 µM resorufin was stable for 7 hours in presence of 10 mg L^{-1} SRFA and 10 mg L^{-1} SRFA plus 1 µM dissolved metals: SRFA+Fe^{2+} (■), SRFA+Fe^{3+}(▲), SRF+Cu^{2+} (△), SRFA+Mn^{2+} (□), SRFA only (○), photo-oxidized SRFA (▽)

B.3 – Degraded catalase experiments

As described in the main text, P_{H2O2} of the unfiltered catalase amended controls were significantly lower when compared to P_{H2O2} of the unamended unfiltered samples from ML-BEM 7/10/13 and CHL 7/19/13 indicating H_2O_2 oxidized AR to resorufin (see section 3.4.3 and Figure 3.3 of the main text). The added catalase from those same sites also decomposed H_2O_2 added from standard additions, as expected, where the molar absorptivities (i.e. slopes) were flat (Figure B.3.1a-b). However, P_{H2O2} of the unfiltered catalase amended controls from SL 7/24/13 and BM 8/7/13 were not significantly lower than P_{H2O2} of their unamended unfiltered counterparts (Figure B.3.2). This result suggests either that something other than H_2O_2 is oxidizing AR to resorufin or that catalase had become degraded or inactive and no longer able to decompose the H_2O_2 produced in the incubation. The latter is most likely the case since H_2O_2

added from standard additions did not decompose via the added catalase (Figure B.3.1c-d for SL 7/24/13 and BM 8/7/13, respectively). In other words, molar absorptivities (i.e. slopes) were unexpectedly measurable in these catalase amended controls supporting the idea that the added catalase had become inactive or decomposed.

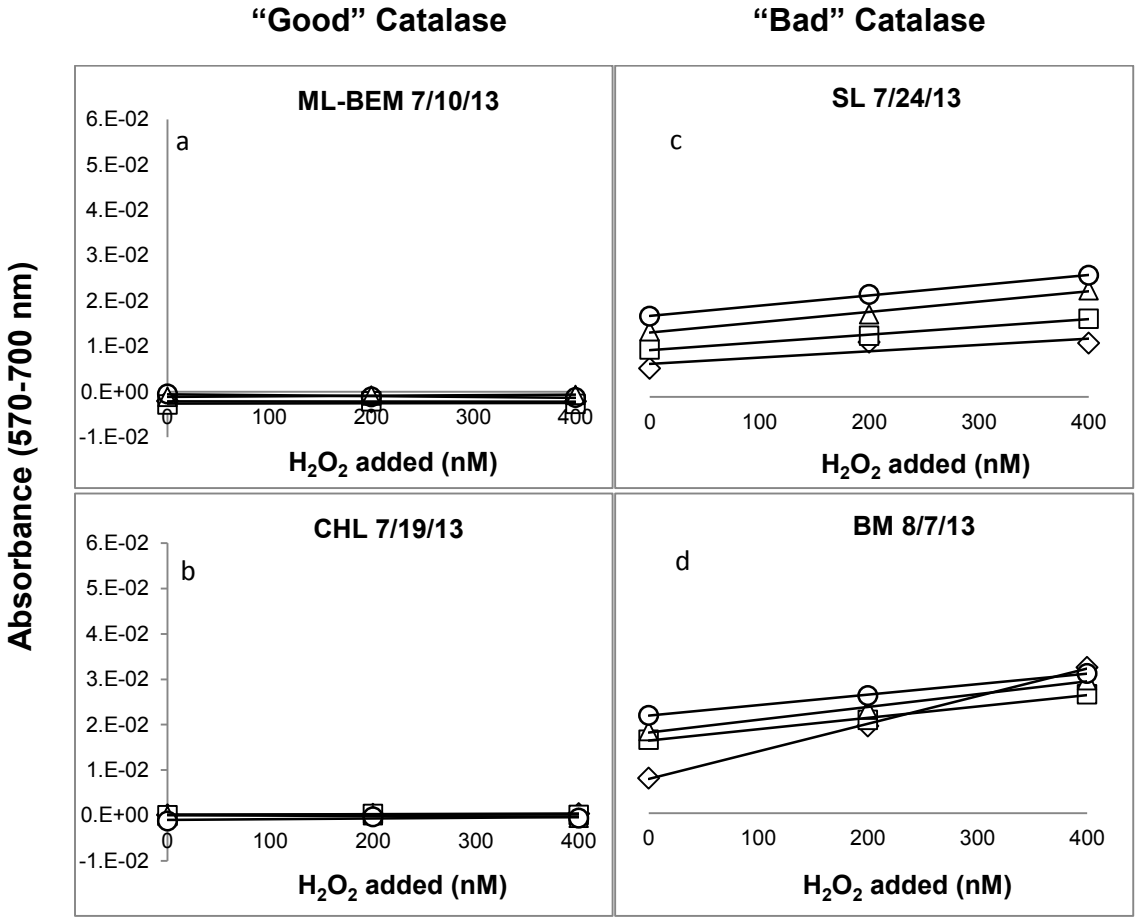

Fig. B.3.1 Examples of a.) and b.) "Good" catalase standard additions from ML-BEM 7/10 and CHL 7/19 compared to c.) and d.) "Bad" catalase standard additions from SL 7/24 and BM 8/7. "Good" catalase means that it expectedly decomposed any H_2O_2 added for standard additions whereas "Bad" catalase means that it unexpectedly did not decomposed any H_2O_2 added for standard additions indicating it had decomposed. The symbols indicate at what point during the incubation an aliquot was removed for standard addition spikes of H_2O_2: time zero of incubation (◇), time 1 hour of incubation (□), time 2 hour of incubation (△), time 3 hour of incubation (○)

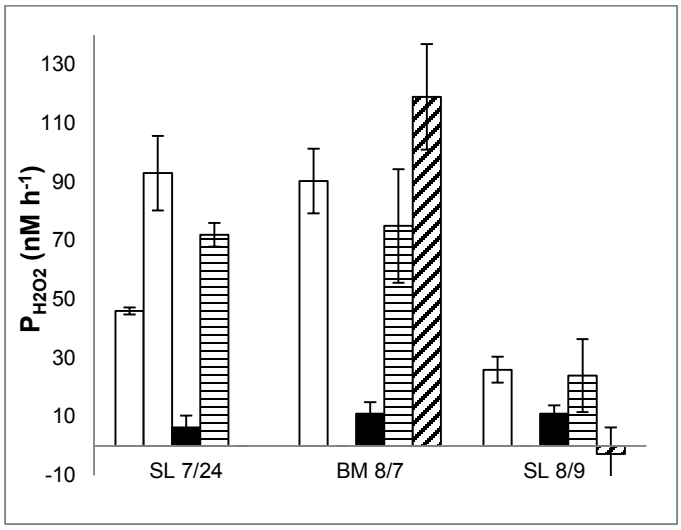

Fig. B.3.2 At SL 7/24, BM 8/7, and SL 8/9 catalase amended unfiltered samples (▤) did not eliminate P_{H2O2} when compared to the unfiltered samples without added catalase (□). Filtered samples (■) did have lower P_{H2O2} than the unfiltered samples, but catalase amended filtered samples (▨) showed an increase in P_{H2O2} at BM 8/7 indicating catalase had decomposed or denatured

Additionally, P_{H2O2} of the filtered catalase amended control from BM 8/7/13 was abnormally large at 119 ± 18 nM h^{-1} even though most of the H_2O_2 source is removed by filtering as seen in the unamended filtered sample (11 ± 4 nM h^{-1}), and resembled P_{H2O2} of the unamended unfiltered sample at 90 ± 11 nM h^{-1} (see Figure B.3.2). It has been previously observed that catalase can produce H_2O_2 when it degrades, and it may be responsible for the observed large P_{H2O2} in the filtered catalase amended control. This further supports that catalase had degraded when used for SL 7/24/13 and BM 8/7/13 incubations, and as a consequence, it is believed H_2O_2 is responsible for AR oxidation to resorufin for those two occurrences.

B.4 – Microbes may contain their own HRP-like enzymes

Here we describe supplementary experiments to determine if HRP-free controls can help detect false positive inferences of the Amplex red method. However, microorganisms may contain HRP-like enzymes and catalyze Amplex red's reaction with H_2O_2.

B.4.1 - Preface

Theoretically, if HRP is not added to a freshwater incubation then resorufin formation (and P_{H2O2}) should not be observed because the system lacks a catalyst for H_2O_2 to oxidize AR to resorufin. Therefore, if there is significant dark P_{H2O2} observed in an unfiltered freshwater incubation *without* added HRP (especially compared to an unfiltered incubation *with* added HRP) it indicates the following: i. microorganisms contain their own HRP-like enzymes capable of catalyzing the AR/H_2O_2 reaction and/or ii. there are particle-associated sources of false positive P_{H2O2} (see section 3.4.2 and Figure 3.1 of the main text and Figure B.4.1). Conversely, if dark P_{H2O2} measured in filtered incubations *without* added HRP is also substantial it may indicate that: i. HRP-like enzymes are located on the cell surface and enter the filtrate via the filtering process and/or ii. there are non-biological dissolved sources of false positive P_{H2O2}. More steps are needed to determine if microorganisms contain HRP-like enzymes, as described in the paragraphs below.

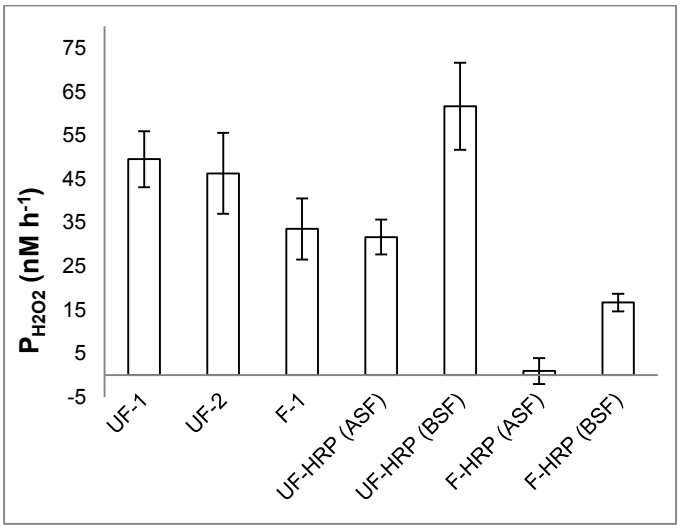

Fig. B.4.1 Comparison of P_{H2O2} from the creek draining Lake Warren, FL for unfiltered and filtered samples *with* HRP (UF and F) and samples *without* HRP (UF-HRP and F-HRP) before and after syringe filtering

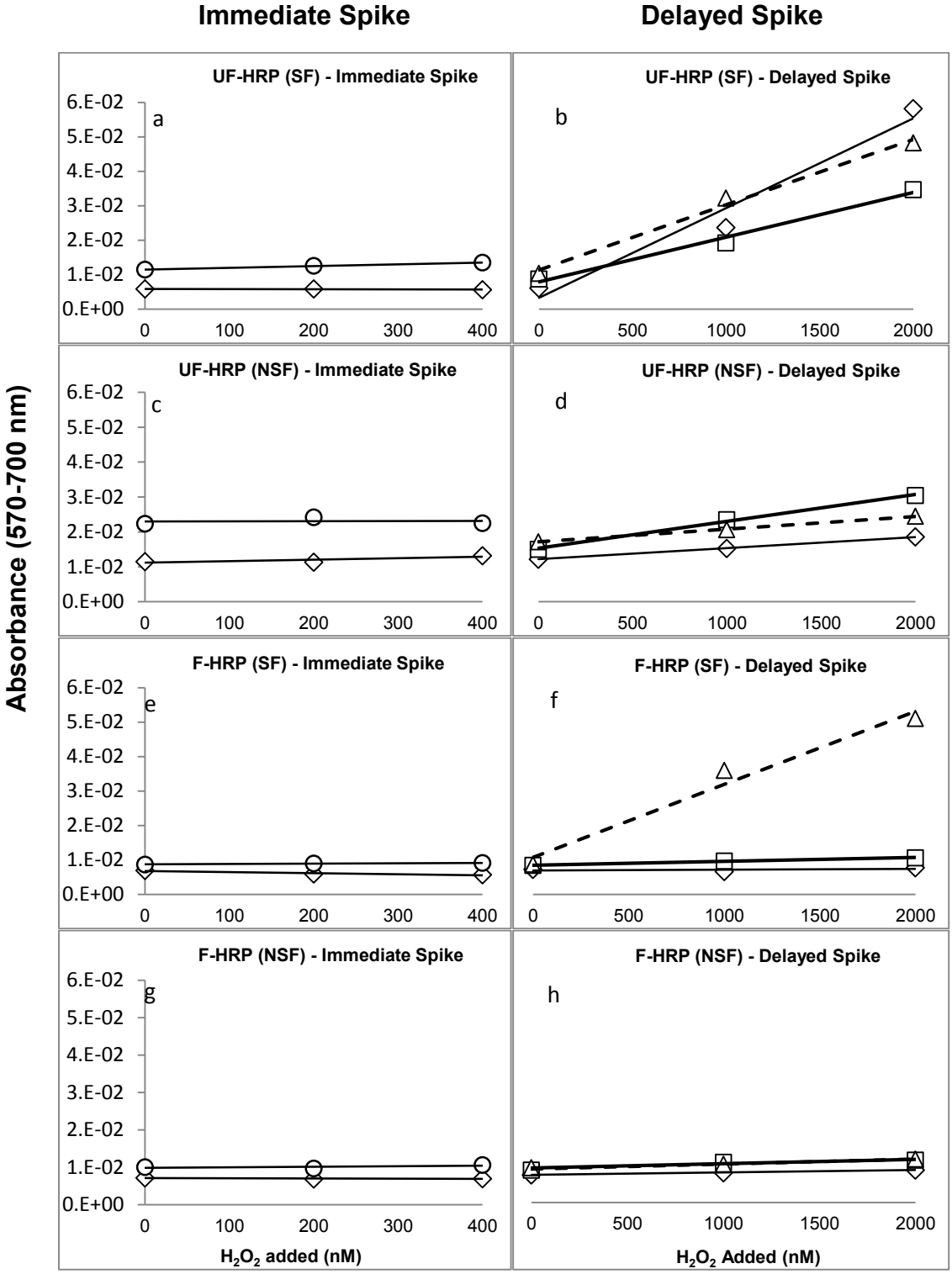

Figure B.4.2 Standard addition spikes with H_2O_2. "Immediate spikes" are absorbance measurements of H_2O_2 standard additions within seconds of spike. "Delayed spikes" are absorbance measurements of H_2O_2 standard additions made at 1.5 and 3 hours after spiking. The symbols indicate at what point during the incubation an aliquot was removed for standard addition spikes of H_2O_2: time zero of incubation (◇), time 1 hour of incubation (□), time 2 hour of incubation (△), time 3 hour of incubation (○)

The first step includes conducting standard additions both *before* and *after* syringe filtering on unfiltered and filtered samples *without* added HRP whereas in a typical AR experiment, standard additions are done only *after* syringe filtering of both unfiltered and filtered samples. Standard additions done "before syringe filtering" are labeled BSF and standard additions done "after syringe filtering" are labeled ASF (Figures B.4.1 and B.4.2). The ASF samples remove particles and microbes so they do not end up in the cuvette before it is analyzed. The opposite is true for BSF. One possible scenario is that there will be a response in absorbance signal by H_2O_2 standard additions before and/or after syringe filtering of the unfiltered sample *without* added HRP. This would strengthen the case that HRP-like enzymes of the microorganisms do in fact exist, although not yet conclusive, and may possibly enter the filtrate via the syringe filtering processes. If a response is not observed either HRP-like enzymes in the microorganisms at this field site do not exist or enough time is not given for them to catalyze the AR/H_2O_2 reaction.

The second step is to measure standard additions both "immediately", within seconds of spiking as per the normal standard addition protocol, and measure standard additions "delayed" within 1.5 hours of each spike. If microorganisms do in fact have their own HRP-like enzymes, then given enough time resorufin should accumulate when H_2O_2 is present in enough quantity (i.e. a relatively large spike of 1 µM H_2O_2). The immediate spikes were done in a typical manner (see section 3.3.6.2 of the main text). The delayed standard additions had spikes with 1 µM H_2O_2 added at the first spike and measured 1.5 hours later (i.e. delayed) followed by another 1 µM H_2O_2 spike and measured another 1.5 hours later. One possible scenario is that there is no response from both the immediate and delayed standard additions, and therefore, HRP-like

enzymes of microorganisms from this field site can be ruled out. The existence of HRP-like enzymes is strengthened if a standard addition response is observed in either case.

All of the below experiments were conducted on incubations containing freshwater from an unnamed creek draining Lake Warren in Orlando, FL from January 5, 2014 (see the following sections: B4.2-4.4).

B.4.2 - P_{H2O2} *with* and *without* HRP added

First, P_{H2O2} of the unfiltered samples *with* added HRP (50 ± 6 and 46 ± 9 nM h^{-1}) were not considerably larger than the filtered sample *with* added HRP (P_{H2O2} = 34 ± 7 nM h^{-1}) shown in Figure B.3.2. This potentially means that dissolved sources play a comparable role to particle-associated sources of P_{H2O2} at this creek. Furthermore, a negligible P_{H2O2} of the filtered sample *without* HRP added (1 ± 3 nM h^{-1}) tells us that there is not a dissolved source of false positive P_{H2O2}, and that HRP-like enzymes of the microorganisms (if they exist) do not end up in filtrate (i.e. the filtered incubated sample).

Furthermore, P_{H2O2} in the unfiltered sample *without* HRP added (P_{H2O2} = 32 ± 4 nM h^{-1}) is somewhat comparable to the unfiltered sample *with* HRP added. Since dissolved sources of false positive P_{H2O2} are ruled out this suggests the presence of either i. microbial HRP-like enzymes or ii. particle-associated false positive P_{H2O2}. Again, comparing these results to the negligible P_{H2O2} of the filtered sample *without* HRP added, it indicates the removal of the particle-associated source of false positive P_{H2O2} and/or that the HRP-like enzymes are attached to cell surfaces and are removed during bulk filtering. Unfortunately, at this point, it remains unclear whether or not microorganisms have their own HRP-like enzymes. Section B4.3 describes the first step to elucidate this issue.

B.4.3 - Immediate standard additions before and after syringe filtering (BSF & ASF)

Immediate standard additions in both unfiltered and filtered incubations *without* added HRP did not show an absorbance response to H_2O_2 added BSF and ASF (Figure B.4.2a,c,e,g) opposed to the unfiltered and filtered incubations *with* added HRP that showed a response to H_2O_2 added ASF, albeit slightly lower than the known literature value (molar absorptivities: UF-1 = 4.04(0.05)x10^{-5}, UF-2 = 4.97(0.1)x10^{-5}, and F-1 = 5.07(0.1)x10^{-5} L nmol^{-1} cm^{-1}). The results of this experiment indicate the lack of microbial HRP-like enzymes, but are still largely inconclusive since enough time may not have been given for the standard addition to react with HRP-like enzymes of the microorganisms. Therefore, standard additions were also conducted in a delayed manner to allow enough time for the reaction to occur (see section B4.4).

B.4.4 - Delayed standard additions before and after syringe filtering

The unfiltered incubations *without* HRP added ASF had a measurable molar absorptivity from delayed H_2O_2 standard additions compared to the non-existent molar absorptivity from immediate standard additions (Figure B.4.2b and B4.2d). In fact, while the molar absorptivity was lower than expected, it was on the same order of magnitude (1.86(0.06)x10^{-5} L nmol^{-1} cm^{-1}) as molar absorptivities for standard additions from unfiltered samples *with* HRP added (e.g. 5.8x10^{-5} L nmol^{-1} cm^{-1}). This is unlike the immediate standard additions from samples *without* HRP added where molar absorptivities are often 2-3 orders of magnitude lower than the expected value or sometimes even negative, and considered non-existent. The unfiltered sample BSF also had a measurable molar absorptivity from delayed H_2O_2 standard additions, but was around an order of magnitude lower (4.7(0.02) x10^{-6} L nmol^{-1} cm^{-1}) than the expected value. This is most likely because microorganisms were placed directly in the cuvette (i.e. not removed by syringe filtering) with subsequent standard additions. Microorganisms are often equipped with enzymes

such as catalase to decompose H_2O_2 and most likely got rid of H_2O_2 added from standard additions.

Both of the delayed standard additions in unfiltered samples *without* HRP added suggest that a component in the spiked aliquot catalyzed AR oxidation to resorufin when H_2O_2 was added. Currently, the only known way for this to occur is to have HRP as a substrate and since it was not artificially added we think that microorganisms at this field site contain their own HRP or HRP-like enzymes. The delayed standard additions also further support that HRP or HRP-like enzymes from the microorganisms were removed during syringe filtering since a molar absorptivity was observed ASF in the unfiltered samples *without* HRP added. Syringe filtering may be forceful enough to remove enzymes loosely bound to cell surfaces opposed to the more passive filtering using a peristaltic pump with an Acropak used for bulk filtering to obtain a filtered sample for incubation purposes. This is supported by the lack of a molar absorptivity observed in delayed standard additions for filtered incubations *without* added HRP BSF and ASF (Figure B.4.2.f and B4.2h), thus, bulk filtering removed the organism along with the bound enzyme. The single outlier in Figure B.4.2.f is believed to be from contamination of the cuvette with added HRP.

B.5 – Raw ε_{app} values for all samples

Table B.1 All ε_{app} values measured at each time point from unfiltered freshwater samples

Site	Time point (h)	ε_{app} x10^{-5} (absorbance cm^{-1} nM^{-1} H_2O_2 added)
BM 7/15/13 Sample 1	0	3.4
	1	3.82
	2	4.03
	3	3.82
BM 7/15/13 Sample 2	0	3.47
	1	3.24
	2	3.74
	3	3.93
BM 8/7/13 Sample 1	0	6.8
	1	7.52
	2	6.69
	3	6.56
BM 8/16/13 Sample 1	0	5.85
	1	7.18
	2	6.54
	3	7.32
BM 8/21/13 Sample 1	0	8.91
	1	7.98
	2	7.99
	3	8.44
BM 8/28/13 Sample 1	0	7.39
	1	7.89
	2	7.49
	3	7.82
BM 3/14/14 Sample 1	0	3.59
	1	4.45
	2	4.86
	3	5.05
CHL 6/28/13 Sample 1	0	5.97
	1	8.42
	2	8.35
	4	7.84
CHL 6/28/13 Sample 2	0	7.2
	1	7.65

Table B.1 Continued

	2	8.65
	4	8.7
CHL 7/1/13 Sample 1	0	6.59
	1	5.87
	2	5.87
	3	6.34
CHL 7/1/13 Sample 2	0	5.62
	1	7.28
	2	7.48
	3	6.67
CHL 7/8/13 Sample 1	1	9.31
	2	8.91
	3	9.2
	4	8.34
CHL 7/8/13 Sample 2	1	8.38
	2	8.71
	3	9.43
	4	9.82
CHL 7/19/13 Sample 1	0	7.66
	1	8.07
	2	7.7
	3	7.85
CHL 7/19/13 Sample 2	0	8.13
	1	8.18
	2	8.11
	3	7.97
CHL 8/19/13 Sample 1	0	6.65
	1	7.83
	2	8.91
	3	9.83
ML-BEM 7/3/13 Sample 1	1	4.93
	2	5.47
	3	5.26
	4	5.59
ML-BEM 7/3/13 Sample 2	1	4.73
	2	5.09
	3	5.68
	4	6.13
ML-BEM 7/10/13 Sample 1	0	6.44
	1	6.95

Table B.1 Continued

	2	7.56
	3	6.81
ML-BEM 7/10/13 Sample 2	0	5.54
	1	7
	2	7.09
	3	6.93
SL 7/24/13 Sample 1	0	8.36
	1	8.31
	2	8.21
	3	8.82
SL 7/24/13 Sample 2	0	5.73
	1	4.85
	2	5.5
	3	6.2
SL 8/9/13 Sample 1	0	10.7
	1	11.6
	2	10.7
	3	11.1
SL 8/30/13 Sample 1	0	16.2
	1	15.4
	2	16.7
	3	17.6
SL 3/13/14 Sample 1	0	5.36
	3	6.64
SL 3/28/14 Sample 1	0	4.43
	1	5.91
	2	6.27
	3	5.21

Table B.2 All ε_{app} values measured at each time point from filtered freshwater samples

Filtered Site	Time point (h)	ε_{app} x10^{-5} (absorbance cm^{-1} nM^{-1} H_2O_2 added)
BM 7/15/13 Sample 1	0	3.46
	1	4.23
	2	4.55
	3	4.44
BM 7/15/13 Sample 2	0	3.71
	1	3.98
	2	3.86
	3	4.48
BM 8/7/13 Sample 1	0	9.1
	1	8.3
	2	10.1
	3	9.79
BM 8/16/13 Sample 1	0	8.06
	1	8.29
	2	9.78
	3	9.4
BM 8/16/13 Sample 2	0	8.25
	1	8.98
	2	7.29
	3	9.38
BM 8/21/13 Sample 1	0	8.19
	1	9.29
	2	8.1
	3	9.51
BM 8/28/13 Sample 1	0	7.97
	1	8.96
	2	7.88
	3	8.15
BM 8/28/13 Sample 2	0	6.8
	1	8.35
	2	7.94
	3	7.81
BM 3/14/14 Sample 1	0	3.36
	1	4.6
	2	5.52
	3	5.61

Table B.2 Continued

CHL 6/28/13 Sample 1	1	7.65
	2	7.54
	4	7.93
CHL 6/28/13 Sample 2	1	7.66
	2	7.73
	4	7.58
CHL 7/1/13 Sample 1	0	5.81
	1	9.1
	2	9.96
	3	8.32
CHL 7/1/13 Sample 2	0	7.15
	1	8.73
	2	9.29
	3	9.36
CHL 7/8/13 Sample 1	1	4.44
	2	8.31
	3	8.33
	4	9.23
CHL 7/8/13 Sample 2	1	5.37
	2	8.81
	3	8.8
	4	7.99
CHL 7/19/13 Sample 2	0	7.55
	1	7.75
	2	8.28
	3	7.3
CHL 8/19/13 Sample 1	0	8.55
	1	9.49
	2	9.88
	3	10.4
ML-BEM 7/3/13 Sample 1	1	4.86
	2	5.1
	3	5.9
	4	6.8
ML-BEM 7/3/13 Sample 2	1	5.86
	2	6.22
	3	5.39
	4	8.49
ML-BEM 7/10/13 Sample 1	0	6.12
	1	7.01

Table B.2 Continued

	2	7.33
	3	7.45
ML-BEM 7/10/13 Sample 2	0	6.13
	1	6.01
	2	7.36
	3	7.02
SL 7/24/13 Sample 1	0	8.04
	1	9.27
	2	8.66
	3	8.46
SL 8/9/13 Sample 1	0	6.36
	1	12.1
	2	12.8
	3	10.7
SL 8/30/13 Sample 1	0	8.62
	1	10.6
	2	8.17
	3	10.2
SL 3/13/14 Sample 1	0	5.23
	3	4.95
SL 3/28/14 Sample 1	0	4.95
	1	5.91
	2	5.59
	3	5.66

Table B.3 All ε_{app} values measured at each time point from 50 mM phosphate buffer (pH 7) controls and laboratory experiment samples

pH 7 phsophate buffer Site	Time point (h)	ε_{app} x10^{-5} (absorbance cm^{-1} nM^{-1} H_2O_2 added)
Control for SL 3/13/14	0	5.36
	3	5.58
Control for BM 3/14/14	0	5.17
	1	5.51
	2	4.93
	3	5.44
Control for SL 3/28/14	0	5.86
	1	5.14
	2	5.71
	3	4.75
Lab experiment 1/17/14	0	3.72
	1	5.39
	2	5.65
	3	4.75
Lab experiment 1/23/14	0	5.29
	1	5.87
	2	5.91
	3	5.52
Lab experiment 1/24/14	0	5.78
	1	5.76
	2	6.09
	3	6.04
Lab experiment 2/28/14	0	4.29
	1	5.9
	2	5.32
	3	5.19

Table B.4 All ε_{app} values measured at each time point from *C. reinhardtii* cultures.

C. reinhardtii Site	Time point (h)	ε_{app} x10^{-5} (absorbance cm^{-1} nM^{-1} H_2O_2 added)
Culture 1 (1/40th dilution)	0	5.71
	1	5.70
	2	5.36
	3	6.44
	4	5.96
Culture 1 (1/20th dilution)	0	5.83
	1	4.70
	2	6.02
	3	5.81
	4	6.03
Culture 1 (1/10th dilution)	0	6.06
	1	5.73
	2	5.98
	3	6.49
	4	7.13
Culture 1(1/5th dilution)	0	5.90
	1	5.74
	2	5.77
	3	6.54
	4	6.68
Culture 2 (1/20th dilution) Sample 1	0	5.30
	1	5.42
	2	6.10
	3	5.86
	4	3.43
Culture 2 (1/20th dilution) Sample 2	0	5.30
	1	5.43
	2	5.64
	3	5.77
	4	3.39
Culture 2 (1/5th dilution) Sample 1	0	5.74
	1	5.81
	2	5.85
	3	5.88
	4	5.93
Culture 2 (1/5th dilution) Sample 2	0	5.38
	1	5.58
	2	5.68
	3	5.77
	4	5.91

APPENDIX C

PERMISSIONS TO USE PREVIOUSLY PUBLISHED MATERIAL

Journal permissions (below) is a license from Springer to use the article "Spatial and Temporal Variability of Widespread Dark Production and Decay of Hydrogen Peroxide in Freshwater," which was published in Aquatic Sciences in June of 2015.

9/2/2015 Rightslink Printable License

SPRINGER LICENSE

TERMS AND CONDITIONS

Sep 02, 2015

This is a License Agreement between Ryan M Marsico ("You") and Springer ("Springer") provided by Copyright Clearance Center ("CCC"). The license consists of your order details, the terms and conditions provided by Springer, and the payment terms and conditions. All payments must be made in full to CCC. For payment instructions, please see information listed at the bottom of this form.

License Number	3700890061631
License date	Sep 02, 2015
Licensed content publisher	Springer
Licensed content publication	Aquatic Sciences Research Across Boundaries
Licensed content title	Spatial and temporal variability of widespread dark production and decay of hydrogen peroxide in freshwater
Licensed content author	Ryan M. Marsico
Licensed content date	Jan 1, 2015

Type of Use	Thesis/Dissertation
Portion	Full text
Number of copies	1
Author of this Springer article	Yes and you are the sole author of the new work
Order reference number	None
Title of your thesis	Implications of Widespread Dark Production and Decay of Reactive Oxygen Species in Natural Waters
Expected completion date	Sep 2015
Estimated size(pages)	137
Customer Tax ID	USColorado
Total	0.00 USD

Terms and Conditions

Introduction

The publisher for this copyrighted material is Springer Science + Business Media. By clicking "accept" in connection with completing this licensing transaction, you agree that the following terms and conditions apply to this transaction (along with the Billing and Payment terms and conditions established by Copyright Clearance Center, Inc. ("CCC"), at the time that you opened your Rightslink account and that are available at any time at http://myaccount.copyright.com).

Limited License

With reference to your request to reprint in your thesis material on which Springer Science and Business Media control the copyright, permission is granted, free of charge, for the use indicated in your enquiry.

Licenses are for onetime use only with a maximum distribution equal to the number that you identified in the licensing process.

This License includes use in an electronic form, provided its password protected or on the university's intranet or repository, including UMI (according to the definition at the Sherpa website: http://www.sherpa.ac.uk/romeo/). For any other electronic use, please contact Springer at (permissions.dordrecht@springer.com or permissions.heidelberg@springer.com).

The material can only be used for the purpose of defending your thesis limited to university use only. If the thesis is going to be published, permission needs to be reobtained (selecting "book/textbook" as the type of use).

Although Springer holds copyright to the material and is entitled to negotiate on rights, this license is only valid, subject to a courtesy information to the author (address is given with the article/chapter) and provided it concerns original material which does not carry references to other sources (if material in question appears with credit to another source, authorization from that source is required as well).

Permission free of charge on this occasion does not prejudice any rights we might have to charge for reproduction of our copyrighted material in the future.

Altering/Modifying Material: Not Permitted

You may not alter or modify the material in any manner. Abbreviations, additions, deletions and/or any other alterations shall be made only with prior written authorization of the author(s) and/or Springer Science + Business Media. (Please contact Springer at (permissions.dordrecht@springer.com or permissions.heidelberg@springer.com)

Reservation of Rights

Springer Science + Business Media reserves all rights not specifically granted in the combination of (i) the license details provided by you and accepted in the course of this licensing transaction, (ii) these terms and conditions and (iii) CCC's Billing and Payment terms and conditions.

Copyright Notice: Disclaimer

You must include the following copyright and permission notice in connection with any reproduction of the licensed material: "Springer and the original publisher /journal title, volume, year of publication, page, chapter/article title, name(s) of author(s), figure number(s), original copyright notice) is given to the publication in which the material was originally published, by adding; with kind permission from Springer Science and Business Media"

Warranties: None

Example 1: Springer Science + Business Media makes no representations or warranties with respect to the licensed material.

Example 2: Springer Science + Business Media makes no representations or warranties with respect to the licensed material and adopts on its own behalf the limitations and disclaimers established by CCC on its behalf in its Billing and Payment terms and conditions for this licensing transaction.

Indemnity

You hereby indemnify and agree to hold harmless Springer Science + Business Media and CCC, and their respective officers, directors, employees and agents, from and against any and all claims arising out of your use of the licensed material other than as specifically authorized pursuant to this license.

No Transfer of License

This license is personal to you and may not be sublicensed, assigned, or transferred by you to any other person without Springer Science + Business Media's written permission.

No Amendment Except in Writing

This license may not be amended except in a writing signed by both parties (or, in the case of Springer Science + Business Media, by CCC on Springer Science + Business Media's behalf).

Objection to Contrary Terms

Springer Science + Business Media hereby objects to any terms contained in any purchase order, acknowledgment, check endorsement or other writing prepared by you, which terms are inconsistent with these terms and conditions or CCC's Billing and Payment terms and conditions. These terms and conditions, together with CCC's Billing and Payment terms and conditions (which are incorporated herein), comprise the entire agreement between you and Springer Science + Business Media (and CCC) concerning this licensing transaction. In the event of any conflict between your obligations established by these terms and conditions and those established by CCC's Billing and Payment terms and conditions, these terms and conditions shall control.

Jurisdiction

All disputes that may arise in connection with this present License, or the breach thereof, shall be settled exclusively by arbitration, to be held in The Netherlands, in accordance with Dutch law, and to be conducted under the Rules of the 'Netherlands Arbitrage Instituut' (Netherlands Institute of Arbitration).*OR:*

All disputes that may arise in connection with this present License, or the breach thereof, shall be settled exclusively by arbitration, to be held in the Federal Republic of Germany, in accordance with German law.

Other terms and conditions:

v1.3

Questions? customercare@copyright.com or +18552393415

(toll free in the US) or

+19786462777.